


<b>Title</b>	A microscopic study of structural and electronic properties of functionalized silicon surfaces based on first-principles
<b>Author(s)</b>	Arefi, Hadi Hassanian
<b>Publication date</b>	2015
<b>Original citation</b>	Arefi, H. H. 2015. A microscopic study of structural and electronic properties of functionalized silicon surfaces based on first-principles. PhD Thesis, University College Cork.
<b>Type of publication</b>	Doctoral thesis
<b>Rights</b>	© 2015, Hadi H. Arefi. <a href="http://creativecommons.org/licenses/by-nc-nd/3.0/">http://creativecommons.org/licenses/by-nc-nd/3.0/</a> 
<b>Embargo information</b>	No embargo required
<b>Item downloaded from</b>	<a href="http://hdl.handle.net/10468/1879">http://hdl.handle.net/10468/1879</a>

Downloaded on 2017-02-12T06:01:40Z



**A Microscopic Study of Structural  
and Electronic Properties of  
Functionalized Silicon Surfaces Based  
on First-Principles**

By

**Hadi Hassanian Arefi**

**Thesis submitted for the degree of Doctor of Philosophy**

**February 2015**

Supervisor: **Dr. Giorgos Fagas**

Advisor: **Dr. Michael Nolan**

Head of Department: **Prof. Nabeel A. Riza**

NATIONAL UNIVERSITY OF IRELAND, CORK  
DEPARTMENT of ELECTRICAL and ELECTRONIC  
ENGINEERING  
TYNDALL NATIONAL INSTITUTE

**To My Beloved Brother, Mahdi ... Rest in Peace!**

# Abstract

Surface modification of silicon with organic monolayers tethered to the surface by different linkers is an important process in realizing future (opto-)electronic devices. Understanding the role played by the nature of the linking group and the chain length on the adsorption structures and electronic properties of these assemblies is vital to advance this technology. This Thesis is a study of such properties and contributes in particular to a microscopic understanding of induced changes in the work function of experimentally studied functionalized silicon surfaces.

Using first-principles density functional theory (DFT), at the first step, we provide predictions for chemical trends in the work function of hydrogenated silicon (111) surfaces modified with various terminations. For nonpolar terminating atomic species such as F, Cl, Br, and I, the change in the work function is directly proportional to the amount of charge transferred from the surface, thus relating to the difference in electronegativity of the adsorbate and silicon atoms. The change is a monotonic function of coverage in this case, and the work function increases with increasing electronegativity. Polar species such as  $-\text{TeH}$ ,  $-\text{SeH}$ ,  $-\text{SH}$ ,  $-\text{OH}$ ,  $-\text{NH}_2$ ,  $-\text{CH}_3$ , and  $-\text{BH}_2$  do not follow this trend due to the interaction of their dipole with the induced electric field at the surface. In this case, the magnitude and sign of the surface dipole moment need to be considered in addition to the bond dipole to generally describe the change in work function. Compared to hydrogenated surfaces, there is slight increase in the work function of  $\text{H}:\text{Si}(111)\text{-XH}$ , where  $\text{X} = \text{Te}$ ,  $\text{Se}$ , and  $\text{S}$ , whereas reduction is observed for surfaces covered with  $-\text{OH}$ ,  $-\text{CH}_3$ , and  $-\text{NH}_2$ .

Next, we study the hydrogen passivated  $\text{Si}(111)$  surface modified with alkyl chains of the general formula  $\text{H}:\text{Si}-(\text{CH}_2)_n\text{-CH}_2$  and  $\text{H}:\text{Si-X}-(\text{CH}_2)_n\text{-CH}_3$ , where  $\text{X} = \text{NH}$ ,  $\text{O}$ ,  $\text{S}$  and  $n = (0, 1, 3, 5, 7, 9, 11)$ , at half coverage. For (X)-Hexyl and (X)-Dodecyl functionalization, we also examined various coverages up to full monolayer grafting in order to validate the result of half covered

surface and the linker effect on the coverage. We find that it is necessary to take into account the van der Waals interaction between the alkyl chains. The strongest binding is for the oxygen linker, followed by S, N, and C, irrespective of chain length. The result revealed that the sequence of the stability is independent of coverage; however, linkers other than carbon can shift the optimum coverage considerably and allow further packing density. For all linkers apart from sulfur, structural properties, in particular, surface-linker-chain angles, saturate to a single value once  $n > 3$ . For sulfur, we identify three regimes, namely,  $n = 0-3$ ,  $n = 5-7$ , and  $n = 9-11$ , each with its own characteristic adsorption structures. Where possible, our computational results are shown to be consistent with the available experimental data and show how the fundamental structural properties of modified Si surfaces can be controlled by the choice of linking group and chain length.

Later we continue by examining the work function tuning of H:Si(111) over a range of 1.73 eV through adsorption of alkyl monolayers with general formula  $[\text{X}^{\text{head-group}}]-(\text{C}_n\text{H}_{2n})-[\text{X}^{\text{tail-group}}]$ ,  $\text{X} = \text{O}(\text{H}), \text{S}(\text{H}), \text{NH}_2$ . The work function is practically converged at 4 carbons (8 for oxygen), for head-group functionalization. For tail-group functionalization and with both head- and tail-groups, there is an odd-even effect in the behavior of the work function, with peak-to-peak amplitudes of up to 1.7 eV in the oscillations. This behavior is explained through the orientation of the terminal-group's dipole. The shift in the work function is largest for  $\text{NH}_2$ -linked and smallest for  $\text{SH}$ -linked chains and is rationalized in terms of interface dipoles. Our study reveals that the choice of the head- and/or tail-groups effectively changes the impact of the alkyl chain length on the work function tuning using self-assembled monolayers and this is an important advance in utilizing hybrid functionalized Si surfaces.

Bringing together the understanding gained from studying single type functionalization of H:Si(111) with different alkyl chains and bearing in mind how to utilize head-group, tail-group or both as well as monolayer coverage, in the final part of this Thesis we study functionalized H:Si(111) with binary SAMs. Aiming at enhancing work function adjustment together with SAM

stability and coverage we choose a range of terminations and linker-chains denoted as  $-X-(\text{Alkyl})$  with  $X = \text{CH}_3, \text{O}(\text{H}), \text{S}(\text{H}), \text{NH}_2$  and investigate the stability and work function of various binary components grafted onto H:Si(111) surface. Using binary functionalization with  $-\text{[NH}_2\text{]/O}(\text{H})\text{[S}(\text{H})\text{]-[Hexyl/Dodecyl]}$  we show that work function can be tuned within the interval of 3.65-4.94 eV and furthermore, enhance the SAM's stability. Although direct Si-C grafted SAMs are less favourable compared to their counterparts with O, N or S linkage, regardless of the ratio, binary functionalized alkyl monolayers with X-alkyl ( $X = \text{NH}, \text{O}$ ) is always more stable than single type alkyl functionalization with the same coverage. Our results indicate that it is possible to go beyond the optimum coverage of pure alkyl functionalized SAMs (50%) by adding a linker with the correct choice of the linker. This is very important since dense packed monolayers have fewer defects and deliver higher efficiency. Our results indicate that binary anchoring can modify the charge injection and therefore bond stability while preserving the interface electronic structure.

# Acknowledgements

First of all, I would like to express my deepest gratitude to my supervisor Dr. Giorgos Fagas, not only for the opportunity to conduct this research, but for the consistent and reliable support, teaching, patience and inspiring encouragement over the last 4 years. I consider myself very lucky to be guided by such an experienced, knowledgeable and kind educator of science.

Special thanks to my advisor, Dr. Michael Nolan for his advice, guidance, fruitful discussions and positive attitude throughout the PhD project. A particular thank you is extended to Dr. Simon Elliot, for his remarkable management and support as the head of the MMD group, for organizing the weekly group meetings, and providing the environment for helpful scientific discussions and transferable skills. I also wish to thank my former supervisors, Dr. M. R. Abolhasani and Dr. S. A. Jafari for providing me the platform to pursue my PhD abroad.

Very big thanks to all of my friends in the Materials Modelling for Devices Group and Electronics Theory Group for creating a friendly working atmosphere and being always enthusiastic to help that is invaluable to any postgraduate experience.

Financial support from The European Commission, through the 7th Framework ICT-FET-Proactive program, project SiNAPS (contract no 257856), is gratefully acknowledged. The author wishes to thank Dr. Simon Elliot for partial support through Science Foundation Ireland (SFI), project “ALDesign” (grant number 09/IN.1/I2628). We also acknowledge computing resources provided by SFI and Irish Centre for High End Computing (ICHEC) to the Tyndall National Institute.

Finally, I wish to convey my sincerest thanks and appreciation to my family, Mum, Dad and my sisters, for all their support and encouragement throughout my education and being always there for me in the hardest times with pure love.

# Publications

1. **Hadi. H. Arefi**, Michael Nolan and Giorgos Fagas, “Density Functional Theory with van der Waals Corrections Study of the Adsorption of Alkyl, Alkylthiol, Alkoxy, and Amino-Alkyl Chains on the H:Si(111) Surface” *Langmuir* 2014, 30 (44) 13255–13265.

2. **Hadi. H. Arefi** and Giorgos Fagas, “Chemical Trends in the Work Function of Modified Si(111) Surfaces: A DFT Study” *J. Phys. Chem. C* 2014, 118 (26), 14346-14354.

3. **Hadi. H. Arefi**, Michael Nolan and Giorgos Fagas, “Role of the Head- and/or Tail Groups of Adsorbed  $-[X^{(\text{head-group})}]\text{-Alkyl-}[X^{(\text{tail-group})}]$  ( $X = \text{O(H)}, \text{NH}_2, \text{S(H)}$ ) Chains on Controlling the Workfunction of Functionalized H:Si(111) Surface” 2014. Submitted to *J. Phys. Chem. C* for review.

4. Dimpay Sharma, **Hadi. H. Arefi** and Giorgos Fagas, “Atomic Basis Sets for First-Principles Studies of Si Nanowires” *Comp. Theor. Chem.* 2012, 991, 32-39.

5. **Hadi. H. Arefi**, Michael Nolan and Giorgos Fagas, “Binary Functionalization of H:Si(111) by Adsorption of Short Alkyl Chains in a Hybrid Organic-Semiconductor Structure: Toward Extra Tuning, Stability and Dense Packing” (In Preparation).



# Conferences and Workshops

1. Hadi H. Arefi and Giorgos Fagas “A Density Functional Theory study of functionalized silicon surfaces.” *Toward Reality in Nanoscale Materials*, 20-22 Feb 2012, Levi, Finland. (Poster)
2. Hadi H. Arefi and Giorgos Fagas “Tuning the Work Function of Functionalized Si(111) for Low-Power Electronics.” NANOENERGY 2013, 10-13 July 2013, Perugia, Italy. (Poster)
3. Hadi H. Arefi and Giorgos Fagas “Tuning the Work Function of Functionalized Si Nanowires.” ICON 2013, 23-26 Sept 2013, Annecy, France. (Poster)

## Attended Schools/Workshops

1. ZEROPOWER Workshop: *Nanoscale Materials for Energy-Efficient Electronics*, 25-27 October 2011, Cork, Ireland.
2. *Toward Reality in Nanoscale Materials workshop*, 20th-22nd February 2012, Levi, Finland.
3. CECAM Tutorial: *GW Quasiparticle Calculations in Condensed Matter Physics and Nanoscience*, 16-20 April 2012, Lausanne, Switzerland.
4. The 6<sup>th</sup> Windsor Summer School on Condensed Matter Theory: *Low-Dimensional Materials, Strong Correlation and Quantum Technologies*, 12-26 August 2012, Windsor, UK.
5. NiPS Summer School 2013: *Energy Management at Micro and Nanoscale*, 8-10 July 2013, Perugia, Italy.

# Declaration

I, Hadi Hassanian Arefi, certify that this thesis is my own work and I have not obtained a degree in this university or elsewhere on the basis of the work submitted in this thesis.

*Hadi Hassanian Arefi*

## Table of Contents

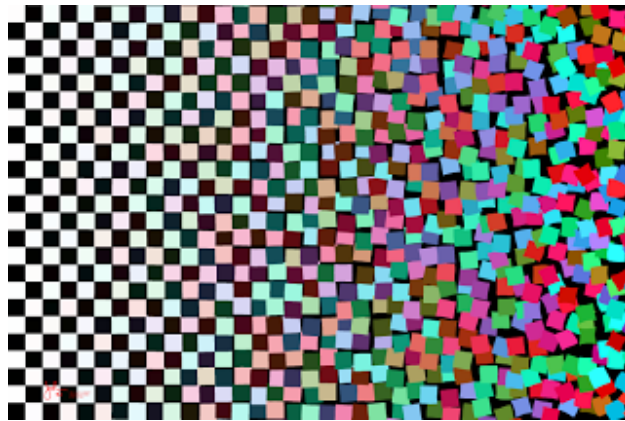
Chapter 1 .....	1
Introduction .....	1
1.1 Motivation .....	1
1.2 My thesis - Understand the interface, control the device .....	4
1.3 An overview of previous studies .....	8
1.3.1 Metallic versus semiconductor surfaces .....	8
1.3.2 Pi-conjugated versus aliphatic self-assembled monolayers .....	9
1.3.3 Head-group and/or Tail-group linkers .....	10
1.4 Thesis overview .....	10
1.5 References .....	12
Chapter 2 .....	17
Background and Methodologies .....	17
2.1 Introduction .....	17
2.1.1 Materials modelling from first-principles .....	17
2.1.2 The many-body problem of electrons around nuclei .....	19
2.2 Density Functional Theory .....	21
2.2.1 Fundamentals .....	21
2.2.2 DFT as an effective single-body theory .....	23
2.3 A practitioner's guide to performing a DFT calculation .....	25
2.3.1 Basis functions .....	26
2.3.2 Pseudopotential .....	28
2.3.3 The Exchange-Correlation term .....	29
2.4 Local functionals: LDA & GGA .....	31
2.5 van der Waals interactions .....	34
2.5.1 van der Waals interactions in DFT .....	36
2.5.2 Higher-accuracy van der Waals density functional .....	36
2.6 Computational package .....	37
2.6.1 Quantum Espresso .....	38
2.7 References .....	39
Chapter 3 .....	41
Chemical Trends in the Work Function of Modified Si(111) Surfaces: A DFT Study .....	41
3.1 Introduction .....	41
3.2 Background and methodology .....	43

3.2.1 Work function calculation from first-principles .....	46
3.3 Results and discussion .....	49
3.3.1 Halogens.....	49
3.3.2 Chalcogens .....	53
3.3.3 Second period.....	56
3.3.4 Comparison with experiment.....	58
3.4 Concluding remarks .....	60
3.5 References .....	62
Chapter 4 .....	65
Density Functional Theory with van der Waals Corrections Study of the Adsorption of Alkyl, Alkylthiol, Alkoxy, and Amino-Alkyl Chains on the H:Si(111) Surface.....	65
4.1. Introduction.....	65
4.2. Computational details.....	70
4.3. Results and discussion .....	73
4.3.1 Adsorption energies and structures with and without the van der Waals correction.....	73
4.3.2 Adsorption energies and structures of H-(X)-alkyl chains at the H:Si(111) surface (X = NH, O, S) .....	76
4.4 Concluding remarks .....	92
4.5 References .....	93
Chapter 5 .....	97
Role of the Head- and/or Tail-groups on Controlling the Work Function of SAM-Functionalized H:Si(111) Surface.....	97
5.1 Introduction .....	97
5.2 Computational Details.....	98
5.3 Results and Discussion.....	99
5.3.1 <i>The effect of the Head-Group on the alkyl- and (O, S, NH)-alkyl-         modified H:Si(111) work function.....</i>	100
5.3.2 <i>The effect of the Tail-Group on the alkyl-modified H:Si(111) work         function.....</i>	103
5.3.3 <i>The effect of the Head- and Tail-Groups [-NH-C<sub>n</sub>H<sub>2n</sub>-NH<sub>2</sub>] on the         alkyl-modified H:Si(111) work function.....</i>	108
5.3.4 <i>Comparison with experiment .....</i>	112
5.4. Concluding remarks .....	113
5.5. References .....	114

Chapter 6 .....	119
Binary Functionalization.....	119
6.1 Introduction .....	119
6.1.1 Motivation for binary functionalization .....	121
6.1.2 Our approach.....	127
6.2 Results and discussion .....	129
6.2.1 Binary functionalization at fixed coverage—Tuning the WF.....	129
6.2.2 Binary functionalization for different coverage—Stability and packing .....	133
6.3 Concluding remarks and future outlook.....	136
6.4 References .....	138
Chapter 7 .....	144
Final Remarks and Perspectives.....	144
7.1 Summary of results and conclusion .....	144
7.2 Future perspectives.....	149

# Chapter 1

## Introduction



### 1.1 Motivation

Remarkable enhancement in functionality and/or cost appears most often when new materials are incorporated into existing technologies. For example, after years of research on materials compatibility replacing copper by aluminum in integrated circuits resulted in huge reduction of interconnect delay times and reliability improvement. Apart from significant impact on current devices newly identified materials can unveil novel technologies and applications. For their unique physical/chemical properties and ubiquitous electrical, optical and environmental applications, Field-Effect-based electronic, optoelectronic and biochemical *hybrid* devices are at the center of attention of many scientific communities and industrial technologies. These hybrid devices are conceptually

based on using molecular functionality to interface with traditional devices made of inorganic materials and modify the features (performance and functionality) of the target electronic devices.

Organic–inorganic hybrid materials represent a new class of materials which are able to combine desirable characteristics of both organic and inorganic building blocks within one combined system. While inorganic materials offer wide range of electronic properties (enabling the design of insulators, semiconductors, and metals), magnetic and dielectric transitions, substantial mechanical hardness, and thermal stability, on the other hand, organic molecules can provide high fluorescence efficiency, large polarizability, plastic mechanical properties, ease of processing, and structural diversity. Adjusting the electronic structure of materials within the nanometre scale can offer unique and potentially higher level of tunability of electronic and optical properties in hybrid materials that cannot be achieved separately from each of their organic and inorganic components.

Properties of materials such as metals or inorganic semiconductors are determined by their atomic structures. Since the final structure depends on total energetics and cannot be changed without a phase transition, manipulating materials properties is possible within certain boundaries, e.g., via doping and nanofabrication or by applying pressure and other external fields. An exciting option to consider is elevating the control over a solid's surface to design materials and devices (based on interfaces) with desired features. Chemisorbed self-assembled organic monolayers on metal or semiconductor substrates can hinge the organic world to inorganic surfaces and create such a hybrid system (Figure 1.1).

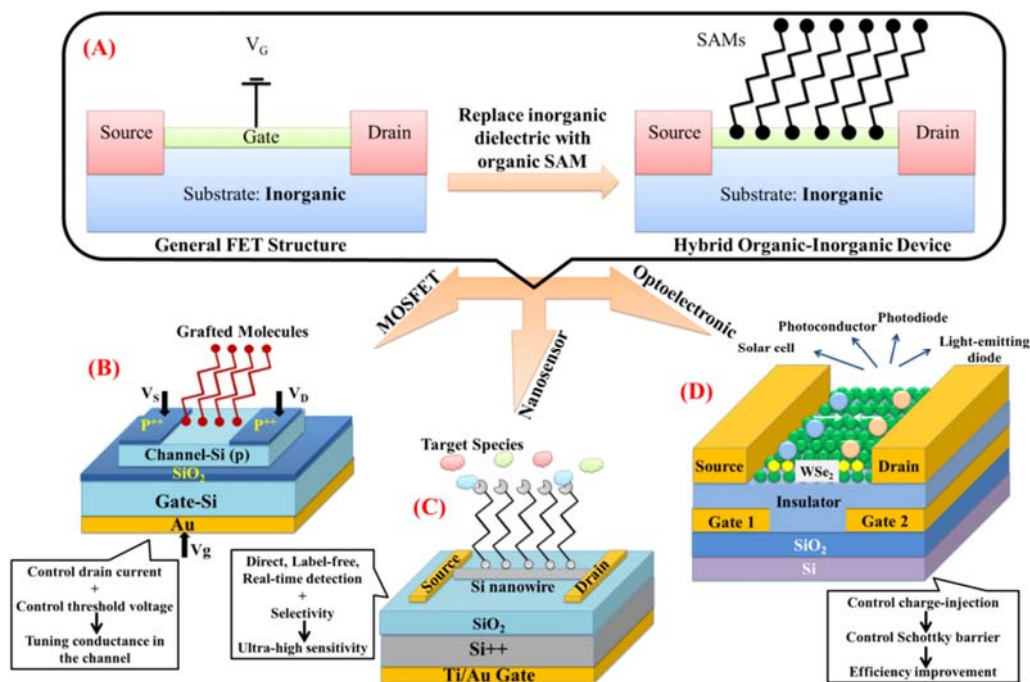


Figure 1.1. (A) Conceptual representation of an organic-inorganic hybrid device; General structure of a traditional Field-Effect-Transistor (FET) is shown on the left. Combining inorganic dielectric with organic self-assembled monolayers (SAMs) is an enabler for increased performance and added functionality to the device (on the right). (B) Schematic side-view representation of a typical MOSFET (metal-oxide-semiconductor field-effect-transistor) device with grafted molecules between source and drain electrodes.  $V_s$ ,  $V_D$ , and  $V_g$  refer to the bias applied on the source, drain, and gate, respectively.<sup>1</sup> (C) Scheme of a molecularly modified SiNW FET (silicon nanowire field-effect-transistor) sensor.<sup>2</sup> (D) Schematic drawing of a lateral monolayer WSe<sub>2</sub> p-n diode with split-gate electrodes. The metal back gates are separated from the WSe<sub>2</sub> monolayer by an insulator, which can be SiN, HfO<sub>2</sub> or BN. Blue and orange spheres represent electrons and holes, respectively.<sup>3</sup>

Molecular structures on metals or semiconductors provide the possibility to benefit from the combined properties of solids (e.g., good electrical conductivity) and molecules (e.g., tuneable photon absorption). Covalent attachment between inorganic surfaces and organic monolayers is a unique path to achieve both surface passivation and induce any sort of bio- and/or chemical functionality into the device. Organic molecules with their numerous and adjustable properties, including size, shape, absorption spectrum, flexibility,



chemical affinity, and conductivity, offer a variety of possibilities to either tune the performance of a device or add new characteristics.

## **1.2 My thesis - Understand the interface, control the device**

To realize this potential in applications, understanding and customized control of the electronic structures of device surfaces via chemical modifications is fundamental. As a scaffold in hybrid electronic devices, semiconductor surfaces have been a leading candidate. Modifying such surfaces offers a wide range of possibilities for tuning device functionality and enhancing performance.<sup>4-5</sup> For example, organosilane SAMs with different end groups grafted on SiO<sub>2</sub> gate insulators cause different monolayer thicknesses and angles, which can be used to tune the mobility of the organic thin-film transistors as well as the threshold voltage (Figure 1.2).<sup>6</sup> Also current-voltage measurements of Schottky diodes composed of p-doped silicon wafers functionalized with different length alkyl chains [Si-C<sub>n</sub>H<sub>2n+1</sub> (n = 10, 12, 16, 22)] shows that the effective barrier height ( $q\phi_{\text{eff}}$ ) of the Schottky diodes is a function of monolayer thickness.<sup>7</sup>

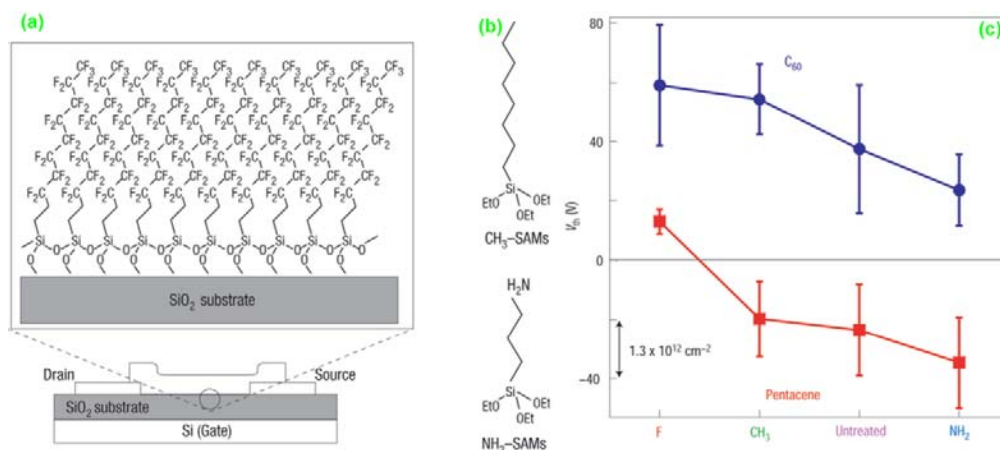


Figure 1.2. (a) Illustration of organic thin-film transistors (TFTs) with F-SAMs on a SiO<sub>2</sub> gate insulator. C<sub>60</sub> and pentacene were deposited on the surface of this monolayer. (b) Used different SAM molecules. (c) Summary of the threshold voltage ( $V_{th}$ ) in n-type C<sub>60</sub> and p-type pentacene TFT devices for different SiO<sub>2</sub> treatments, untreated and with three kinds of SAMs.<sup>6</sup>

One of the key parameters that determine the threshold voltage in a field effect transistor (FET) is the work function (WF) of the gate contact materials,<sup>8</sup> whereas, surface reactivity and interface charge reorganization have a significant effect on the sensitivity of biosensors (Figure 1.3).<sup>9-13</sup> The band edge profile at the surface also plays an important role in nanoscale optoelectronic devices (e.g. in schottky barrier tuning), light absorption and emission due to the strong dependence on electron affinity (EA) and ionization potential (IP).<sup>14</sup> The type of chemical termination and its structural characteristics are primarily responsible for the charge reorganization at the interface and its significant effect on key device parameters.<sup>1,2</sup> Structural properties include termination type, monolayer thickness, angle *etc.* and a better microscopic understanding of these properties is required before addressing the electrical characteristics of an interface.

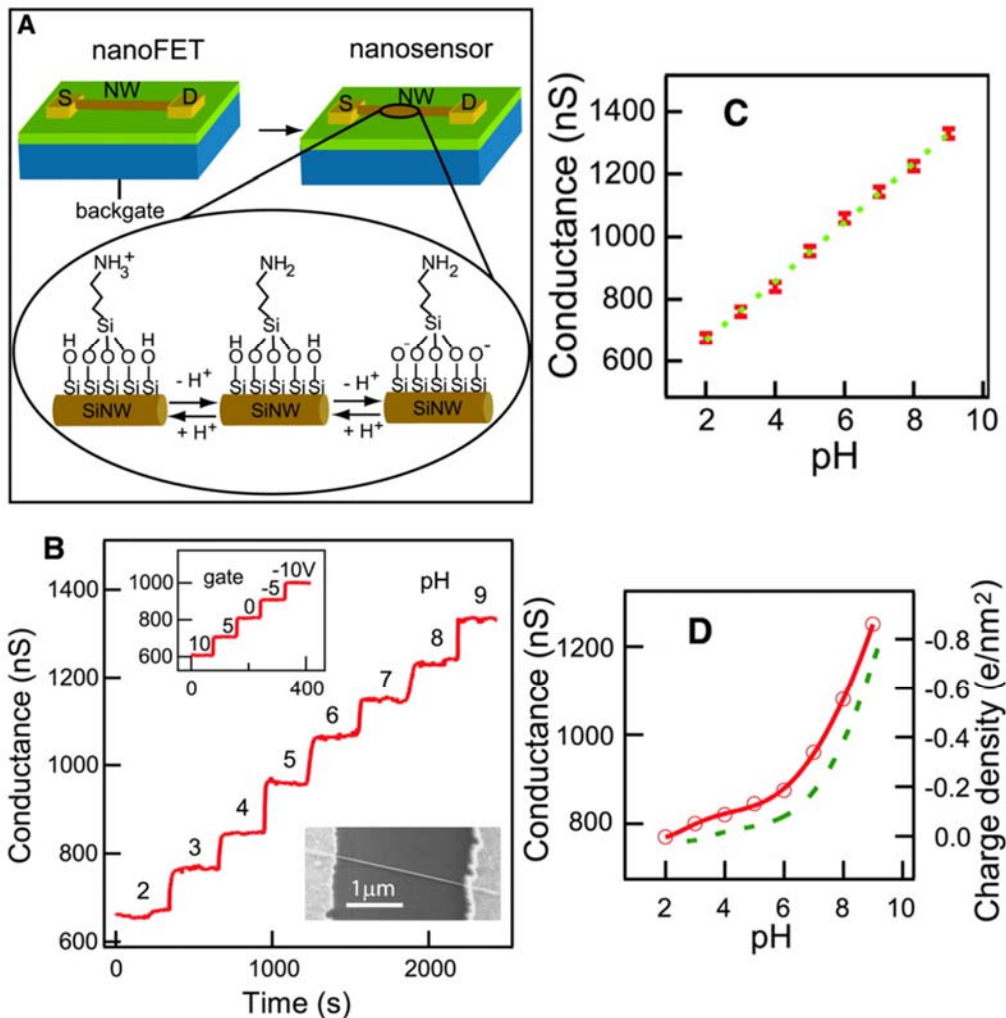


Figure 1.3. Nanowire (NW) nanosensor for pH detection. (A) Schematic illustrating the FET-based NW nanosensors for pH sensing. (B) Real-time detection of the conductance for 3-aminopropyltriethoxysilane (APTES)-modified SiNW for pHs from 2 to 9. (C) Plot of the conductance versus pH; the red points are experimental data, and the dashed green line is linear fit through this data. (D) The conductance of unmodified SiNW (red) versus pH.<sup>10</sup>

Silicon is the most widely used material in the electronics industry. There are an increasing number of applications, including hybrid electronics or sensors, where hybrid organic semiconductor structures assembled by grafting organic monolayers onto Si play a dominant role.<sup>11, 15-18</sup> Key to these applications is finding suitable combinations of organics<sup>5</sup> with Si that will display the desired electronic properties and this has limited their potential to date. Grafted SAMs of

organic molecules onto Si surfaces can modify the interfacial structure and tune the electronic properties,<sup>1, 19-20</sup> in particular the WF.<sup>21-24</sup>

Studies of the surface work function offer significant information towards a microscopic understanding of the changes at interfaces. The work function is sensitive to surface chemistry and morphology, providing valuable insights to surface interactions and the reorganization of electronic charges caused by surface modifications.<sup>25</sup> The WF tuning allows control over the charge injection<sup>26</sup> and Schottky energy barrier<sup>27</sup> in solar cells<sup>28</sup> and light emitting diodes,<sup>29</sup> the threshold voltage in a FET transistor<sup>30</sup> or the sensitivity in a biosensor<sup>9-10, 31</sup> constructed from these organic-semiconductor assemblies.

In fact, interactions of atoms and molecules with metal surfaces and their effect on the work function have been at the center of attention for many years. However, there is still no comprehensive analysis which can explain and anticipate the work function variations due to different functionalization schemes on semiconductors. This is despite several experimental studies and the importance of interface engineering. From the theory perspective, multiple dipole decomposition analysis, charge re-organization at the interface and polarization due to different dipoles, electrostatic potential shift and levels alignment between Fermi level and SAMs states have been investigated.<sup>25, 28-29, 31, 33, 36-37, 47</sup> However, as explained below further understanding of this mechanism in semiconductors is important in enabling the use of these structures in the aforementioned applications. This is exactly the topic of this Thesis. Taking a small step, we address functionalized silicon surfaces from microscopic principles and focus on the analysis of their electronic, (predominantly the work function) and structural properties.

## 1.3 An overview of previous studies

### 1.3.1 Metallic versus semiconductor surfaces

The underlying microscopic mechanism of WF tuning has been explored comprehensively for various metallic substrates such as gold<sup>32-46</sup>, silver<sup>28-29, 35-36</sup> and copper<sup>45, 47-49</sup> functionalized with different monolayers that are primarily aromatic compounds<sup>33-34, 38, 41-42, 45, 50</sup> and alkyl chains with different head and/or tail-groups.<sup>35, 37, 39-40, 43-44</sup> Despite several studies<sup>4, 7, 21-22, 51</sup> semiconductor surfaces such as silicon have not received significant attention in this regard. Silicon is still the most technologically important material in the electronic industry due to its versatile properties: high mobility, low band gap, easy doping and optical activity in visible, ultraviolet and infrared range. In this area, alkyl monolayers with sulfur and oxygen head groups on Si have been studied with regard to WF tuning.<sup>22</sup> The WF tuning mechanism for metals is examined using approaches including Kelvin-probe measurements<sup>32, 50, 52</sup> and photoelectron spectroscopy.<sup>41, 43, 53</sup>

Despite extensive study of metal substrates for functionalization purposes, semiconductor surfaces, which are fundamentally different, have not been given enough attention. The much larger screening length in semiconductor surfaces than metal surfaces creates an extended space charge layer.<sup>54</sup> Unlike with metal substrates, the band edge demonstrates a richer behavior and band bending can be modified by the molecule that is attached to the semiconductor surface.<sup>51, 55-57</sup> As a result the WF can vary significantly from linker to linker, and this tuneability is of course very important for electronic device applications.

In fact if we separate the WF change at the (metal/semiconductor)-organic interface into two contributions, one from the intrinsic SAM dipole and the other from the bond dipole at the Metal-SAM or semiconductor-SAM junction, the former is independent of the substrate, but the latter is directly influenced by the chemistry of the surface. It has been shown that most SAMs create covalent bonds with semiconductors,<sup>58-59</sup> whereas in the case of metals the bond is weaker than a covalent bond but stronger than van der Waals bonding.<sup>60-61</sup> In the case of

silicon and gold substrates, this comparison is very trivial as Si-(S, C, O, N) bonds are all covalent so the created SAMs are immobile. However due to the weaker Au-S bond, thiolated-SAMs on gold are able to move from one site to another even at room temperature.<sup>25</sup> This indicates that in semiconductors, the bond dipole is the key parameter for the magnitude of the WF change. However for gold, the intrinsic dipole of the SAM (by creating an image charge) dominates.

It must also be mentioned that even the intrinsic dipole of a SAM is not the same for different substrates as it is very much dependent on the geometry of the SAMs, which is primarily determined by the nature of the bond between the SAM and substrate. Therefore there is some competition between the intrinsic dipole and the SAM bonding to the substrate that can give the same WF change for two different materials (metal and semiconductor) functionalized with the same type of SAMs. However, the underlying mechanisms can be different. Therefore there is a need to examine the SAM-semiconductor systems in detail as the mechanisms developed for SAM-metal systems may not necessarily be determining the WF in the SAM-semiconductor systems.

### **1.3.2 Pi-conjugated versus aliphatic self-assembled monolayers**

Although the WF of metal functionalized surfaces with thiolated pi-conjugated SAMs has been extensively studied, semiconductor surfaces functionalized with aliphatic alkyl chains are fundamentally different. Moreover, the SAMs of aliphatic chains that we investigate are dielectric in nature, due to the very large gap between the highest occupied molecular orbital and the lowest unoccupied molecular orbital.<sup>62</sup> The aromatic SAMs have delocalized orbitals allowing electron movement which, compared to the more localized orbitals in aliphatic SAMs, increases the possibility of instantaneous dipole formation. Regarding the previous discussion on substrate materials, this can affect the bond stability via charge injection at the interface and consequently the WF change mechanism.

This is not the case for semiconductor surfaces as they can create strong covalent bonds with various linkers (C, O, S, N etc.), thereby offering more flexibility.<sup>63</sup>

### **1.3.3 Head-group and/or Tail-group linkers**

Although some studies have highlighted that the interfacial bonding between the Si surface and the organic chain is chiefly responsible for the alteration of the interface electronic properties,<sup>22, 51</sup> these studies have primarily focussed on alkyl chains linked to the surface by carbon (Si-C).<sup>4, 7, 64-65</sup> There are a few studies of alkyl chain modified Si in the literature,<sup>11</sup> in which Si was modified with an alkyl chain with 10 and 18 carbons, linked to Si by C, O, S and the electronic structure was examined experimentally through different spectroscopic techniques, including X-ray and ultraviolet photoemission spectroscopy and this showed changes in the WF, compared to unmodified Si, of up to  $\sim 0.4$  eV. In the metal functionalized surfaces the focus is on the SAM attachment via thiolated bonds. The modification of Si with alkyl chains that have different chain lengths, other linker (head)-groups such as nitrogen or oxygen and terminating (tail) groups such as  $-NH_2$  or  $-SH$  has not been studied with respect to electronic properties. This is an area of great interest because surface tuning by chemistry variation (head-or tail groups) is an attractive approach to modify the interface electronic structure.<sup>66-69</sup> Since sulfur and nitrogen radicals are very often used for different purposes in SAM technology such as creating fibre surfaces either for analyte interaction or further modification,<sup>70-78</sup> it is therefore imperative to know how the modification of Si with alkyl chains with different head- and/or tail-groups as well as different alkyl chain lengths can be used to modify the WF of Si in a well understood manner.

## **1.4 Thesis overview**

The work of this Thesis is structured as follows:

- In the second Chapter, the methodological background applied through this study is explained along with a brief introduction to the computational methods and packages that have been employed.
- In Chapter 3, we study the effect of different terminations on the electronic structure of a hydrogenated silicon surface. We identify the basic chemical trends for a selection of polar and non-polar species. For non-polar terminations the WF change is directly proportional to the amount of charge transfer and therefore the electronegativity of the attached species and is a monotonic function of the coverage. However, polar molecules do not follow this trend and the radical dipole as well as linker electronegativity must be considered at the same time to interpret the WF changes.
- In the fourth Chapter, focusing on the structural properties we expand our study to functionalized silicon surfaces with alkyl monolayers of different length and coverage, and investigate various head-groups. We find that including vdW interaction is absolutely necessary as chain-chain interactions can effectively change the obtained structural and electronic results. Applying different head-groups can change the stability of the monolayer. Oxygen delivers the most stable monolayer followed by sulfur, nitrogen and carbon itself and this is independent of the chain length. Apart from sulfur, structural properties are converged for chains longer than three carbons. Adding linkers can enhance the coverage up to 75% however the stability ordering seems independent.
- With the insights from chapters three and four, in Chapter 5 we study functionalized silicon surfaces at fixed coverage with various combinations of (head-group)-alkyl-(tail-group) linker chains. Depending on implement only head-group, only tail-group or both, we observe different dependence of WF on chain length. An oscillatory behavior in the WF is identified when tail-group is used. For chains only with head-group, the oscillations are less significant especially for chains



longer than eight carbons. Depending on the type of head- and/or tail-groups the WF swings for odd and even number of carbons can vary significantly. The oscillations are explained in terms of variation of terminal-group dipole angle with respect to surface normal.

- In Chapter 6, we study a more complex case of binary functionalized silicon surfaces for both fixed and varying ratio of the components, drawing attention to the structural stability and coverage enhancement. We find that mixed surface functionalization obtains a WF which is within the interval of each linker's WF. Control over the ratio of individual linkers can increase the tuning. In the case of alkyl monolayer functionalization, adding a monolayer with either oxygen or nitrogen can enhance the stability and improve the coverage. The results still indicate that full coverage of alkyl monolayers for chains longer than six carbons is not possible.
- The recap of the overall results and perspective on future work in the context of this study are presented in the final Chapter 7.

## 1.5 References

1. He, T.; He, J.; Lu, M.; Chen, B.; Pang, H.; Reus, W. F.; Nolte, W. M.; Nackashi, D. P.; Franzon, P. D.; Tour, J. M., Controlled modulation of conductance in silicon devices by molecular monolayers. *J. Am. Chem. Soc.* **2006**, *128*, 14537-14541.
2. Wang, B.; Cancilla, J. C.; Torrecilla, J. S.; Haick, H., Artificial sensing intelligence with silicon nanowires for ultrasensitive detection in the gas phase. *Nano Lett.* **2014**, *14*, 933-8.
3. Bratschitsch, R., Optoelectronic devices: Monolayer diodes light up. *Nat. Nano* **2014**, *9*, 247-248.
4. Lavi, A.; Cohen, H.; Bendikov, T.; Vilan, A.; Cahen, D., Si-C-bound alkyl chains on oxide-free Si: towards versatile solution preparation of electronic transport quality monolayers. *Phys. Chem. Chem. Phys.* **2011**, *13*, 1293-1296.
5. Koch, N., Organic electronic devices and their functional interfaces. *ChemPhysChem* **2007**, *8*, 1438-1455.
6. Kobayashi, S.; Nishikawa, T.; Takenobu, T.; Mori, S.; Shimoda, T.; Mitani, T.; Shimotani, H.; Yoshimoto, N.; Ogawa, S.; Iwasa, Y., Control of carrier density by self-assembled monolayers in organic field-effect transistors. *Nat. Mater.* **2004**, *3*, 317-322.

7. Faber, E. J.; de Smet, L. C.; Olthuis, W.; Zuilhof, H.; Sudholter, E. J.; Bergveld, P.; van den Berg, A., Si-C linked organic monolayers on crystalline silicon surfaces as alternative gate insulators. *ChemPhysChem* **2005**, *6*, 2153-2166.
8. Ashkenasy, G.; Cahen, D.; Cohen, R.; Shanzer, A.; Vilan, A., Molecular Engineering of Semiconductor Surfaces and Devices. *Acc. Chem. Res.* **2002**, *35*, 121-128.
9. Nair, P. R.; Alam, M. A., Screening-limited response of nanobiosensors. *Nano Lett.* **2008**, *8*, 1281-1285.
10. Cui, Y.; Wei, Q.; Park, H.; Lieber, C. M., Nanowire nanosensors for highly sensitive and selective detection of biological and chemical species. *Science* **2001**, *293*, 1289-1292.
11. Patolsky, F.; Lieber, C., Nanowire nanosensors. *Mater. Today* **2005**, *8*, 20-28.
12. Patolsky, F.; Zheng, G.; Lieber, C. M., Nanowire-based biosensors. *Anal. Chem.* **2006**, *78*, 4260-9.
13. Nair, P. R.; Alam, M. A., Design considerations of silicon nanowire biosensors. *IEEE Trans. Electron Devices* **2007**, *54*, 3400-3408.
14. Shirota, Y., Organic materials for electronic and optoelectronic devices. *J. Mater. Chem.* **2000**, *10*, 1-25.
15. Hahn, J.-i.; Lieber, C. M., Direct ultrasensitive electrical detection of DNA and DNA sequence variations using nanowire nanosensors. *Nano Lett.* **2004**, *4*, 51-54.
16. Haick, H.; Hurley, P. T.; Hochbaum, A. I.; Yang, P.; Lewis, N. S., Electrical characteristics and chemical stability of non-oxidized, methyl-terminated silicon nanowires. *J. Am. Chem. Soc.* **2006**, *128*, 8990-8991.
17. Cattani-Scholz, A.; Pedone, D.; Dubey, M.; Neppl, S.; Nickel, B.; Feulner, P.; Schwartz, J.; Abstreiter, G.; Tornow, M., Organophosphonate-based PNA-functionalization of silicon nanowires for label-free DNA detection. *ACS Nano* **2008**, *2*, 1653-1660.
18. Shen, X.; Sun, B.; Yan, F.; Zhao, J.; Zhang, F.; Wang, S.; Zhu, X.; Lee, S., High-performance photoelectrochemical cells from ionic liquid electrolyte in methyl-terminated silicon nanowire arrays. *ACS Nano* **2010**, *4*, 5869-5876.
19. Segev, L.; Salomon, A.; Natan, A.; Cahen, D.; Kronik, L.; Amy, F.; Chan, C. K.; Kahn, A., Electronic structure of Si(111)-bound alkyl monolayers: Theory and experiment. *Phys. Rev. B* **2006**, *74*, 165323-6.
20. Yu, H. B.; Webb, L. J.; Heath, J. R.; Lewis, N. S., Scanning tunneling spectroscopy of methyl- and ethyl-terminated Si(111) surfaces. *Appl. Phys. Lett.* **2006**, *88*, 252111-252111.
21. Jaeckel, B.; Hunger, R.; Webb, L. J.; Jaegermann, W.; Lewis, N. S., High-resolution synchrotron photoemission studies of the electronic structure and thermal stability of CH<sub>3</sub>- and C<sub>2</sub>H<sub>5</sub>-functionalized Si(111) surfaces. *J. Phys. Chem. C* **2007**, *111*, 18204-18213.
22. Hacker, C. A., Modifying electronic properties at the silicon–molecule interface using atomic tethers. *Solid-State Electron.* **2010**, *54*, 1657-1664.
23. Cooper, A. J.; Keyvanfar, K.; Deberardinis, A.; Pu, L.; Bean, J. C., Dopant passivation and work function tuning through attachment of heterogeneous organic monolayers on silicon in ultrahigh vacuum. *Appl. Surf. Sci.* **2011**, *257*, 6138-6144.
24. Kuo, C. H.; Liu, C. P.; Lee, S. H.; Chang, H. Y.; Lin, W. C.; You, Y. W.; Liao, H. Y.; Shyue, J. J., Effect of surface chemical composition on the work function of silicon substrates modified by binary self-assembled monolayers. *Phys. Chem. Chem. Phys.* **2011**, *13*, 15122-15126.
25. Ulman, A., Formation and Structure of Self-Assembled Monolayers. *Chem. Rev.* **1996**, *96*, 1533-1554.

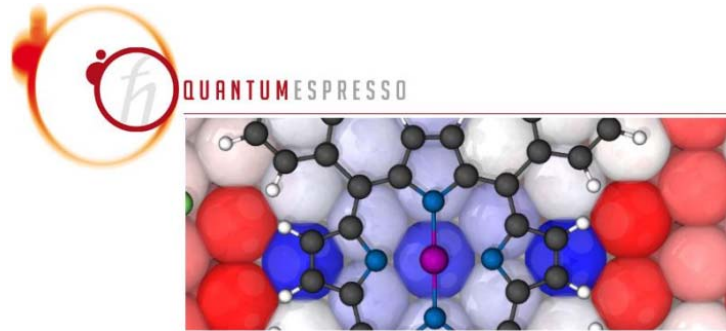
26. Greiner, M. T.; Helander, M. G.; Tang, W.-M.; Wang, Z.-B.; Qiu, J.; Lu, Z.-H., Universal energy-level alignment of molecules on metal oxides. *Nat. Mater.* **2012**, *11*, 76-81.
27. Campbell, I. H.; Rubin, S.; Zawodzinski, T. A.; Kress, J. D.; Martin, R. L.; Smith, D. L.; Barashkov, N. N.; Ferraris, J. P., Controlling Schottky energy barriers in organic electronic devices using self-assembled monolayers. *Phys. Rev. B* **1996**, *54*, 14321-14324.
28. Nattestad, A.; Mozer, A. J.; Fischer, M. K.; Cheng, Y. B.; Mishra, A.; Bauerle, P.; Bach, U., Highly efficient photocathodes for dye-sensitized tandem solar cells. *Nat. Mater.* **2010**, *9*, 31-35.
29. Kabra, D.; Lu, L. P.; Song, M. H.; Snaith, H. J.; Friend, R. H., Efficient single-layer polymer light-emitting diodes. *Adv. Mater.* **2010**, *22*, 3194-3198.
30. Li, T.; Balk, J. W.; Ruden, P. P.; Campbell, I. H.; Smith, D. L., Channel formation in organic field-effect transistors. *J. Appl. Phys.* **2002**, *91*, 4312-4318.
31. Buitrago, E.; Fagas, G.; Badia, M. F. B.; Georgiev, Y. M.; Berthome, M.; Ionescu, A. M., Junctionless silicon nanowire transistors for the tunable operation of a highly sensitive, low power sensor. *Sensor Actuat. B-Chem.* **2013**, *183*, 1-10.
32. Evans, S. D.; Ulman, A., Surface potential studies of alkyl-thiol monolayers adsorbed on gold. *Chem. Phys. Lett.* **1990**, *170*, 462-466.
33. Evans, S. D.; Urankar, E.; Ulman, A.; Ferris, N., Self-assembled monolayers of alkanethiols containing a polar aromatic group: Effects of the dipole position on molecular packing, orientation, and surface wetting properties. *J. Am. Chem. Soc.* **1991**, *113*, 4121-4131.
34. Romaner, L.; Heimel, G.; Zojer, E., Electronic structure of thiol-bonded self-assembled monolayers: Impact of coverage. *Phys. Rev. B* **2008**, *77*, 045113-9.
35. Alloway, D. M.; Hofmann, M.; Smith, D. L.; Gruhn, N. E.; Graham, A. L.; Colorado, R.; Wysocki, V. H.; Lee, T. R.; Lee, P. A.; Armstrong, N. R., Interface dipoles arising from self-assembled monolayers on gold: UV-photoemission studies of alkanethiols and partially fluorinated alkanethiols. *J. Phys. Chem. B* **2003**, *107*, 11690-11699.
36. Rusu, P. C.; Brocks, G., Surface dipoles and work functions of alkylthiolates and fluorinated alkylthiolates on Au(111). *J. Phys. Chem. B* **2006**, *110*, 22628-22634.
37. Rusu, P. C.; Brocks, G., Work functions of self-assembled monolayers on metal surfaces by first-principles calculations. *Phys. Rev. B* **2006**, *74*, 073414-4.
38. Heimel, G.; Romaner, L.; Zojer, E.; Bredas, J. L., Toward control of the metal-organic interfacial electronic structure in molecular electronics: A first-principles study on self-assembled monolayers of pi-conjugated molecules on noble metals. *Nano Lett.* **2007**, *7*, 932-940.
39. Sushko, M. L.; Shluger, A. L., Dipole-dipole interactions and the structure of self-assembled monolayers. *J. Phys. Chem. B* **2007**, *111*, 4019-4025.
40. Sushko, M. L.; Shluger, A. L., Intramolecular dipole coupling and depolarization in self-assembled monolayers. *Adv. Funct. Mater.* **2008**, *18*, 2228-2236.
41. Bröker, B.; Blum, R. P.; Frisch, J.; Vollmer, A.; Hofmann, O. T.; Rieger, R.; Müllen, K.; Rabe, J. P.; Zojer, E.; Koch, N., Gold work function reduction by 2.2eV with an air-stable molecular donor layer. *Appl. Phys. Lett.* **2008**, *93*, 243303-3.
42. Heimel, G.; Romaner, L.; Zojer, E.; Bredas, J. L., The interface energetics of self-assembled monolayers on metals. *Acc. Chem. Res.* **2008**, *41*, 721-729.
43. Ge, Y.; Weidner, T.; Ahn, H.; Whitten, J. E.; Zharnikov, M., Energy level pinning in self-assembled alkanethiol monolayers. *J. Phys. Chem. C* **2009**, *113*, 4575-4583.

44. Alloway, D. M.; Graham, A. L.; Yang, X.; Mudalige, A.; Colorado, R.; Wysocki, V. H.; Pemberton, J. E.; Lee, T. R.; Wysocki, R. J.; Armstrong, N. R., Tuning the effective work function of gold and silver using omega-functionalized alkanethiols: Varying surface composition through dilution and choice of terminal groups. *J. Phys. Chem. C* **2009**, *113*, 20328-20334.
45. Hofmann, O. T.; Egger, D. A.; Zojer, E., Work-function modification beyond pinning: When do molecular dipoles count? *Nano Lett.* **2010**, *10*, 4369-4374.
46. Heimel, G.; Rissner, F.; Zojer, E., Modeling the electronic properties of pi-conjugated self-assembled monolayers. *Adv. Mater.* **2010**, *22*, 2494-2513.
47. Kondoh, H.; Saito, N.; Matsui, F.; Yokoyama, T.; Ohta, T.; Kuroda, H., Structure of alkanethiolate monolayers on Cu(100): Self-assembly on the four-fold-symmetry surface. *J. Phys. Chem. B* **2001**, *105*, 12870-12878.
48. Laibinis, P. E.; Whitesides, G. M.; Allara, D. L.; Tao, Y. T.; Parikh, A. N.; Nuzzo, R. G., Comparison of the structures and wetting properties of self-assembled monolayers of n-alkanethiols on the coinage metal surfaces, copper, silver, and gold. *J. Am. Chem. Soc.* **1991**, *113*, 7152-7167.
49. Bussolotti, F.; Betti, M.; Mariani, C., Anchoring methane thiol on Cu(100) in different structural configurations: Electronic state dispersion. *Phys. Rev. B* **2006**, *74*, 125422-8.
50. Zehner, R. W.; Parsons, B. F.; Hsung, R. P.; Sita, L. R., Tuning the Work Function of Gold with Self-Assembled Monolayers Derived from X-[C<sub>6</sub>H<sub>4</sub>-C(C)-]nC<sub>6</sub>H<sub>4</sub>-SH (n= 0, 1, 2; X = H, F, CH<sub>3</sub>, CF<sub>3</sub>, and OCH<sub>3</sub>). *Langmuir* **1999**, *15*, 1121-1127.
51. Vilan, A.; Yaffè, O.; Biller, A.; Salomon, A.; Kahn, A.; Cahen, D., Molecules on si: Electronics with chemistry. *Adv. Mater.* **2010**, *22*, 140-159.
52. Lü, J.; Delamarche, E.; Eng, L.; Bennewitz, R.; Meyer, E.; Güntherodt, H. J., Kelvin Probe Force Microscopy on Surfaces: Investigation of the Surface Potential of Self-Assembled Monolayers on Gold. *Langmuir* **1999**, *15*, 8184-8188.
53. De Renzi, V.; Rousseau, R.; Marchetto, D.; Biagi, R.; Scandolo, S.; del Pennino, U., Metal work-function changes induced by organic adsorbates: A combined experimental and theoretical study. *Phys. Rev. Lett.* **2005**, *95*, 046804-4.
54. Lüth, H., *Solid Surfaces, Interfaces and Thin Films*, Fifth ed.; Springer Berlin Heidelberg, 2010.
55. Cahen, D.; Kahn, A., Electron energetics at surfaces and interfaces: Concepts and experiments. *Adv. Mater.* **2003**, *15*, 271-277.
56. Salomon, A.; Boecking, T.; Seitz, O.; Markus, T.; Amy, F.; Chan, C.; Zhao, W.; Cahen, D.; Kahn, A., What is the Barrier for Tunneling Through Alkyl Monolayers? Results from n- and p-Si-Alkyl/Hg Junctions. *Adv. Mater.* **2007**, *19*, 445-450.
57. Zhang, Z.; Yates, J. T., Band Bending in Semiconductors: Chemical and Physical Consequences at Surfaces and Interfaces. *Chem. Rev.* **2012**, *112*, 5520-5551.
58. Ma, Z.; Zaera, F., Organic chemistry on solid surfaces. *Surf. Sci. Rep.* **2006**, *61*, 229-281.
59. Tao, F.; Bernasek, S. L.; Xu, G. Q., Electronic and structural factors in modification and functionalization of clean and passivated semiconductor surfaces with aromatic systems. *Chem. Rev.* **2009**, *109*, 3991-4024.
60. G. A. Somorjai; Y. Li, *Introduction to Surface Chemistry and Catalysis*, 2nd ed.; Wiley: Hoboken, NJ, 2010.
61. G. Ertl, *Reactions at Solid Surface*; Wiley, 2009.
62. Wang, W.; Lee, T.; Reed, M. A., Elastic and Inelastic Electron Tunneling in Alkane Self-Assembled Monolayers. *J. Phys. Chem. B* **2004**, *108*, 18398-18407.

63. DiBenedetto, S. A.; Facchetti, A.; Ratner, M. A.; Marks, T. J., Molecular Self-Assembled Monolayers and Multilayers for Organic and Unconventional Inorganic Thin-Film Transistor Applications. *Adv. Mater.* **2009**, *21*, 1407-1433.
64. Uosaki, K.; Fukumitsu, H.; Masuda, T.; Qu, D., Construction of a metal-organic monolayer-semiconductor junction on a hydrogen-terminated Si(111) surface via Si-C covalent linkage and its electrical properties. *Phys. Chem. Chem. Phys.* **2014**, *16*, 9960-9965.
65. Wong, K. T.; Lewis, N. S., What a difference a bond makes: the structural, chemical, and physical properties of methyl-terminated Si(111) surfaces. *Acc. Chem. Res.* **2014**, *47*, 3037-3044.
66. Vilan, A.; Shanzer, A.; Cahen, D., Molecular control over Au/GaAs diodes. *Nature* **2000**, *404*, 166-168.
67. Selzer, Y.; Cahen, D., Fine tuning of Au/SiO<sub>2</sub>/Si diodes by varying interfacial dipoles using molecular monolayers. *Adv. Mater.* **2001**, *13*, 508-511.
68. Hunger, R.; Jaegermann, W.; Merson, A.; Shapira, Y.; Pettenkofer, C.; Rappich, J., Electronic structure of methoxy-, bromo-, and nitrobenzene grafted onto Si(111). *J. Phys. Chem. B* **2006**, *110*, 15432-15441.
69. He, T.; Ding, H.; Peor, N.; Lu, M.; Corley, D. A.; Chen, B.; Ofir, Y.; Gao, Y.; Yitzchaik, S.; Tour, J. M., Silicon/molecule interfacial electronic modifications. *J. Am. Chem. Soc.* **2008**, *130*, 1699-1710.
70. Wagner, P.; Nock, S.; Spudich, J. A.; Volkmuth, W. D.; Chu, S.; Cicero, R. L.; Wade, C. P.; Linford, M. R.; Chidsey, C. E., Bioreactive self-assembled monolayers on hydrogen-passivated Si(111) as a new class of atomically flat substrates for biological scanning probe microscopy. *J. Struct. Biol.* **1997**, *119*, 189-201.
71. Zhao, Y. D.; Pang, D. W.; Hu, S.; Wang, Z. L.; Cheng, J. K.; Dai, H. P., DNA-modified electrodes; part 4: Optimization of covalent immobilization of DNA on self-assembled monolayers. *Talanta* **1999**, *49*, 751-756.
72. Strother, T.; Cai, W.; Zhao, X. S.; Hamers, R. J.; Smith, L. M., Synthesis and characterization of DNA-modified silicon (111) surfaces. *J. Am. Chem. Soc.* **2000**, *122*, 1205-1209.
73. Frutos, A. G.; Brockman, J. M.; Corn, R. M., Reversible protection and reactive patterning of amine- and hydroxyl-terminated self-assembled monolayers on gold surfaces for the fabrication of biopolymer arrays. *Langmuir* **2000**, *16*, 2192-2197.
74. Yang, Z.; Frey, W.; Oliver, T.; Chilkoti, A., Light-activated affinity micropatterning of proteins on self-assembled monolayers on gold. *Langmuir* **2000**, *16*, 1751-1758.
75. Li, H. L.; Fu, A. P.; Xu, D. S.; Guo, G. L.; Gui, L. L.; Tang, Y. Q., In situ silanization reaction on the surface of freshly prepared porous silicon. *Langmuir* **2002**, *18*, 3198-3202.
76. Harant, A. W.; Khire, V. S.; Thibodaux, M. S.; Bowman, C. N., Thiol-ene photopolymer grafts on functionalized glass and silicon surfaces. *Macromolecules* **2006**, *39*, 1461-1466.
77. Goddard, J. M.; Hotchkiss, J. H., Polymer surface modification for the attachment of bioactive compounds. *Prog. Polym. Sci.* **2007**, *32*, 698-725.
78. Campos, M. A.; Paulusse, J. M.; Zuilhof, H., Functional monolayers on oxide-free silicon surfaces via thiol-ene click chemistry. *Chem. Commun.* **2010**, *46*, 5512-5514.

# Chapter 2

## Background and Methodologies



### 2.1 Introduction

#### 2.1.1 Materials modelling from first-principles

There are many areas within the physical sciences and engineering where the key to scientific and technological progress is understanding and controlling the properties of matter at the level of individual atoms and molecules. This can be provided by the combination of methodological and algorithmic innovations and ever-increasing computer power which is delivering a simulation revolution in materials modelling, starting from the nanoscale up to bulk materials and devices.

Electronic structure calculations based on first-principle methods have become increasingly important in condensed matter physics, quantum chemistry and material science since they are an ideal tool to study and comprehend the atomic energy levels, molecular spectra and energy bands of solids and it also gives insights into all properties derived from electronic spectra and wavefunctions. The behavior of electrons in particular governs most of the properties of materials and quantum mechanics provides a reliable way to calculate what electrons and atomic nuclei do. This is true for both single atoms and assemblies of atoms in condensed matter, because quantum mechanics describes and explains chemical bonds. Hence, it is in principle possible to understand the

properties of any material based on fundamental physical laws and without using free parameters by solving the Schrödinger equation for the electrons in that material, that is, from first-principles.

In general, first-principles methods allow us to determine structural properties (e.g., angle, bond length etc.), reactivity (via calculating the free energy), electrical conductivity (via calculating density of states, band structures,  $I$ - $V$  characteristics, transmittance etc.), optical properties (e.g. by calculating dielectric function, photo adsorption spectra, optical indices) etc. of a material system only by giving basic structural information without any adjustable parameters. These can be investigated without ever synthesizing the material. This uniqueness of first-principle methods enables us to provide predictions regarding material properties and to estimate their use in potential applications. For example, current-voltage simulations based on first-principles allow prediction of the performance of new materials in field-effect-transistors, sensors and photovoltaic cells. Technology computer aided design (TCAD) reduces substantially both the development time and the cost of new technologies. In addition to path-finding, first-principle methods are widely used as a complementary component of experimental investigations to interpret results.

In this Chapter we introduce the theoretical background to the computational methodologies applied later in the Thesis. The Chapter starts with posing the many-body problem and the necessity of adopted approximations. We continue with a brief overview of elementary quantum mechanical concepts before introducing DFT. This is followed by a bird's eye view of the overall computational approach with particular emphasis on basis functions, pseudopotentials, the exchange-correlation term and the van der Waals correction that are applied in this study.<sup>1-2</sup> The final section introduces the computational code that implements DFT for electronic structure simulation and material analysis as applied in this Thesis.

## 2.1.2 The many-body problem of electrons around nuclei

Material modelling from first-principles relies on simulating the physics and chemistry at the atomic scale using the quantum mechanical description. These systems increase in complexity with different types of atoms or molecules, in for example atomic clusters or quantum dots, and solids, including covalent, ionic, metallic, and molecular solids as well as layered structures, surfaces and quasi-crystals.

Dealing with any physical problem based on the accurate description of the quantum mechanics of the system components (microscopic point of view), in general involves having to solve the Schrödinger equation for a large number of interacting particles. Finding the wavefunction of such a system is a many-body problem and it is computationally a very challenging task. As we know from Quantum Mechanics, all information about any (many-body) system is in principle extractable from the quantum mechanical wavefunction of that system. For any material, this is represented as:

$$\Psi_{MB} = \Psi(r_1, r_2, \dots, r_N | R_1, R_2, \dots, R_N | t) \text{ (eq. 2.1)}$$

in which  $t$  is the time variable and the  $(r, R)$  are the electronic and nuclei coordinates respectively.

Apart from a few trivial cases such as a simple 2D square potential or a hydrogen atom, the Schrödinger equation cannot be solved exactly. This is due to the fact that even an independent many-body equation has  $3N_e$  degrees of freedom for electrons and  $3N_n$  for nuclei. Eventually, we need to involve some approximation to solve the problem although such an approximation is not often easy to find. The first technical move in any many-body problem is to reduce the degrees of freedom of the system under study and it is in fact what the Born-Oppenheimer approximation readily does.

***Born-Oppenheimer approximation-*** Due to similar order of magnitude between the applied forces on electrons and nuclei, they have comparable momentum



values. However the massive weights of nuclei compared to electrons result in the kinetic energy of nuclei being much smaller than for electrons. This is the key concept of the Born-Oppenheimer approximation. Electrons are expected to have an instantaneous response to the movement of nuclei. At any nuclear configuration, the electrons are assumed to be in an instantaneous ground-state and then the total energy of the system is calculated within this condition. By variation over the nuclear positions, a multi-dimensional potential energy surface is defined. Accordingly, the motion of the nuclei then can be treated like classical particles moving in this potential.

Applying these insights into the many-body wavefunction, Born and Oppenheimer proposed to break it into its electronic and nuclear components:

$$\Psi_{MB} = \Psi_e \times \Psi_n. \text{ (eq. 2.2)}$$

As the first step, they solved the electronic Schrödinger equation to calculate  $\Psi_e$  which only depends on electrons as variables. Within this process, the nuclei are assumed to be fixed at their initial configuration. The total electronic energy is then a summation over the following terms: inter-nuclear potential, electron kinetic energy, electron-electron interaction and electron-nuclear attraction. In the second step, the nuclear kinetic energy is added to the nuclear potential energy of the system and the nuclei's wavefunction,  $\Psi_n$ , is calculated.

Many approaches have been developed so far to deal with the many-body problem of finding  $\Psi_e$ . These include mean-field based methods and extensions, Configuration Interaction (CI), Coupled Cluster (CC), Monte-Carlo based methods and Density Functional Theory (DFT). The DFT approach has been employed in this study due to its conceptual simplicity, computational efficiency and relative accuracy as explained in the next sections.

## 2.2 Density Functional Theory

### 2.2.1 Fundamentals

DFT is one of the most popular and straightforward methods of obtaining an approximate solution to the Schrödinger equation of an  $N$ -particle system among the various available methods so far and is applicable to many systems.<sup>3</sup> It is now routine to apply DFT for calculating, for example, the binding energy of molecules or the band structure of solids. In fact this flexibility of the DFT is mainly due to its universal fundamental concepts and many ways to implement them. Although flexible, Density Functional Theory is based on a rigorous conceptual framework. Core elements of DFT are the Hohenberg-Kohn theorems and the Kohn-Sham system (and equations derived thereafter).

Since the electronic structure is the main focus of this thesis, assuming the non-relativistic situation for a single electron moving in the potential  $v(r)$ , from Schrödinger's equation the electronic wavefunction is calculated as (atomic units are used;  $\hbar = m_e = e = 1$ ):

$$\left[-\frac{1}{2}\nabla^2 + v(\mathbf{r})\right]\psi(\mathbf{r}) = \epsilon\psi(\mathbf{r}) \text{ (eq. 2.3)}$$

The nuclear degrees of freedom (e.g., the crystal lattice in a solid) appear only in the form of a potential  $v(r)$  applied on the electrons as a result of the Born-Oppenheimer approximation.

If there is more than one electron (i.e., a many-body problem) then Schrödinger's equation for the electronic part becomes:

$$\left[\sum_i^N \left(-\frac{1}{2}\nabla_i^2 + v(\mathbf{r}_i)\right) + \sum_{i<j} U(\mathbf{r}_i, \mathbf{r}_j)\right]\Psi(\mathbf{r}_1, \mathbf{r}_2, \dots, \mathbf{r}_N) = E\Psi(\mathbf{r}_1, \mathbf{r}_2, \dots, \mathbf{r}_N) \text{ (eq. 2.4)}$$

where  $N$  is the number of electrons and  $U(r_i, r_j)$  is the electron-electron interaction.\* Considering a Coulombic system one has:

$$\hat{U} = \sum_{i<j} U(\mathbf{r}_i, \mathbf{r}_j) = \sum_{i<j} \frac{1}{|\mathbf{r}_i - \mathbf{r}_j|} \text{ (eq. 2.5)}$$

---

\*Please note the drop of the subscript 'e' as from this point we deal only with electrons unless stated otherwise.

Note that this is the same operator for any system of particles interacting via the Coulomb interaction, just as the kinetic energy operator,

$$\hat{T} = -\frac{1}{2} \sum_i \nabla_i^2 \text{ (eq. 2.6)}$$

is the same for any non-relativistic system. Whether the system is an atom, a molecule, or a solid thus depends only on the potential  $v(r_i)$ . Extracting measurable quantities from the usual quantum-mechanical approach to Schrödinger's equation (SE) can be simply explained by the following sequence:

$$v(\mathbf{r}) \xrightarrow{SE} \Psi(\mathbf{r}_1, \mathbf{r}_2, \dots, \mathbf{r}_N) \xrightarrow{\langle \Psi | \dots | \Psi \rangle} \text{Observables (eq. 2.7)}$$

i.e., one specifies the system by choosing  $v(r)$ , plugs it into Schrödinger's equation, solves that equation for the wavefunction  $\Psi$ , and then calculates observables by taking expectation values of operators with this wavefunction.

One among the observables that are calculated in this way is the particle density:

$$n(\mathbf{r}) = N \int d^3\mathbf{r}_2 \int d^3\mathbf{r}_3 \dots \int d^3\mathbf{r}_N \Psi^*(\mathbf{r}_1, \mathbf{r}_2, \dots, \mathbf{r}_N) \Psi(\mathbf{r}_1, \mathbf{r}_2, \dots, \mathbf{r}_N). \text{ (eq. 2.8)}$$

The particle density is the central quantity in DFT and allows for simplifications that make the many-body problem computationally tractable.

Unlike solving for the many-body electronic wavefunction, which is a function of  $3N$  variables (the coordinates of all  $N$  particles in the system), as in the Hartree-Fock (HF) theory or post-HF methods, in DFT everything is expressed as a function of the electron density, which is only a function of three variables  $x$ ,  $y$  and  $z$ . This includes the wavefunction:

$$\Psi = \Psi[n](\mathbf{r}_1, \mathbf{r}_2, \dots, \mathbf{r}_N) \text{ (eq. 2.9)}$$

indicating that  $\Psi$  is a function of its  $N$  spatial variables, but a functional of  $n(r)$ , i.e., a function of a function.

The basis of this mapping was provided by the Hohenberg-Kohn theorems. These theorems simply demonstrate that the density of any system is sufficient to derive all the ground-state properties of the system. For example, the ground state energy of a many-electron system is a functional of the density. Strictly speaking, if we know the electron density functional, then we know the total energy of the system. The ground-state wavefunction  $\Psi_0$  must not only

reproduce the ground-state density, but also minimize the energy. For a given ground-state density  $n_0(r)$ , we can write this requirement as

$$E_{v,0} = \min_{\Psi \rightarrow n_0} \langle \Psi | \hat{T} + \hat{U} + \hat{V} | \Psi \rangle \quad (\text{eq. 2.10})$$

where  $E_{v,0}$  represents the ground-state energy in potential  $v(r)$ . The previous equation tells us that for a given density  $n_0(r)$  the ground-state wavefunction  $\Psi_0$  is that which reproduces this  $n_0(r)$  and minimizes the energy. For an arbitrary density  $n(r)$ , we define the functional:

$$E_v[n] = \min_{\Psi \rightarrow n} \langle \Psi | \hat{T} + \hat{U} + \hat{V} | \Psi \rangle \quad (\text{eq. 2.11})$$

If  $n$  is a density different from the ground-state density  $n_0$  in potential  $v(r)$ , then the  $\Psi$  that produce this  $n$  are different from the ground-state wavefunction  $\Psi_0$ , and based on the variational principle the minimum obtained from  $E_v[n]$  is higher than (or equal to) the ground-state energy  $E_{v,0} = E_v[n_0]$ . Thus, the functional  $E_v[n]$  is minimized by the ground-state density  $n_0$ , and its value at the minimum is  $E_{v,0}$ . The total-energy functional can be written as:

$$E_v[n] = \min_{\Psi \rightarrow n} \langle \Psi | \hat{T} + \hat{U} | \Psi \rangle + \int d^3\mathbf{r} n(\mathbf{r})v(\mathbf{r}) = F[n] + V[n] \quad (\text{eq. 2.12})$$

where the internal-energy functional  $F[n] = \min_{\Psi \rightarrow n} \langle \Psi | \hat{T} + \hat{U} | \Psi \rangle$  is independent of the potential  $v(r)$ , and thus determined only by the structure of the operators  $\hat{U}$  and  $\hat{T}$ . This universality of the internal-energy functional allows us to define the ground-state wavefunction  $\Psi_0$  as that antisymmetric  $N$ -particle function that delivers the minimum of  $F[n]$  and reproduces  $n_0$ . If the ground state is non-degenerate, this double requirement uniquely determines  $\Psi_0$  in terms of  $n_0(r)$ , without having to specify  $v(r)$  explicitly.

## 2.2.2 DFT as an effective single-body theory

There are plenty of ways of implementing density-functional theory. The first method is based on minimization of an explicit energy functional, which in fact is not normally very efficient. Kohn-Sham is the most widely used approach. It is based on mapping the complicated problem of a system of interacting electrons into that of a non-interacting electrons moving in an effective potential.

The success and popularity of this approach is partly due to the fact that it does not exclusively work in terms of the particle (or charge) density, but brings a special kind of wavefunction (single-particle orbitals) back into the game. As a result DFT then looks formally like a single-particle theory, although many-body effects are still included via the so-called exchange-correlation functional.

### 2.2.2.1 Deriving Kohn-Sham equations

Kohn and Sham separated  $E[n]$  into the following parts:

$$E[n] = T[n] + U[n] + V[n] = T_s[\{\phi_i[n]\}] + U_H[n] + E_{xc}[n] + V[n] \quad (\text{eq. 2.13})$$

where  $T_s$  indicates the kinetic energy of non-interacting particles,  $U_H$  is the Hartree potential and  $E_{xc}$  is the exchange-correlation energy, which will be explained later. Since  $T_s$  is an orbital functional one cannot directly minimize the energy with respect to  $n$ . Kohn and Sham introduced an indirect minimization scheme. This scheme starts by writing the minimization as:

$$0 = \frac{\delta E[n]}{\delta n(\mathbf{r})} = \frac{\delta T_s[n]}{\delta n(\mathbf{r})} + \frac{\delta V[n]}{\delta n(\mathbf{r})} + \frac{\delta U_H[n]}{\delta n(\mathbf{r})} + \frac{\delta E_{xc}[n]}{\delta n(\mathbf{r})} = \frac{\delta T_s[n]}{\delta n(\mathbf{r})} + v(\mathbf{r}) + v_H(\mathbf{r}) + v_{xc}(\mathbf{r}) \quad (\text{eq. 2.14})$$

Assume now a system of non-interacting particles moving in the potential  $v_s(r)$ .

For this system the minimization condition is simply:

$$0 = \frac{\delta E_s[n]}{\delta n(\mathbf{r})} = \frac{\delta T_s[n]}{\delta n(\mathbf{r})} + \frac{\delta V_s[n]}{\delta n(\mathbf{r})} = \frac{\delta T_s[n]}{\delta n(\mathbf{r})} + v_s(\mathbf{r}) \quad (\text{eq. 2.15})$$

since there are no Hartree and  $xc$  terms in the absence of interactions. Comparing this with the preceding equation we find that both minimizations have the same solution  $n_s(r) \equiv n(r)$ , if  $v_s$  is chosen to be:

$$v_s(\mathbf{r}) = v(\mathbf{r}) + v_H(\mathbf{r}) + v_{xc}(\mathbf{r}). \quad (\text{eq. 2.16})$$

Consequently, one can calculate the density of the interacting (many-body) system in a potential  $v(r)$ , described by a many-body Schrödinger equation, by solving the equations of a non-interacting (single-body) system in potential  $v_s(r)$ .

In particular, the Schrödinger equation of this auxiliary system,

$$\left[-\frac{1}{2}\nabla^2 + v_s(\mathbf{r})\right]\phi_i(\mathbf{r}) = \epsilon_i\phi_i(\mathbf{r}) \quad (\text{eq. 2.17})$$

gives orbitals that reproduce the density  $n(r)$  of the original system:

$$n(\mathbf{r}) = n_s(\mathbf{r}) = \sum_i^N f_i |\phi_i(\mathbf{r})|^2 \quad (\text{eq. 2.18})$$

where  $f_i$  is the occupation of the  $i$ 'th orbital. The above three equations are the famous Kohn-Sham (KS) equations. They replace the problem of minimizing  $E[n]$  by that of solving a non-interacting Schrödinger equation.

Because both  $v_H$  and  $v_{xc}$  depend on  $n$ , which depends on the  $\varphi_i$ , which in turn depends on  $v_s$ , the problem of solving the KS equations is a nonlinear problem. The typical way of solving such problems is to start with an initial guess for  $n(r)$ , calculate the corresponding  $v_s(r)$ , and then solve the differential equation (2.17) for the  $\varphi_i$ . From these one calculates a new density, using (2.18), and starts again. The process is repeated until the convergence criterion is satisfied. The technical name for this procedure is 'self-consistency cycle'. Different convergence criteria (such as convergence in the energy, the density, or some observable calculated from these) and various convergence-accelerating algorithms (such as mixing of old and new effective potentials) are commonly in use. Once one has a converged solution of  $n_0$ , then the total energy can be calculated from equation (2.13).

## 2.3 A practitioner's guide to performing a DFT calculation

Based on which specific technical criteria are included while solving a typical DFT calculation, different approaches can be realized. This has led to a variety of modern DFT methods which are mainly categorized on the basis of the following options:

- Which basis set is used to expand the KS eigenfunctions? (planewaves and localized basis functions are the two most common choices)
- How core and valence electrons are treated in terms of interactions with the nuclei? A full-potential (all-electron) picture can be applied or a pseudopotential approach can be chosen, neglecting core orbitals.
- The choice of functionals to describe electron-electron interaction.

Obviously there are several cases where KS DFT does not provide a reasonable solution, such as strongly correlated electron systems or excited states. Methods such as many-body perturbation theory or dynamical mean field theory can enhance the DFT predictions where needed.

### **2.3.1 Basis functions**

In practice, the numerical solution of the KS differential equation (2.17) normally proceeds by expanding the KS orbitals in a suitable set of basis functions and solving the resulting equation for the coefficients in this expansion and/or for the eigenvalues for which it has a solution. The construction of suitable basis functions is a major enterprise within electronic-structure theory. Planewaves, real-space grids and atom-centred orbitals are most commonly used.

In physics much is known about the construction of basis functions for solids due to decades of experience with band-structure calculations. This includes many calculations that predate the widespread use of DFT in physics. There is a fundamental difference between methods that work with fixed basis functions that do not depend on energy, and methods that employ energy dependent basis functions. Fixed basis functions are used e.g., in planewave expansions, tight-binding or linear combination of atomic orbitals (LCAO) approximations, or the orthogonalized planewave (OPW) method. Examples for methods using energy-dependent functions are the augmented planewave (APW) or Korringa-Kohn-Rostoker (KKR) approaches. This distinction became less clear-cut with the introduction of ‘linear methods’,<sup>4</sup> in which energy-dependent basis functions are linearized (Taylor expanded) around some fixed reference energy. The most widely used methods for solving the Kohn-Sham equation in solid-state physics, linear muffin tin orbitals (LMTO) and linear augmented planewaves (LAPW), are of this latter type. Development of better basis functions is an ongoing task.

The situation is quite similar in chemistry. Due to decades of experience with Hartree-Fock and CI calculations much is known about the construction of basis functions that are suitable for molecules. Almost all of this continues to hold in DFT, a fact that has greatly contributed to the recent popularity of DFT in chemistry. Chemical basis functions are classified with respect to their behavior as a function of the radial coordinate into Slater type orbitals (STOs), which decay exponentially far from the origin, and Gaussian type orbitals (GTOs), which have a Gaussian behavior. STOs more closely resemble the true behavior of atomic wavefunctions, but GTOs are easier to handle numerically because the product of two GTOs located at different atoms is another GTO located in between, whereas the product of two STOs is not an STO. The so-called ‘contracted basis functions’, in which STO basis functions are re-expanded in a small number of GTOs, represent a compromise between the accuracy of STOs and the convenience of GTOs. The most common methods for solving the Kohn-Sham equations in quantum chemistry are of this type.

**Planewave.** Traditionally planewaves have been used in electronic structure calculations of crystalline solids where the underlying lattice provides periodicity to the Kohn-Sham wavefunction. To use these implementations in more general cases where periodicity does not apply (or exists only in certain directions), a repeating unit (supercell) can be set up with sufficient vacuum to make the interaction between repeated atoms, molecules or finite clusters negligible. In any case, the Kohn-Sham wavefunction can be expanded in planewaves

$$\psi_i(\mathbf{r}) = \sum_{\mathbf{G} < \mathbf{G}_{max}} c_{i,\mathbf{G}} \cdot e^{i(\mathbf{K}+\mathbf{G})\cdot\mathbf{r}} \text{ (eq. 2.19)}$$

where  $\mathbf{K}$  and  $\mathbf{G}$  are planewaves and reciprocal lattice vector that satisfies the periodicity imposed to the supercell respectively. Systematic convergence can be achieved by increasing the number of planewaves, that is, increasing  $G_{max}$ . To allow for that, one sets a single variational parameter, that is, the maximum kinetic energy  $E_{cutoff} = \frac{1}{2}|\mathbf{G}_{max}|^2$  of the planewaves. However, calculations with converged sets of planewaves are computational demanding.



**Atomic orbitals basis sets.** The method builds on expressing the Kohn-Sham wavefunction  $\psi_i$  as a linear combination of atomic-like basis functions  $\varphi_j$  located at the various atomic sites:

$$\psi_i(\mathbf{r}) = \sum_n \sum_{j=1}^k c_{ij} \varphi_j(\mathbf{r} - \mathbf{r}_n) \quad (\text{eq. 2.20})$$

where  $n$  is the site index and  $j$  includes the angular momentum  $l$ , magnetic quantum number  $m$  and the multiplicity index  $p$ , namely,  $j \rightarrow p, l, m$ . The  $\{\varphi_j\}$  basis is obtained by the eigenvectors of the Schrödinger equation for an atom in a slightly modified environment that accounts to some extent for the orbital relaxation when bonding.

### 2.3.2 Pseudopotential

A very popular approach to larger systems in DFT, in particular solids, is based on the concept of a pseudopotential (PP). The idea behind the PP is that chemical binding in molecules and solids is dominated by the outer (valence) electrons of each atom. The inner (core) electrons retain, to a good approximation, an atomic-like configuration, and their orbitals do not change much if the atom is put in a different environment. Hence, it is possible to approximately account for the core electrons in a solid or a large molecule by means of an atomic calculation, leaving only the valence density to be determined self-consistently for the system of interest.

In the original Kohn-Sham equation the effective potential  $v_s(r) = v_{ext}(r) + v_H(r) + v_{xc}(r)$  is determined by the full electronic density  $n(r)$ , and the self-consistent solutions are single-particle orbitals reproducing this density. In the PP approach the Hartree and  $xc$  terms in  $v_s[n]$  are evaluated only for the valence density  $n_v$ , and the core electrons are accounted for by replacing the external potential  $v_{ext}$  by a pseudopotential  $v_{ext}^{PP}$ . Hence  $v_s^{PP}[n_v] = v_{ext}^{PP} + v_H[n_v] + v_{xc}[n_v]$ . The PP  $v_{ext}^{PP}$  is determined in two steps. First, one determines, in an auxiliary atomic calculation, an effective PP,  $v_s^{PP}$ , such that for a suitably chosen atomic reference configuration the single-particle orbitals resulting from  $v_s^{PP}$  agree, outside a cut-off radius  $r_c$  separating the core from the valence region,

with the valence orbitals obtained from the all-electron KS equation for the same atom. As a consequence, the valence densities  $n_v^{at}$  obtained from the atomic KS and the atomic PP equation are the same. Next, one subtracts the atomic valence contributions  $v_H[n_v^{at}]$  and  $v_{xc}[n_v^{at}]$  from  $v_s[n_v^{at}]$  to obtain the external potential  $v_{ext}^{PP}$ , which is then used in the molecular or solid-state calculation, together with  $v_H[n_v]$  and  $v_{xc}[n_v]$  taken at the proper valence densities for these systems. The pseudopotential approach is very convenient because it reduces the number of electrons treated explicitly, making it possible to perform density-functional calculations on systems with tens of thousands of electrons. Moreover, the pseudopotentials  $v_{ext}^{PP}$  are much smoother than the bare nuclear potentials  $v_{ext}$ . Hence removes need for high frequency planewaves to describe high kinetic energy core electrons (lower  $E_{cutoff}$ ). The remaining valence electrons are thus well described by planewave basis sets.

### 2.3.3 The Exchange-Correlation term

An accurate scheme for treating the kinetic-energy functional of interacting electrons,  $T[n]$ , is based on decomposing it into one part that represents the kinetic energy of non-interacting particles of density  $n$ , i.e., the quantity called above  $T_s[n]$ , and one that indicates the remainder, denoted  $T_c[n]$  (the subscripts  $s$  and  $c$  stand for ‘single-particle’ and ‘correlation’, respectively):

$$T[n] = T_s[n] + T_c[n] \text{ (eq. 2.21)}$$

$T_s[n]$  is not known exactly as a functional of  $n$  but it is easily expressed in terms of the single-particle orbitals,  $\phi_i(\mathbf{r})$ , of a non-interacting system with density  $n$ , as:

$$T_s[n] = -\frac{1}{2} \sum_i^N \int d^3\mathbf{r} \phi_i^*(\mathbf{r}) \nabla^2 \phi_i(\mathbf{r}) \text{ (eq 2.22)}$$

as for non-interacting particles the total kinetic energy is just the sum of the individual kinetic energies. Since all  $\phi_i(\mathbf{r})$  are functionals of  $n$ , this expression for  $T_s$  is an explicit orbital functional but an implicit density functional,  $T_s[n] = T_s[\{\phi_i[n]\}]$ , where the notation indicates that  $T_s$  depends on the full set of

occupied orbitals  $\phi_i$ , each of which is a functional of  $n$ . We can now rewrite the exact energy functional as:

$$E[n] = T[n] + U[n] + V[n] = T_s[\{\phi_i[n]\}] + U_H[n] + E_{xc}[n] + V[n] \text{ (eq. 2.13)}$$

where by definition  $E_{xc}$  contains the differences  $T-T_s$  (i.e.  $T_c$ ) and  $U-U_H$ . This definition shows that a significant part of the correlation energy  $E_c$  is due to the difference  $T_c$  between the non-interacting and the interacting kinetic energies. It is often decomposed as  $E_{xc} = E_x + E_c$ , where  $E_x$  is due to the Pauli principle (exchange energy) and  $E_c$  is due to correlations ( $T_c$  is then a part of  $E_c$ ).

A ladder of approximate functionals has been developed for the purpose of solving the many-electron Schrödinger equation (the KS equations). The way that exchange-correlation functionals are designed is to satisfy the most possible exact constraints.

The exchange-correlation term first was approximated by the Local Density Approximation (LDA) that will be explained in the next section. Within this approximation, at any small region, the exchange-correlation energy is described by the evaluated value for electronic gas of the same electron density. In other words, the modelled exchange-correlation hole is not the exact one. Instead, it is replaced by the hole taken from an electron gas with the same density as the local density around the electron. Although the exchange-correlation hole may not be represented exactly as its real shape, surprisingly, the overall effective charge is modelled very accurately. This basically demonstrates that the attractive potential felt by each electron is well described.

In practice LDA is shown to predict accurate results for a wide range of ionic, covalent and metallic materials, even though they do not have slowly varying or homogeneous electron densities.

An alternative, slightly more sophisticated approximation is the Generalized Gradient Approximation (GGA) which estimates the contribution of each volume element to the exchange-correlation based upon the magnitude and gradient of the electron density within that element. The more mathematical details of LDA, GGA etc. are given in the following sections.

## 2.4 Local functionals: LDA & GGA

From both historical and practical point of view, the local density approximation (LDA) is the most important type of DFT approximation. To comprehend the concept of the LDA, remember first how the non-interacting kinetic energy  $T_s[n]$  is treated in the Thomas-Fermi approximation: In a homogeneous system one knows that, per volume:

$$t_s^{hom}(n) = \frac{3h^2}{10m} [(3\pi^2)^{2/3}] n^{5/3} \text{ (eq. 2.23)}$$

where  $n = \text{constant}$  in space. In an inhomogeneous system, with  $n = n(\mathbf{r})$ , one approximates locally:

$$t_s(\mathbf{r}) \approx t_s^{hom}(n(\mathbf{r})) = \frac{3h^2}{10m} [(3\pi^2)^{2/3}] n^{5/3} \text{ (eq. 2.24)}$$

and obtains the full kinetic energy by integration over all space:

$$T_s^{LDA}[n] = \int d^3\mathbf{r} t_s^{hom}(n(\mathbf{r})) = \frac{3h^2}{10m} (3\pi^2)^{2/3} \int d^3\mathbf{r} n(\mathbf{r})^{5/3} \text{ (eq. 2.25)}$$

For the kinetic energy, the approximation  $T_s[n] \approx T_s^{LDA}[n]$  is much weaker compared to the exact treatment of  $T_s$  in terms of orbitals, offered by the Kohn-Sham equations. However, the LDA concept appeared to be highly useful for another component of the total energy (eq 2.13), the exchange-correlation energy  $E_{xc}[n]$ . For the exchange energy,  $E_x[n]$ , the procedure is very simple, since the per volume exchange energy of the homogeneous electron liquid is known exactly as:

$$e_x^{hom}(n) = -\frac{3q^2}{4} \left(\frac{3}{\pi}\right)^{1/3} n^{4/3} \text{ (eq. 2.26)}$$

So that:

$$E_x^{LDA}[n] = -\frac{3q^2}{4} \left(\frac{3}{\pi}\right)^{1/3} \int d^3\mathbf{r} n(\mathbf{r})^{4/3} \text{ (eq. 2.27)}$$

This is the LDA for  $E_x$ .

For the correlation energy  $E_c[n]$  the situation is more complicated because  $e_c^{hom}(n)$  is not known exactly: the determination of the correlation energy of a homogeneous interacting electron system (an electron liquid) is yet a difficult many-body problem on its own! Early approximate expressions for  $e_c^{hom}(n)$  were based on applying perturbation theory (e.g. the random-phase

approximation) to this problem.<sup>5</sup> Independently of the parametrization, the LDA for  $E_{xc}[n]$  formally consists in:

$$E_{xc}[n] \approx E_{xc}^{LDA}[n] = \int d^3r e_{xc}^{hom}(n)|_{n \rightarrow n(r)} = \int d^3r e_{xc}^{hom}(n(\mathbf{r})) \quad (\text{eq. 2.28})$$

where  $e_{xc}^{hom} = e_x^{hom} + e_c^{hom}$ . This approximation for  $E_{xc}[n]$  has proved amazingly successful, even when applied to systems that are quite different from the electron liquid that forms the reference system for the LDA. A partial explanation for this success of the LDA is systematic error cancellation: typically, LDA underestimates  $E_c$  but overestimates  $E_x$ , resulting in unexpectedly good values of  $E_{xc}$ . This error cancellation is not accidental, but systematic, and caused by the fact that for any density the LDA  $xc$  hole satisfies the correct sum rule  $\int d^3r' n_{xc}^{LDA}(\mathbf{r}, \mathbf{r}') = -1$  which is only possible if integrated errors in  $n_x^{LDA}$  cancel with those of  $n_c^{LDA}$ .

What real systems, such as atoms, molecules, clusters and solids, have in common, is that at the same time, they are both inhomogeneous (the electrons are exposed to spatially varying electric fields produced by the nuclei) and interacting (the electrons interact via the Coulomb interaction). The way density-functional theory, in the local-density approximation, deals with this inhomogeneous many-body problem is by decomposing it into two simpler (but still highly nontrivial) problems: the solution of a spatially homogeneous interacting problem (the homogeneous electron liquid) yields the uniform  $xc$  energy  $e_{xc}^{hom}(n)$ , and the solution of a spatially inhomogeneous non-interacting problem (the inhomogeneous electron gas described by the KS equations) yields the particle density. Both steps are connected by the local-density potential,<sup>6</sup> which shows how the  $xc$  energy of the uniform interacting system enters the equations for the inhomogeneous non-interacting system.

In the LDA one exploits knowledge of the density at point  $r$ . Any real system is spatially inhomogeneous, i.e., it has a spatially varying density  $n(r)$ , and it would clearly be useful to also include information on the rate of this variation in the functional. First attempts at doing these were the so-called ‘gradient-expansion approximations’ (GEA). In this class of approximation one tries to systematically calculate gradient-corrections of the form  $|\nabla n(r)|$ ,  $|\nabla n(r)|^2$ ,

$\nabla^2 n(\mathbf{r})$ , etc, to the LDA. A common example is the lowest-order gradient correction to the Thomas-Fermi approximation for  $T_s[n]$ ,

$$T_s[n] \approx T_s^W[n] = T_s^{LDA} \left[ \frac{\hbar^2}{8m} \int d^3r \frac{|\nabla n(\mathbf{r})|^2}{n(\mathbf{r})} \right]. \quad (\text{eq. 2.29})$$

This second term on the right-hand side is called the Weizsacker term.<sup>7</sup> Similarly, in

$$E_x[n] \approx E_x^{GEA(2)}[n] = E_x^{LDA}[n] - \frac{10q^2}{432\pi(3\pi^2)^{1/3}} \int d^3r \frac{|\nabla n(\mathbf{r})|^2}{n(\mathbf{r})^{4/3}} \quad (\text{eq. 2.30})$$

the second term on the right-hand side is the lowest-order gradient correction to  $E_x^{LDA}[n]$ . Practically, including low-order gradient corrections almost makes no improvement on the LDA, even often making it worse. Also, higher-order corrections are increasingly difficult to calculate.

In this situation it was a significant advance when it was realized, in the early eighties, that instead of power-series-like systematic gradient expansions one could experiment with more general functions of  $n(\mathbf{r})$  and  $\nabla n(\mathbf{r})$ , which need not proceed order by order. Such functionals, of the general form

$$E_x^{GGA}[n] = \int d^3r f(n(\mathbf{r}), \nabla n(\mathbf{r})) \quad (2.31)$$

have become known as generalized-gradient approximations (GGAs).<sup>8</sup> Different GGAs differ in the choice of the function  $f(n, \nabla n)$ . Note that this makes different GGAs much more different from each other than the different parametrizations of the LDA: essentially there is only one correct expression for  $e_{xc}^{hom}(n)$ , and the various parametrizations of the LDA<sup>9-10</sup> are merely different ways of writing it. On the other hand, depending on the method of construction employed for obtaining  $f(n, \nabla n)$  one can obtain very different GGAs. In particular, GGAs used in quantum chemistry typically proceed by fitting parameters to test sets of selected molecules. Then again, GGAs used in physics tend to emphasize exact constraints. Nowadays the most popular (and most reliable) GGAs are PBE (denoting the functional proposed in 1996 by Perdew, Burke and Ernzerhof<sup>11</sup>) in physics, and BLYP (denoting the combination of Becke's 1988 exchange functional<sup>12</sup> with the 1988 correlation functional of Lee, Yang and Parr<sup>13</sup>) in chemistry. Many other GGA-type functionals are also available, and new ones continue to appear.

Generally, current GGAs seem to give reliable results for all kinds of chemical bonds (covalent, ionic, metallic and hydrogen bonds). However, for van der Waals interactions, typical GGAs and LDAs fail.<sup>14</sup> To describe these very weak interactions, several approaches have been developed within DFT (section 2.5).<sup>15-17</sup> Overall, popularity of the GGAs in both physics and chemistry has led to substantial improvements as compared to LDA. Although ‘chemical accuracy’, as mentioned earlier, has not yet been achieved, it is not too far away.

So far various exchange-correlation functionals have been developed to improve the output of DFT calculations. In terms of accuracy enhancement in the exchange-correlation energy, a sequence of methods is proposed which is sometimes referred to as the ‘Jacob’s ladder’ of DFT. At the lowest step of this ladder, the contribution to the energy from a 3-D volume element in the space is determined by the local charge density in that volume. Higher levels include more complicated components constructed from the density or the KS orbitals in or around this volume element. The four important levels of Jacob’s ladder are: LDA, GGA, meta-GGA and hybrid functionals. The last of these mixes DFT and exact HF exchange functionals.

## **2.5 van der Waals interactions**

Apart from forces owing to the covalent bond, the hydrogen bond, or electrostatic interaction of ions with one another in neutral or charged molecules, there is another type of force called van der Waals (vdW) forces which is the summation over attractive or repulsive forces between molecules. vdW interactions are also known as London dispersion interactions. From the quantum-mechanical point of view they arise when charge fluctuations in one part of an atomic system are electro-dynamically correlated with charge fluctuations in another. This creates an attractive vdW force in the system. Hence, the vdW force at one place is dependent on charge fluctuations at another area. As a result, vdW forces are nonlocal correlation effects.

To properly describe the van der Waals interactions, treatment of dynamic long-range correlation effects are required. The van der Waals force includes: (a) force between two permanent dipoles (Kessom force), (b) force between a permanent dipole and a corresponding induced dipole (Debye force) and (c) force between two instantaneously induced dipoles (London force).

*London forces* arise in non-polar molecules as a result the correlated movement of electrons in interacting molecules. The electrons in neighboring molecules move away as they repel each other. Consequently, electron density is redistributed in the vicinity of another molecule. This redistribution of electron density creates instantaneous dipoles that attract each other. Larger molecules have stronger London forces. An increase of the polarizability of a molecule will make the electron clouds more scattered.

van der Waals (vdW) interactions play an important role in the self-assembly processes of organic monolayers.<sup>18-20</sup> In fact, the structure and stability of biomolecules,  $\pi$ -conjugated systems, molecular crystals, and adsorbed molecules on weakly reactive surfaces are strongly affected by vdW forces. Therefore, being aware of such an effect with its accurate theoretical description is primarily important when dealing with the systems such as solar cells, gas sensors and organic semiconductor devices, in which SAMs are included as an essential part.<sup>21</sup> Due to the high technological interest in hybrid organic-inorganic systems, it is vital to improve the agreement between theory and experiment and vdW corrections have been shown to have an effective contribution to that objective.<sup>22-23</sup>

The usefulness of density-functional theory (DFT) in describing structure, cohesion and other static properties of dense matter is now well established. The standard DFT approach these days involves the general-gradient approximation (GGA), which is in particular successful for describing valence bonds. In order to make DFT a practical tool applicable to the larger classes of matter, soft and condensed, it is very desirable to improve DFT by the inclusion of the vdW interactions.



### 2.5.1 van der Waals interactions in DFT

As we explained earlier, the practical DFT is based on approximations. The most common approaches, LDA and GGA, depend on the density in local and semilocal ways respectively. However, nonlocal interactions like vdW are not taken into account. Empirical and semi-empirical approaches based on the asymptotical form  $-r^{-4}$  for insulating sheets and  $-r^{-6}$  for atoms and molecules do exist that account for the vdW or London dispersion forces.<sup>15-17</sup> However, using this method the predicted forces at the scale of the vdW bond length are significantly different from the correct values.

The procedure of the vdW-DF method can be generally described as:

$$E_{xc}[n] = E_x^{GGA}[n] + E_c^{new}[n]. \text{ (eq. 2.32)}$$

The first term on the right hand side indicates an appropriate GGA exchange functional. The second term is constructed by a nonlocal correlation functional that includes an account of vdW forces. This is now an efficient and more accurate electron-structure scheme, which can be computed with planewave and real-space codes with a computational cost comparable with ordinary DFT-GGA. The correlation energy is then divided into short- and long-range pieces:

$$E_c^{new}[n] = E_c^o[n] + E_c^{nl}[n]. \text{ (eq. 2.33)}$$

The short-range term,  $E_c^o[n]$ , is evaluated in LDA, however the longer-range part,  $E_c^{nl}[n]$ , depends nonlocally on the density. A simple dielectric function is used in the nonlocal piece. In principle, the latter contains the vdW terms and it is also much smaller in magnitude and positional sensitivity.

### 2.5.2 Higher-accuracy van der Waals density functional

First-principles approaches for treating vdW in DFT started in the form of asymptotic interaction between fragments and ultimately developed into vdW-DF for arbitrary geometries.<sup>24-25</sup> Although successful in describing dispersion

and better than all non-empirical methods,<sup>26</sup> this approach overestimates equilibrium separations<sup>24-26</sup> and underestimates hydrogen-bond strength.<sup>27</sup>

A new version of the van der Waals density functional (vdW-DF2) was proposed<sup>28</sup> which employs the more accurate semilocal exchange functional PW86<sup>8</sup> and also uses a large- $N$  ( $N$  is number of electrons) asymptote gradient correction<sup>29</sup> for the vdW kernel determination. By comparing the potential energy curve with accurate quantum chemistry (QC) results for 22 molecular duplexes, it is shown that vdW-DF2 makes significant improvements in equilibrium spacings between noncovalently bound complexes, as well as in binding energy, especially when hydrogen bonding plays a role. This approach, implemented in the Quantum Espresso package, was used in our study wherever vdW correction was included in the calculations.

The vdW-DF method shows promise to extend the broad successes of density-functional theory to new classes of matter.<sup>23</sup> This is shown in several applications that cannot be done by any other nonempirical method.<sup>26</sup> Calculations for molecular systems and crystalline solids with wavefunction (i.e. Hartree-Fock) compared to vdW-DF method show that the latter can be fruitfully applied to more extended systems, and provide more favorable results.<sup>24-28</sup> The calculated adsorption energies of different systems can be tested with experimental values which usually are measured in desorption experiments. Comparisons with experiments in general indicate that the vdW-DF has improved the accuracy.<sup>23</sup> Interfacial dipoles and bonding are also better explained with vdW-DF.<sup>23</sup>

## 2.6 Computational package

Below a brief description follows of the computational tools I have used in my calculations.

## 2.6.1 Quantum Espresso

Quantum Espresso is an open source integrated suite of computer codes for geometrical optimizations of the atomic structure and electronic structure calculations.<sup>30</sup> It is based on a planewave implementation of DFT. Pseudopotentials (both norm-conserving and ultrasoft) are employed to eliminate core states. Quantum Espresso builds onto newly-restructured electronic-structure codes (PWscf, PHONON, CP90, FPMD, and Wannier) that have been developed and tested by some of the original authors of novel electronic structure algorithms —from Car-Parrinello molecular dynamics to density-functional perturbation theory— and applied in the last twenty years by some of the leading materials modelling groups worldwide. Quantum Espresso can perform the following types of calculations:

- 1) Geometrical optimization
- 2) Band structure, projected density of states
- 3) Electron-phonon interactions

The most important input parameters in Quantum Espresso are the atomic geometries (number and types of atoms in the periodic cell, bravais-lattice index, crystallographic or lattice constants), the kinetic energy cutoff and the type of pseudopotentials.

Despite the high computational cost when applied to a large number of atoms, Quantum Espresso is an easy approach to use towards predicting the electronic properties of materials or a combined system. As Quantum Espresso uses planewave basis sets it is relatively an appropriate DFT tools for studying crystalline solids and their surfaces. Applying a broad range of pseudopotentials with different flavors of LDA and GGA and many post-processing codes, it can calculate the electronic properties of the system as well as geometry optimization and structural properties. In particular for our interest, Quantum Espresso is capable of calculating the electrostatic potential of a slab supercell in a desired direction and charge reorganization can be monitored at the interface.

Density of states (DOS) and partial DOS is also extractable in a sequence of self-consistent and non-self-consistent calculations which is useful for a local analysis of the electronic densities and chemical bond interpretations. It has various optional corrections to the standard DFT, such as including London forces via vdW-DF(2), which can be implemented for better description of long-range forces and low-density structures wherever needed.

## 2.7 References

1. Robert G. Parr, W. Y., *Density-Functional Theory of Atoms and Molecules*; Oxford University Press, 1989.
2. David Sholl, J. A. S., *Density Functional Theory: A Practical Introduction*; John Wiley & Sons, 2011.
3. Capelle, K., A bird's-eye view of density-functional theory. *Braz. J. Phys.* 2006, *36*, 1318-1343.
4. Andersen, O. K., Linear methods in band theory. *Phys. Rev. B* 1975, *12*, 3060-3083.
5. Gunnarsson, O.; Lundqvist, B. I., Exchange and correlation in atoms, molecules, and solids by the spin-density-functional formalism. *Phys. Rev. B* 1976, *13*, 4274-4298.
6. Troullier, N.; Martins, J. L., Efficient pseudopotentials for plane-wave calculations. *Phys. Rev. B* 1991, *43*, 1993-2006.
7. Gázquez, J. L.; Ludeña, E. V., The weizsacker term in density functional theory. *Chem. Phys. Lett.* 1981, *83*, 145-148.
8. Perdew, J. P.; Yue, W., Accurate and simple density functional for the electronic exchange energy: Generalized gradient approximation. *Phys. Rev. B* 1986, *33*, 8800-8802.
9. Perdew, J. P.; Zunger, A., Self-interaction correction to density-functional approximations for many-electron systems. *Phys. Rev. B* 1981, *23*, 5048-5079.
10. Perdew, J. P.; Wang, Y., Accurate and simple analytic representation of the electron-gas correlation energy. *Phys. Rev. B* 1992, *45*, 13244-13249.
11. Staroverov, V. N.; Scuseria, G. E.; Perdew, J. P.; Davidson, E. R.; Katriel, J., High-density limit of the Perdew-Burke-Ernzerhof generalized gradient approximation and related density functionals. *Phys. Rev. A* 2006, *74*, 044501.
12. Becke, A. D., Density-functional exchange-energy approximation with correct asymptotic behavior. *Phys. Rev. A* 1988, *38*, 3098-3100.
13. Lee, C.; Yang, W.; Parr, R. G., Development of the Colle-Salvetti correlation-energy formula into a functional of the electron density. *Phys. Rev. B* 1988, *37*, 785-789.
14. Sham, L. J.; Schlüter, M., Density-Functional Theory of the Energy Gap. *Phys. Rev. Lett.* 1983, *51*, 1888-1891.
15. Andersson, Y.; Langreth, D. C.; Lundqvist, B. I., van der Waals Interactions in Density-Functional Theory. *Phys. Rev. Lett.* 1996, *76*, 102-105.

16. Dobson, J. F.; Dinte, B. P., Constraint Satisfaction in Local and Gradient Susceptibility Approximations: Application to a van der Waals Density Functional. *Phys. Rev. Lett.* 1996, *76*, 1780-1783.
17. Kohn, W.; Meir, Y.; Makarov, D. E., van der Waals Energies in Density Functional Theory. *Phys. Rev. Lett.* 1998, *80*, 4153-4156.
18. Bjork, J.; Matena, M.; Dyer, M. S.; Enache, M.; Lobo-Checa, J.; Gade, L. H.; Jung, T. A.; Stohr, M.; Persson, M., STM fingerprint of molecule-atom interactions in a self-assembled metal-organic surface coordination network on Cu(111). *Phys. Chem. Chem. Phys.* 2010, *12*, 8815-8821.
19. Caplan, M. R.; Moore, P. N.; Zhang, S.; Kamm, R. D.; Lauffenburger, D. A., Self-Assembly of a  $\beta$ -Sheet Protein Governed by Relief of Electrostatic Repulsion Relative to van der Waals Attraction. *Biomacromolecules* 2000, *1*, 627-631.
20. Turchanin, A.; Golzhauser, A., Carbon nanomembranes from self-assembled monolayers: Functional surfaces without bulk. *Prog. Surf. Sci.* 2012, *87*, 108-162.
21. Sony, P.; Puschnig, P.; Nabok, D.; Ambrosch-Draxl, C., Importance of Van Der Waals Interaction for Organic Molecule-Metal Junctions: Adsorption of Thiophene on Cu(110) as a Prototype. *Phys. Rev. Lett.* 2007, *99*, 176401.
22. Brede, J.; Atodiresei, N.; Kuck, S.; Lazić, P.; Caciuc, V.; Morikawa, Y.; Hoffmann, G.; Blügel, S.; Wiesendanger, R., Spin- and Energy-Dependent Tunneling through a Single Molecule with Intramolecular Spatial Resolution. *Phys. Rev. Lett.* 2010, *105*, 047204.
23. Lüder, J.; Sanyal, B.; Eriksson, O.; Puglia, C.; Brena, B., Comparison of van der Waals corrected and sparse-matter density functionals for the metal-free phthalocyanine/gold interface. *Phys. Rev. B* 2014, *89*, 045416.
24. Dion, M.; Rydberg, H.; Schroder, E.; Langreth, D. C.; Lundqvist, B. I., Van der Waals density functional for general geometries. *Phys. Rev. Lett.* 2004, *92*, 246401-4.
25. Thonhauser, T.; Cooper, V. R.; Li, S.; Puzder, A.; Hyldgaard, P.; Langreth, D. C., Van der Waals density functional: Self-consistent potential and the nature of the van der Waals bond. *Phys. Rev. B* 2007, *76*, 125112-11.
26. Langreth, D. C.; Lundqvist, B. I.; Chakarova-Kack, S. D.; Cooper, V. R.; Dion, M.; Hyldgaard, P.; Kelkkanen, A.; Kleis, J.; Kong, L.; Li, S.; Moses, P. G.; Murray, E.; Puzder, A.; Rydberg, H.; Schroder, E.; Thonhauser, T., A density functional for sparse matter. *J. Phys. Condens. Matter* 2009, *21*, 084203-15.
27. Kelkkanen, A. K.; Lundqvist, B. I.; Nørskov, J. K., Density functional for van der Waals forces accounts for hydrogen bond in benchmark set of water hexamers. *J. Chem. Phys.* 2009, *131*, 046102.
28. Lee, K.; Murray, E. D.; Kong, L. Z.; Lundqvist, B. I.; Langreth, D. C., Higher-accuracy van der Waals density functional. *Phys. Rev. B* 2010, *82*, 081101-4.
29. Elliott, P.; Burke, K., Non-empirical derivation of the parameter in the B88 exchange functional. *Can. J. Chem.* 2009, *87*, 1485-1491.
30. Giannozzi, P.; Baroni, S.; Bonini, N.; Calandra, M.; Car, R.; Cavazzoni, C.; Ceresoli, D.; Chiarotti, G. L.; Cococcioni, M.; Dabo, I.; Dal Corso, A.; de Gironcoli, S.; Fabris, S.; Fratesi, G.; Gebauer, R.; Gerstmann, U.; Gougoussis, C.; Kokalj, A.; Lazzeri, M.; Martin-Samos, L.; Marzari, N.; Mauri, F.; Mazzarello, R.; Paolini, S.; Pasquarello, A.; Paulatto, L.; Sbraccia, C.; Scandolo, S.; Sclauzero, G.; Seitsonen, A. P.; Smogunov, A.; Umari, P.; Wentzcovitch, R. M., QUANTUM ESPRESSO: A modular and open-source software project for quantum simulations of materials. *J. Phys. Condens. Matter* 2009, *21*, 395502-39521.

# Chapter 3

## Chemical Trends in the Work Function of Modified Si(111) Surfaces: A DFT Study

### 3.1 Introduction

In this Chapter we apply density functional theory to extract the work function of silicon surfaces with various terminations and the induced charge reorganization. Our aim is to provide a detailed microscopic analysis and to understand several chemical trends that have been observed in a series of experimental studies. By measuring the work function for pure H:Si(111) and after sulfur exposure and CuInS<sub>2</sub> deposition at different thicknesses, Hunger *et al.*<sup>1</sup> showed an increase in the work function at each stage respectively. Based on higher binding energy of the Si–S bond compared to the Si–Si bond, they proposed the formation of a surfacial SiS<sub>2</sub> phase on Si(111)/(100) and therefore the epitaxial growth of CuInS<sub>2</sub> on these surfaces. Later, the same group investigated the chemical state, electronic properties, and geometric structure of methyl-terminated Si(111) surfaces prepared using a two-step chlorination/alkylation process, high-resolution synchrotron photoelectron spectroscopy and low-energy electron diffraction methods.<sup>2</sup> The authors reported the possibility of full methyl-terminated surface which showed a decrease in the work function. Another group observed that chlorine termination of low-doped n-type Si(111) leads to an increase in conductance relative to the hydrogen-terminated surface.<sup>3</sup> The authors attributed this enhancement to formation of a

two dimensional hole gas resulting from the strong electron withdrawing nature of the adsorbed chlorine. Based on the fact that electronic properties at the semiconductor–molecule interface can be altered by changing the nature of covalent attachment, Hacker<sup>4</sup> examined the change in work function of the silicon surface after formation of Si–O–C, Si–C–C, and Si–S–C bonded alkyl monolayers, and separated charge transfer and dipolar contributions. A similar study was performed by Ashley *et al.*<sup>5</sup> using different terminations. Also Kuo *et al.*<sup>6</sup> used binary SAMs (self-assembled monolayers) with various ratios to modify the surface of Si to fine-tune the work function of Si to an arbitrary energy level. Most recently, Yan Li *et al.*<sup>7</sup> presented a combined theoretical and experimental study of the band edge position of –H, –Cl, –Br, –CH<sub>3</sub>, and –C<sub>2</sub>H<sub>5</sub> terminated Si(111) surfaces. These authors found an increase in the *WF* for the –Br and –Cl terminated surface; the *WF* decreased for methyl- and –C<sub>2</sub>H<sub>5</sub> terminations. They provided various theoretical methods to calculate *WF* and *IP*. Both were shown to be consistent with experimental data.

In what follows we present first-principles calculations of the work function of modified Si(111) surface with various terminating species. The unsaturated surface Si atoms form bonds with halogens, chalcogens and atoms from the second row of the periodic table. Due to the selected tether atoms relative to the hydrogenated surface, different charge reorganization, changes in electrical dipole moment of the interface as well as work function variations are observed and studied in detail. Surface terminations can be broadly divided into two general classes, that is, modifications by polar and nonpolar adsorbates. As may be expected for non-polar species, the change in the work function is readily interpreted by interface charge transfer and shows a monotonic behavior. For polar adsorbates, it is found that the electronegativity of the linker and the radical dipole moment of the precursor play a crucial role in the strength and direction of the changes in the work function. Coverage seems to have a minor effect to the work function in most cases.

The structure of the Chapter is as follows. In Section 3.2 we discuss briefly the background and the methodology used for our first-principle calculations. The

main body of our study follows in Section 3.3 with the presentation of results and discussion. We conclude with few remarks in Section 3.4.

## 3.2 Background and methodology

The work function in metals is defined as the minimum energy required to extract one electron from the solid. In this context it is the energy difference between the ground state energy of the neutral crystal of  $N$  electrons,  $E_N$ , and the energy of the new configuration which includes the  $N-1$  electrons at ground state,  $E_{N-1}$ , of the crystal and the removed electron at rest. The extracted electron has only electrostatic energy determined by the vacuum level,  $E_{\text{vac}}$ , so  $WF = E_{N-1} + E_{\text{vac}} - E_N$ . The change between  $E_N$  and  $E_{N-1}$  can be described thermodynamically in terms of the electrochemical potential as the derivative of free energy ( $F$ ) with respect to  $N$  at constant volume and temperature,  $E_{N-1} - E_N = \left(\frac{\partial F}{\partial N}\right)_{T,V} = \mu$ . At low temperatures  $\mu \approx E_F$ , thus the work function simplifies to:

$$WF = E_{\text{vac}} - E_F \text{ (eq. 3.1)}$$

where  $E_F$  is the Fermi energy. In a finite size crystal,  $E_{\text{vac}}$  is set by the final position of the electron, assuming that it is well away from the surface to avoid interaction with its image charge. There are a number of methods to experimentally measure the  $WF$ . Generally they are divided into two main categories: absolute measurements (field emission, thermionic emission and photoemission) and relative measurements (Kelvin probe).<sup>8</sup>



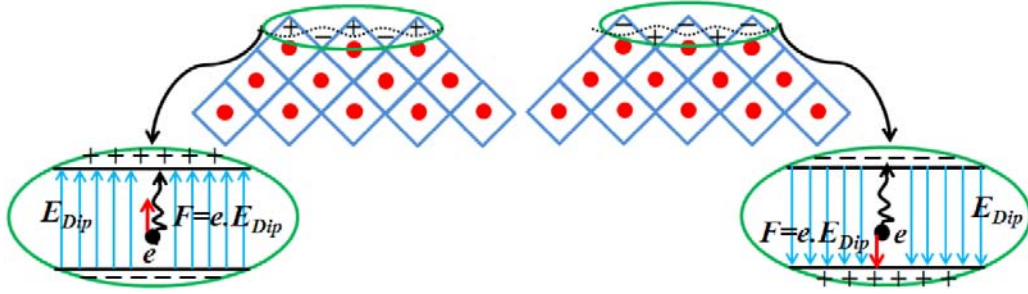


Figure 3.1. Electron acceleration across the interface for outward (left) and inward (right) surface dipoles.

Since the work function expresses the thermodynamic work of an electron moved from the material to a state at rest in the vacuum, it is expected that the  $WF$  is quantitatively determined by the electrostatic dipole at the surface. This is shown schematically in Figure 3.1. Materials surfaces, even different facets of the same crystal, can have varying surface dipole moments as a consequence of different atomic packing. Also atoms or molecules adsorbed on the surface can alter the total dipole moment of the surface. Adsorbates on the surface effectively redistribute the charges through chemical bonds and if they have static dipole moment they modify the surface elementary dipoles. Consequently the presence of such adsorbates may result in large changes in the work function. In semiconductors, charge neutrality causes band bending at the surface and the  $WF$  is interpreted as a contribution of three terms:

$$WF = \chi + eV_s + (E_C - E_F)_{\text{bulk}} \quad (\text{eq. 3.2})$$

where  $\chi$ ,  $eV_s$  and  $(E_C - E_F)$  represent the electron affinity, the band bending and the energy difference between the Fermi level and the conduction band minimum in the bulk, respectively. Electronic band diagrams for a clean surface and a surface with adsorbates are shown in Figure 3.2. Since both electron affinity and band bending are characteristic features of the surface, adsorbates-induced dipoles resulting from attaching atoms or molecules to the surface can only affect the first two terms in the above equation. Doping levels in the bulk of the semiconductor vary the third term inside the bracket.

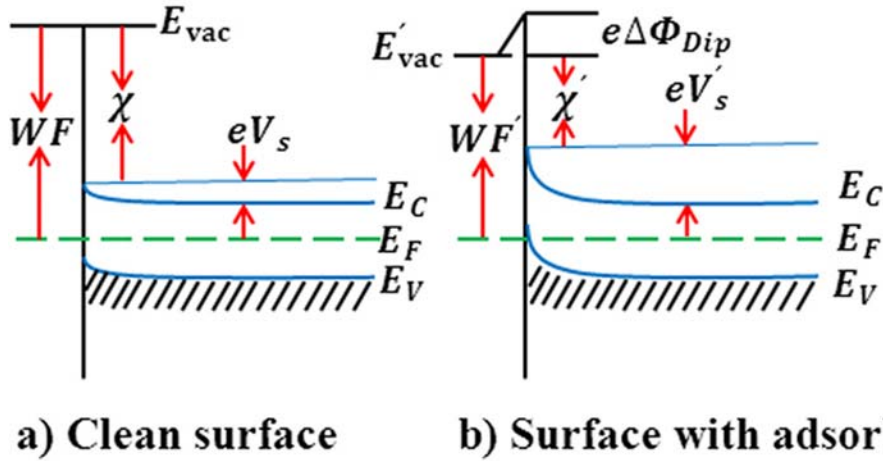


Figure 3.2. A schematic of the electronic-band diagrams of a clean and modified semiconductor surface. (a) A clean surface with its work function,  $WF$ , electron affinity,  $\chi$ , band bending at the surface,  $eV_s$ , conduction band minimum,  $E_C$ , valence band maximum,  $E_V$ , and vacuum level just outside the surface,  $E_{vac}$ . (b) Adsorbate-modified band diagram. Change in the band bending,  $eV_s$ , and electron affinity,  $\chi'$ , are exaggerated in the figure. Charge transfer within the bonds induces dipoles at the surface,  $\Delta\Phi_{Dip}$ , thus shifts the vacuum level,  $E'_{vac}$ , and varies the work function,  $WF$ .

Using the above definitions we use first principles methods in the Density Functional Theory (DFT) formulation to calculate the work function and separate contributions to its changes upon the various surface modifications.<sup>9-10</sup> This approach has been an increasingly valuable tool for such studies,<sup>11-16</sup> predicting changes for the adsorbate-induced substrate work function in agreement with experimental results.<sup>17-19</sup> DFT studies of the WF without the inclusion of long-range dispersion forces found reasonable agreement with the experiment, even for physisorbed systems.<sup>18-20</sup> In this chapter, only chemisorbed species are studied, hence, we do not include dispersion forces in identifying chemical trends.

Our DFT calculations are carried out using the PWSCF code of the QUANTUM-ESPRESSO distribution.<sup>21</sup> The Perdew-Burke-Ernzerhof (PBE) functional within the generalized gradient approximation (GGA) and ultrasoft pseudopotentials (USPPs) is used in all cases. The kinetic-energy cutoff for the planewave basis of 55 Ry for the wave function and 525 Ry for the charge

density are well converged for all elements in the calculations. We consider thin slabs of silicon separated by twelve equivalent vacuum layers in supercell geometry. Brillouin-zone integrations are performed using a  $10 \times 10 \times 1$  (a denser mesh of  $20 \times 20 \times 1$  for the  $WF$  calculation and charge analysis) Monkhorst-Pack k-points mesh for relax calculations. The fixed occupation technique was employed using ten additional bands to ensure energy convergence. The steps to extracting the necessary parameters to carry out the  $WF$  calculations are described below.

### 3.2.1 Work function calculation from first-principles

First we investigate the slab thickness effects on the precision of our calculations. We start with two layers thickness and proceed to 16 layers, and calculate distances between layers after relaxation. All surfaces are saturated by hydrogens. The work function for both relaxed and unrelaxed structure and the results are plotted in Figure 3.3. As we can see from Figure 3.3(a), convergence is achieved after a thickness of 14 layers. Nevertheless, even for 6-layer thickness deviation from the converged result is 0.5%. In Figure 3.3(b), the work function with varying thickness is shown for fully relaxed, unrelaxed and top layer relaxed. As we can see, there is a constant shift between relaxed and unrelaxed structures. Considering just top layer relaxation improves the precision more than 30%. Based on these observations we investigated several schemes that would allow speeding up our calculations by using only slabs with 6-layer thickness. As indicated in Figure 3.3(b), the schemes involved several approximations to slab relaxation and considerations about the Fermi energy. Considering relaxation of only the outermost layers (“top-down”: TD) yields the work function of the fully relaxed 6-layer slab. The remaining deviation from the converged result can be removed by replacing the Fermi energy of the 6-layer slab with the converged Fermi energy (bulk  $E_F$ ). We have confirmed that this also applies to polar terminating species. This scheme allows us extracting

converged results with much thinner slabs and reduced time spent on atomic relaxations, that is, 6-layer thickness with top and bottom layer relaxations.

The basic steps of the procedure to find the work function of silicon surfaces are as follows:

- 1) Starting with a 6-layer thick slab a geometry optimization is performed at the outset (top, bottom layers and interfaces only as discussed above). The force acting on each atom is converged to less than  $0.01 \text{ eV/\AA}$ . The rest of the four silicon layers (core layers) are fixed during geometry optimization.
- 2) After determining the electronic structure of the optimized geometry, the electrostatic potential is extracted from the converged Kohn-Sham equations using post-processing tools. The vacuum level is determined by calculating the macroscopic and planar averages of the electrostatic potential. The vacuum level is determined by the region

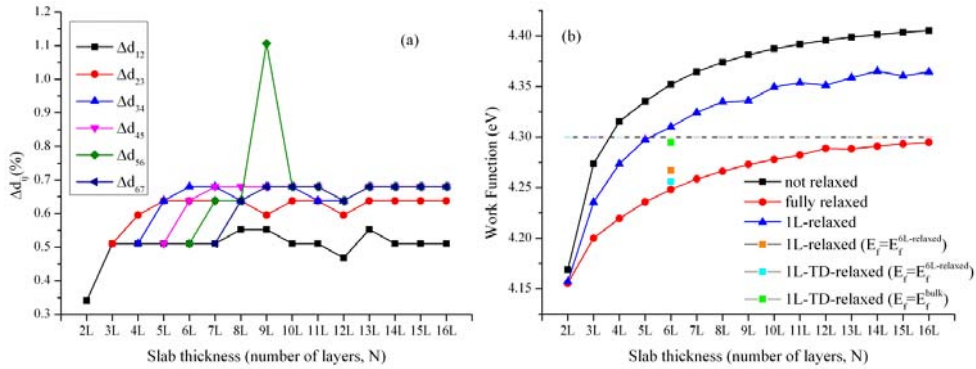


Figure 3.3. (a) Percentage change of interlayer distance versus slab thickness ( $\Delta d_{ij}$  is the distance between layers  $i$  and  $j$  normalized to the initial layer spacing  $d_0$ ). (b) The work function of H:Si(111) with respect to slab thickness.

outside the surface when the potential reaches a constant flat level. Due to periodic boundary conditions, a slab calculation with nonsymmetrical interfaces at each side will cause an artificial electric field. Dipole correction using a saw tooth electric field with zero amplitude along the non-periodic component of the slab has been implemented to remove the

additional field.<sup>22</sup> The same method was applied to extract radical dipoles. The induced surface dipole has been calculated by subtracting the radical dipole from the total dipole.

- 3) Finally the work function is determined after subtracting the bulk Fermi energy, calculated independently, from the vacuum level:

$$WF = E_{vac} - E_F \text{ (eq. 3.3)}$$

The structure of our hydrogenated slab supercell and the average electrostatic potential are plotted in Figure 3.4. For surface-modified slabs, we replace only the hydrogens of the top surface with selected terminations to achieve the specified concentration.

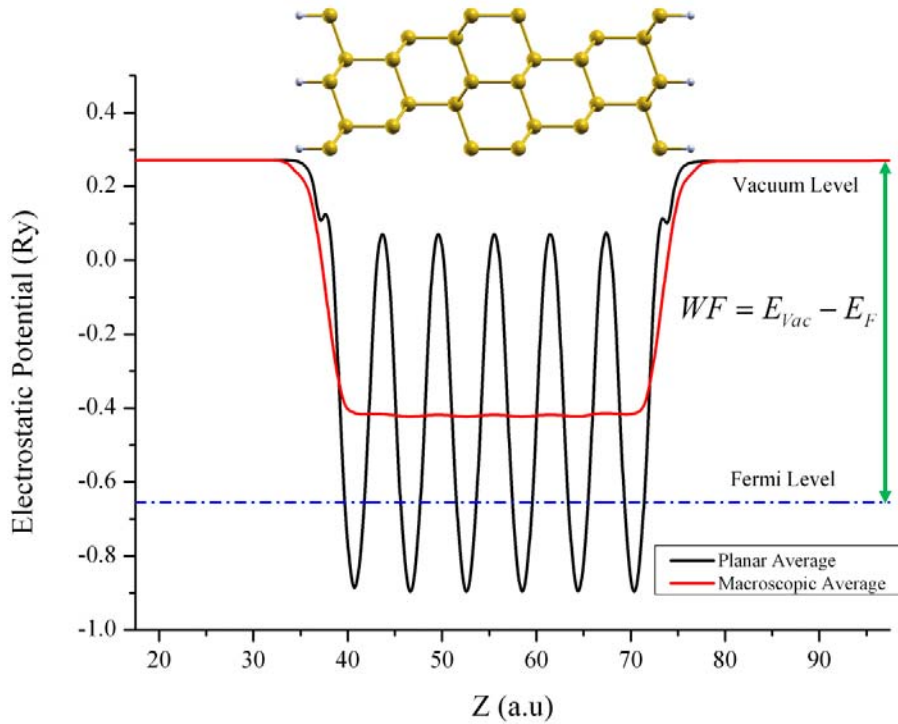


Figure 3.4. Macroscopic and planar average of the electrostatic potential across the 6-layer thick slab.

## 3.3 Results and discussion

In order to understand how the work function depends on surface properties, we study various types of terminating species with 50% and 100% coverage assembled on a Si(111) surface. As it is depicted in Figure 3.5, there is a significant change in the work function for the considered variety of surface terminations (see table 3.2, 3.5 and 3.8 for tabulated  $WF$  values along with  $IP$  and  $EA$  data). Our analysis attributes this to electron valency and electronegativity. We analyze the work function change for elements from group 16 (chalcogens) and 17 (halogens) of the periodic table and from the second period starting from boron. Surface termination species are sorted along the horizontal axis based on electronegativity of the tether/terminating atomic species, starting from the lowest value in each case. The work function for hydrogenated silicon surface is also shown for comparison. Below we discuss separately the work function trends for each classification.

### 3.3.1 Halogens

As seen in Figure 3.5(a), the work function increases with increasing halogen atom electronegativity; this trend is observed for each percentage separately. The increase is readily explained. Radical halogens (halides) do not have permanent dipole, therefore the work function is determined solely from the bond dipole. Each linker has a higher electronegativity compared to silicon, so they are chemisorbed with positive charge accumulation at the substrate (p-doped). This creates a dipole layer and the resultant field opposes electron acceleration towards outside the surface. Table 3.1 shows the Löwdin charge analysis for halogen modification. As the difference between the terminating atom electronegativity and the silicon atom increases more charge is withdrawn and consequently the bond dipole and surface potential are higher. Doubling the coverage has almost no effect on the local charge transfer at the adsorption sites to justify large work function change with coverage. However, the total charge

transfer at the interface is twice for full coverage compared to 50% adsorption and we attribute the sensitivity in the vacuum level to the decreased interaction between adsorbates as the covalent radius decreases from iodine to fluorine. This is exemplified in Figure 3.6(a) and (b) where the excess charge density of iodine and fluorine-terminated silicon surface compared to H:Si(111) is shown. Orbital overlap between neighboring iodine atoms (iodine has the largest diatomic distance among all investigated halogens) that is pronounced at full coverage, compensates the increased field strength due to charge injection into the substrate compared to half coverage and results in a slightly lower work function shift for fully iodine covered silicon surface.

Table 3.1. Löwdin charge analysis for halogen-modified Si(111) surface for half and full coverage  $\Delta q_{Si(1n)}$  indicates charge change of Si atoms in contact with halogen elements, and  $\Delta q_{Si(2n)}$  corresponds to charge change averaged over neighboring atoms.  $\Delta q_{tot}$  is the total charge difference after modification, and  $q_x$  is the local charge on the halogen species. The electron charge is used as unit.

	-I		-Br		-Cl		-F	
Coverage	50%	100%	50%	100%	50%	100%	50%	100%
$\Delta q_{Si(1n)}$	-0.03	-0.03	-0.13	-0.14	-0.22	-0.23	-0.53	-0.56
$\Delta q_{Si(2n)}$	0.01	0.02	0.02	0.03	0.02	0.05	0.06	0.12
$\Delta q_{tot}$	-0.01	-0.01	-0.07	-0.11	-0.11	-0.18	-0.23	-0.45
$q_x$	-7.07	-7.03	-7.16	-7.12	-7.22	-7.19	-7.46	-7.44

Several experimental results compare favorably with our predictions. For p-doped/n-doped H:Si(111), the work function of 4.35/4.17 eV was measured by Hacker.<sup>4</sup> The p-doped value is surprisingly close to our obtained result for undoped H:Si(111), however, it is expected that the real value lies somewhere between 4.17 and 4.35 eV. In another work by Lopinski *et al.*,<sup>3</sup> chlorine termination of low-doped n-type Si(111) induces a large (1.2-1.5 eV) increase in the work function which is consistent with our calculated value for full coverage. Partial coverage of H:Si(111) with  $-C_6H_4-Br$  termination results in a work function around 5.13 eV.<sup>7</sup>

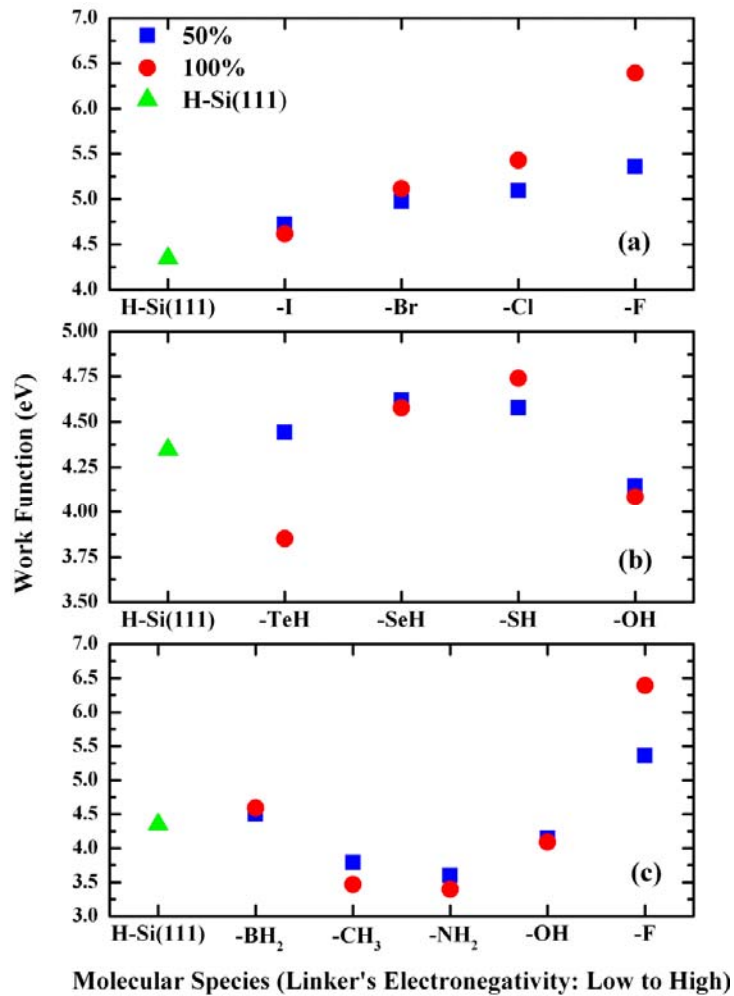


Figure 3.5. Work function changes due to different surface termination for half and full coverage: (a) halogens, (b) chalcogens and (c) linkers from second row of the periodic table.

The increase is almost the same as in our calculations for the bromine covered surface. In recent experiments carried out for samples with two different doping levels, the reported  $WF$  values follow the trends observed here;  $WF$  is 4.16/4.24 eV for H-terminated surface, 4.32 for the  $WF$  of Br-terminated surface, and 4.60 eV for Cl-terminated surface.<sup>7</sup> Additionally, our calculated values for ionization potentials (see table 3.2) are in agreement with other theoretical and experimental studies.<sup>7</sup>



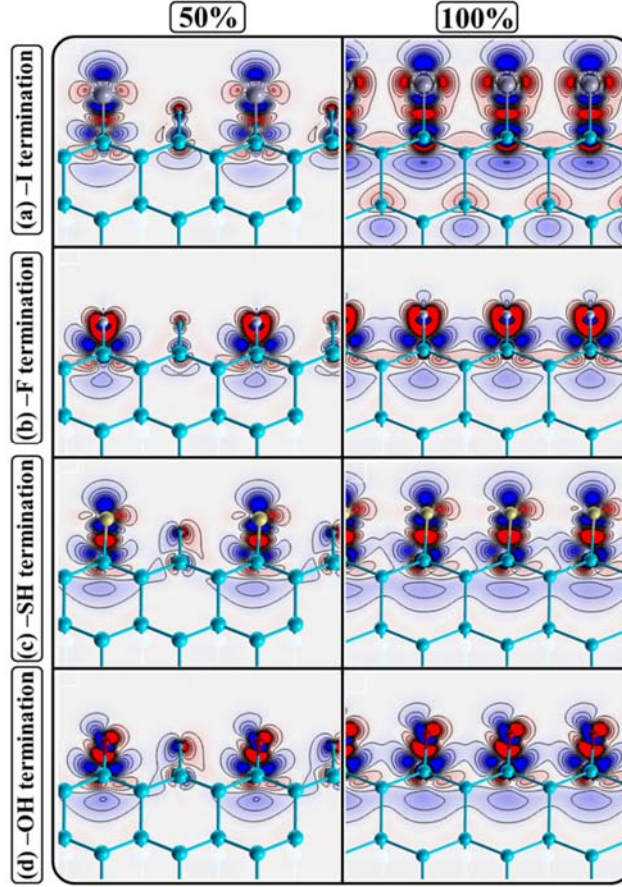


Figure 3.6. Charge density difference,  $\Delta n = (n_{\text{H:Si(111)-M}} - [n_{\text{H:Si(111)}} + n_{\text{M}}])$ , for three different surface modifications (M): (a) and (b) are iodine and fluorine, non-polar adsorbates that increase the  $WF$ , (c)  $-SH$ , a polar species that increases the  $WF$ , and (d)  $-OH$ , a polar adsorbate that decreases the  $WF$ . The contours are drawn in linear scale from  $-0.01$  to  $0.01 e/a_0^3$ , with the increment of  $0.002 e/a_0^3$  and isosurfaces of  $\pm 0.005 e/a_0^3$  are shown. The charge flows from blue to red regions.

Table 3.2. Work function,  $WF$ , electron affinity,  $EA$  ( $E_{\text{vac}} - E_{\text{C}}$ ), and ionization potential,  $IP$  ( $E_{\text{vac}} - E_{\text{V}}$ ), for halogen-modified H:Si(111) surfaces at half and full coverage. Values for H:Si(111) surface are tabulated for comparison.

	50%			100%		
	$WF$ (eV)	$EA$ (eV)	$IP$ (eV)	$WF$ (eV)	$EA$ (eV)	$IP$ (eV)
<b>H:Si(111)</b>	4.35	3.88	4.72	4.35	3.88	4.72
<b>-I</b>	4.72	4.23	4.96	4.62	4.12	4.40
<b>-Br</b>	4.98	4.51	5.33	5.12	4.65	5.40
<b>-Cl</b>	5.09	4.62	5.45	5.43	4.95	5.74
<b>-F</b>	5.36	4.89	5.70	6.39	5.91	6.67

### 3.3.2 Chalcogens

Using chalcogen tether atoms, we calculated the work function variation of H:Si(111)–XH surfaces where X = O, S, Se, Te. Figure 3.5(b) shows the  $WF$  for two coverage. Compared to the halogen-terminated surfaces, the work function does not increase monotonically with increasing tether electronegativity. The difference is attributed to the non-zero dipole moment of the surface radicals and yields a more complex behavior. For example, Hacker<sup>4</sup> observed that the Si–O–C surface bonding exhibited a lower work function than Si–C–C and Si–S–C. In this study, the Si(111)–CH<sub>3</sub> surface shows lower work function than –OH terminated surface and both are lower than the Si(111)–SH surface. Hunger *et al.*<sup>1</sup> measured the work function of the H:Si(111) after sulfur exposure and they got the value of 4.85 eV which is close to our calculated value for –SH termination. In the same work, the value of 4.42 eV has been reported for the  $WF$  of unmodified H:Si(111) surface. The charge transfer trend tabulated in Table 3.3 shows that the change in  $WF$  does not follow the electronegativity trend for different chalcogen tethers. Similar to non-polar species, the local charge transfer is insensitive to surface coverage. Except than Te (note that Te results are less accurate due to the large covalent radius) there is positive charge accumulation on backbond silicon atoms which increases with linker electronegativity and almost doubles from 50% to 100% coverage.

To interpret the  $WF$  results, we further analyzed the electronic structure and the various contributions to the dipole moments (see Table 3.4). The calculated dipole moment of radicals in isolation on its own cannot account for this behavior, however, the induced dipole (both sign and magnitude) offers an interpretation. In the case of oxygen, the –OH bond is strongly polarized and charges are shifted towards the oxygen atom which causes a large radical dipole moment. The bonding of –OH to the silicon substrate involves positive charge donation and the polarity of the bond causes an increase in the work function. At the same time  $WF$  decreases by the induced dipole moment of –OH. Therefore, the change has two components: one from the induced dipole moment of –OH and one from the associated dipole moment of the Si–O bond. The total dipole is

described by  $p = p_0 + p(\text{OH})\cos\alpha$ , where  $\alpha$  is the angle between the OH-plane and the surface normal. The values of  $\alpha$  for  $-\text{OH}$ ,  $-\text{SH}$ ,  $-\text{SeH}$  and  $-\text{TeH}$  for half (full) coverage are  $59.93^\circ$  ( $60.93^\circ$ ),  $83.81^\circ$  ( $80.73^\circ$ ),  $86.9^\circ$  ( $85.09^\circ$ ), and  $89.84^\circ$  ( $92.3^\circ$ ), respectively. As a result, the value of  $\cos\alpha$  decreases as the covalent radius increases. The radical dipole moment along the surface normal vector ( $p(\text{OH})\cos\alpha$ ) also decreases. This explanation is consistent with the trends of work function observed in Figure 3.5(b). Note that the biggest change in  $\alpha$  happens for  $-\text{SH}$  and  $-\text{TeH}$  which significantly alters the surface potential, hence the  $WF$ , by going from half to full coverage.

In the case of Te, the second component completely vanishes and the same situation occurs for Se. Considering  $-\text{TeH}$  termination, the direction of the radical dipole changes by moving from half to full coverage. This behavior can explain the significant change in the work function from half to full coverage. The surface dipole supports this interpretation. Among all the species in this group, only oxygen (and tellurium at full coverage) show a decrease in the work function which is related to the surface dipole behavior. The dipole inversion between chalcogen species is evident in Figure 3.6(c) and 3.6(d).

Our results for chalcogen-terminated Si substrate are also consistent with experimental studies. Besides the previously mentioned agreement on thiolated surfaces,<sup>3</sup> the work function value of 4.22 eV, measured by Hunger *et al.*<sup>23</sup> in the case of H:Si(111) partially modified by  $-\text{OH}$  group, compares favorably with our calculation. In the same work, the work function for the same structure partially modified with  $-\text{C}_6\text{H}_4-\text{OCH}_3$  yielded a value of 4.06 eV.

Table 3.3. Löwdin charge analysis for chalcogen-modified Si(111) surface for half and full coverage.  $\Delta q_{\text{Si}(1n)}$  indicates charge change for Si atoms in contact with chalcogen elements, and  $\Delta q_{\text{Si}(2n)}$  corresponds to charge change averaged over neighboring atoms.  $\Delta q_{\text{tot}}$  is the total charge difference after modification, and  $q_x$  is the local charge on the chalcogen species.  $q_x + q_H$  is the total charge on the  $-\text{XH}$  radical (X=Te, Se, S, O). The electron charge is used as unit.

	<b>-TeH</b>		<b>-SeH</b>		<b>-SH</b>		<b>-OH</b>	
	50%	100%	50%	100%	50%	100%	50%	100%
$\Delta q_{\text{Si}(1n)}$	0.04	0.05	-0.04	-0.04	-0.12	-0.11	-0.47	-0.46
$\Delta q_{\text{Si}(2n)}$	0.00	0.00	0.01	0.02	0.02	0.04	0.06	0.11
$\Delta q_{\text{tot}}$	0.02	0.05	-0.02	-0.02	-0.04	-0.08	-0.18	-0.35
$q_x$	-5.99	-5.95	-6.12	-6.10	-6.20	-6.21	-6.73	-6.74
$q_x + q_H$	-6.98	-6.96	-7.03	-7.02	-7.05	-7.05	-7.31	-7.32

Table 3.4. Dipole analysis and surface potential changes for chalcogen-modified H:Si(111) surface for half and full coverage.  $\mu_R$ ,  $\mu_{\text{ind}}$ ,  $\mu_{\text{surf}}$  ( $\mu_{\text{ind}} = \mu_{\text{surf}} - \mu_R$ ) are the radical dipole, induced dipole and surface dipole in Debye, respectively.  $\Delta V$  (eV) is the change in surface potential of the new surface compare to H:Si(111).

<b>R</b>	50%				100%			
	<b>Radical <math>\mu_R</math></b>	$\mu_{\text{ind}}$	$\mu_{\text{surf}}$	$\Delta V$	<b>Radical <math>\mu_R</math></b>	$\mu_{\text{ind}}$	$\mu_{\text{surf}}$	$\Delta V$
<b>-OH</b>	0.83	-0.76	0.07	0.20	0.79	-0.70	0.09	0.26
<b>-SH</b>	0.12	-0.20	-0.08	-0.23	0.12	-0.25	-0.13	-0.40
<b>-SeH</b>	0.02	-0.12	-0.09	-0.26	0.04	-0.12	-0.08	-0.23
<b>-TeH</b>	0.00	-0.03	-0.03	-0.09	0.00	0.17	0.17	0.49

Selenium adsorption on Si(111)7×7 surface increases the work function locally<sup>24-27</sup> similar to our calculations from first-principles. There are no experimental data on tellurium-modified surface as some previous works predict a low adsorption of tellurium on Si(100).<sup>28</sup> However, recent studies have claimed successful passivation of Si nanowires with tellurium,<sup>29</sup> which was highlighted for being highly sensitive to ammonia and propylamine at room temperature.<sup>30</sup>

Table 3.5. Work function,  $WF$ , electron affinity,  $EA$  ( $E_{vac}-E_C$ ), and ionization potential,  $IP$  ( $E_{vac}-E_V$ ), for chalcogen-modified H:Si(111) surfaces at half and full coverage. Values for H:Si(111) surface are tabulated for comparison.

	50%			100%		
	$WF$ (eV)	$EA$ (eV)	$IP$ (eV)	$WF$ (eV)	$EA$ (eV)	$IP$ (eV)
<b>H:Si(111)</b>	4.35	3.88	4.72	4.35	3.88	4.72
<b>-TeH</b>	4.44	3.96	4.76	3.85	-	-
<b>-SeH</b>	4.62	4.14	4.96	4.58	4.11	4.44
<b>-SH</b>	4.58	4.11	4.88	4.74	4.27	4.70
<b>-OH</b>	4.15	3.68	4.46	4.09	3.61	4.31

### 3.3.3 Second period

The previous investigations were carried out considering bonding to the Si surface with atoms belonging to the same group, i.e., the number of valence electrons is fixed. Now we consider tether atoms along the second row of the periodic table, from boron up to fluorine. As we can see in Figure 3.5(c), the work function follows the same non-monotonic behavior for the both coverage. As surface Si passivation through boron and fluorine bonds shows a  $WF$  increase, the other tethers induce a decrease in the work function relative to the hydrogenated silicon surface. Full coverage gives slightly bigger decrease than half coverage.

As before, we explain the observed behavior using the analysis of the charge transfer and dipoles. The electronegativity of the tethers increases with increasing valency by a nearly fix step of 0.5 Pauling, thus explaining the charge withdrawal seen in Table 3.6. By comparing the change of surface dipole moments (see Table 3.7) with the work function changes across different species, we see that the negative surface dipole increases the work function while the inverse holds for a positive dipole. This trend is corroborated by the radical dipole changes. The dipole rearrangement in this case is exemplified in Figure 3.6 (d) by the plotted charge density difference between the oxygen-terminated silicon surface and H:Si(111).

Our values for methyl modifications are very close to experiment. The work function of the methyl-terminated surface was found to be 3.86 eV with a surface dipole of -0.4 eV.<sup>2</sup> Our predictions are consistent with measurements performed by Kuo *et al.*<sup>6</sup> which showed both the increase and decrease of the *WF* for sulfur and amine modified surfaces, respectively. It is worth noting that for Si(100) surface modified by  $-\text{C}_6\text{H}_4-\text{NH}_2$ , He *et al.*<sup>31</sup> measured the *WF* in the range of 4.04-4.11 eV (for different doping types and concentration at low surface coverage) which is in line with our results for  $-\text{NH}_2$  modification. Our analysis of the change in electron affinity for H:Si(111) and methylated Si(111) surface is also in good agreement with the experimental results. For example, Hunger *et al.*<sup>1-2</sup> measured the value of 4.17 eV<sup>1</sup> and 3.68 eV<sup>2</sup> for the electron affinity of H:Si(111) surface and methylated Si(111) surface respectively. Our results for these surfaces show 0.55 eV shift in the electron affinity of the H:Si(111) after 50% methylation, which is comparable to the measured difference of 0.49 eV (see table 3.5 and 3.8 for complete table and other linkers).

Table 3.6. Löwdin charge analysis for half and full coverage for Si(111) surface modified with elements from second period.  $\Delta q_{\text{Si}(1n)}$  indicates charge change for Si atoms in contact with the element, and  $\Delta q_{\text{Si}(2n)}$  corresponds to charge change averaged over neighboring atoms.  $\Delta q_{\text{tot}}$  is the total charge difference after modification, and  $q_x$  is the local charge on the element.  $q_x+q_H$  is the total charge on the  $-\text{XH}$  radical.

	$-\text{BH}_2$		$-\text{CH}_3$		$-\text{NH}_2$		$-\text{OH}$		$-\text{F}$	
<b>Coverage</b>	50%	100%	50%	100%	50%	100%	50%	100%	50%	100%
$\Delta q_{\text{Si}(1n)}$	-0.02	-0.01	-0.20	-0.18	-0.36	-0.34	-0.47	-0.46	-0.53	-0.56
$\Delta q_{\text{Si}(2n)}$	-0.02	-0.03	0.02	0.04	0.05	0.09	0.06	0.11	0.06	0.12
$\Delta q_{\text{tot}}$	-0.03	-0.05	-0.06	-0.15	-0.12	-0.26	-0.18	-0.35	-0.23	-0.45
$q_x$	-3.21	-3.20	-4.74	-4.73	-5.85	-5.85	-6.73	-6.74	-7.46	-7.44
$q_x+q_H$	-5.05	-5.05	-7.12	-7.15	-7.20	-7.23	-7.31	-7.32	-	-

Table 3.7. Dipole analysis and surface potential changes for modified H:Si(111) surface using second period elements for bonding terminating species.  $\mu_R$ ,  $\mu_{ind}$ ,  $\mu_{surf}$  ( $\mu_{ind}=\mu_{surf}-\mu_R$ ) are the radical dipole, induced dipole and surface dipole in Debye, respectively.  $\Delta V$  (eV) is the change in surface potential of the new surface compare to H:Si(111).

R	50%				100%			
	Radical $\mu_R$	$\mu_{ind}$	$\mu_{surf}$	$\Delta V$	Radical $\mu_R$	$\mu_{ind}$	$\mu_{surf}$	$\Delta V$
-BH <sub>2</sub>	0.56	-0.61	-0.05	-0.16	0.57	-0.65	-0.08	-0.24
-CH <sub>3</sub>	0.71	-0.52	0.19	0.56	0.71	-0.42	0.30	0.88
-NH <sub>2</sub>	1.30	-1.05	0.25	0.75	1.18	-0.86	0.32	0.95
-OH	0.83	-0.76	0.07	0.20	0.79	-0.70	0.09	0.26
-F	0.00	-0.34	-0.34	-1.01	0.00	-0.69	-0.69	-2.05

Table 3.8. Work function,  $WF$ , electron affinity,  $EA$  ( $E_{vac}-E_C$ ), and ionization potential,  $IP$  ( $E_{vac}-E_V$ ), for H:Si(111) surfaces modified using tethers from the second row of the periodic table at half and full coverage. Values for H:Si(111) surface are tabulated for comparison.

	50%			100%		
	$WF$ (eV)	$EA$ (eV)	$IP$ (eV)	$WF$ (eV)	$EA$ (eV)	$IP$ (eV)
H:Si(111)	4.35	3.88	4.72	4.35	3.88	4.72
-BH <sub>2</sub>	4.50	4.26	4.86	4.59	4.58	4.93
-CH <sub>3</sub>	3.79	3.32	4.15	3.47	2.99	3.82
-NH <sub>2</sub>	3.59	3.12	3.91	3.39	2.92	3.60
-OH	4.15	3.68	4.46	4.09	3.61	4.31
-F	5.36	4.89	5.70	6.39	5.91	6.67

### 3.3.4 Comparison with experiment

Compared to available experimental results, our simulations are not only consistent with the literature but offer important insights into the origin of changes in the WF upon modifying the termination of the Si (111) surface. For example the obtained value for the WF of bare H:Si(111) in this study, 4.35 eV, is consistent with the measured WF<sup>4</sup> (determined from the secondary electron cutoffs obtained from ultraviolet photoemission spectroscopy (UPS) data) for p-doped/n-doped H:Si(111), 4.35/4.17 eV, where the value for undoped H:Si(111) lies in this interval. Measured WFs (calculated from the secondary electron cutoff energies) of the H:Si(111) before/after sulfur exposure in ref. 1 are

4.42/4.85 eV, in agreement with our calculated values for bare and –SH terminated Si(111). Another WF measurement<sup>3</sup> (using Kelvin probe) on chlorinated n-type Si(111) revealed a large (1.2-1.5 eV) increase in the WF which is entirely consistent with our computed shift for a fully chlorinated silicon surface. Recent experiments on two samples with different doping levels showed WF (determined from UPS spectra) values as follows: 4.16/4.24 eV for H-terminated surface, 4.32 eV for Br-terminated surface, and 4.60 eV for Cl-terminated surface.<sup>7</sup> This trend is completely in agreement with our findings. Another measurement for the WF of H:Si(111) partially modified by –OH groups gives a WF (determined from secondary electron onset in UPS spectra) of 4.22 eV<sup>23</sup> which compares favorably with our work. Similar to our calculations, other studies showed that selenium adsorption on Si(111)7×7 surface increases the WF up to 0.5 eV.<sup>25-27</sup>

The calculated WF shifts for the various terminations are tabulated in Table 3.9 using the H:Si(111) surface as reference. Trends are in agreement with available experimental data as described above. This gives us confidence regarding the computational method. Since surface passivation is an important part of the surface functionalization process, playing a key-role in controlling the reactivity and electronic properties of the surface, the results of this Chapter can help experimentalists to choose terminating species with detailed knowledge of how they modify surface properties. In particular, one can get direct insight of surface reactivity as the latter can be related to the shifts in the WF or the substantial charge transfer into/from the surface.



Table 3.9. WF shift compared to bare H:Si(111) surface at half and full coverage and comparison with available experimental data.

Termination	<i>Calculated</i> $\Delta WF$ (eV); 50%	<i>Calculated</i> $\Delta WF$ (eV); 100%	<i>Measured WF shift</i> (eV)	<i>Method (Reference)</i>
-H	0.00	0.00	-	-
-I	0.37	0.27	-	-
-Br	0.63	0.77	0.16	UPS (Ref. 7)
-Cl	0.74	1.08	0.44, 1.2-1.5	UPS (Ref. 7), Kelvin probe (Ref. 3)
-F	1.01	2.04	-	-
-TeH	0.09	-0.5	-	-
-SeH	0.27	0.23	0.50	UPS (ref. 25-27)
-SH	0.23	0.39	0.07/0.68	UPS (ref. 1)
-OH	-0.20	-0.26	-	-
-BH <sub>2</sub>	0.15	0.24	-	-
-CH <sub>3</sub>	-0.56	-0.88	-	-
-NH <sub>2</sub>	-0.76	-0.96	-	-

### 3.4 Concluding remarks

Calculations based on density functional theory have been carried out for modified silicon (111) surfaces. Several polar and non-polar adsorbates such as halogens, chalcogens and second row elements in the periodic table have been considered on a H:Si(111) surface. Our comprehensive study allows reasonable interpretation for chemical trends to be predicted from first-principles based on work function variation in each case. To explain the changes of the work function for different adsorbates at different coverage, we found radical dipole, bond dipole, the electronegativity and range of interatomic interaction of the tether atoms to be of profound importance.

A larger radical dipole component along the surface normal causes increased change in the work function with the sign of the  $WF$  shift determined by the direction of the dipole. A bond dipole is formed by charge reorganization across the tether bond with the surface silicon. This creates the surface dipole layer which affects the electron acceleration towards the vacuum and the

corresponding work. The strength and the direction of the dipole field depend on the amount and sign of charge transfer. The valency and electronegativity of the linker specify the transferred charge as confirmed by our charge analysis. All selected tethers have higher electronegativity than silicon. This results in electron withdrawal from the silicon surface and the inward (bond) dipole field is expected to increase the  $WF$ . This is the case for surface termination by halogens for which a monotonic increase is predicted with increasing halogen electronegativity. However for other adsorbates the radical dipole moment can reduce or even negate this effect. With the exception of H:Si(111)–OH, modification of H:Si(111)–XH via other chalcogen tethers, tends to increase the work function, but to a lesser degree than halogen termination. Reduction compared to the hydrogenated surface is observed for surfaces covered with –CH<sub>3</sub> and –NH<sub>2</sub>. The electronic profile may also depend on the surface coverage. However, due to the covalent radius of the tether atoms there are no large changes occurring on local charges on the surface Si atoms, therefore, the work function shows overall weak dependence on coverage percentage. Finally, halogens seem to increase the  $WF$  more than other species, that is, with the exception of iodine that has the largest size and the lowest electronegativity among the studied halogens.

Controlling the structure of silicon surfaces, their chemical and physical properties, is scientifically interesting and particularly important for technology. Aiming at a microscopic understanding of the chemical trends, here we took a first step of studying silicon surfaces modified with experimentally accessible terminations. Our approach is able to predict from first-principles the  $WF$  and values very close to measurements have been obtained. Also all the identified chemical trends are in good agreement with currently available experimental data. This analysis forms a basis for efforts in creating surfaces by design.

## 3.5 References

1. Hunger, R.; Pettenkofer, C.; Scheer, R., Dipole formation and band alignment at the Si(111)/CuInS<sub>2</sub> heterojunction. *J. Appl. Phys.* **2002**, *91*, 6560.
2. Hunger, R.; Fritsche, R.; Jaeckel, B.; Jaegermann, W.; Webb, L. J.; Lewis, N. S., Chemical and electronic characterization of methyl-terminated Si(111) surfaces by high-resolution synchrotron photoelectron spectroscopy. *Phys. Rev. B* **2005**, *72*, 045317-045317.
3. Lopinski, G.; Eves, B.; Hul'ko, O.; Mark, C.; Patitsas, S.; Boukherroub, R.; Ward, T., Enhanced conductance of chlorine-terminated Si(111) surfaces: Formation of a two-dimensional hole gas via chemical modification. *Phys. Rev. B* **2005**, *71*, 125308-125308.
4. Hacker, C. A., Modifying electronic properties at the silicon–molecule interface using atomic tethers. *Solid-State Electron.* **2010**, *54*, 1657-1664.
5. Cooper, A. J.; Keyvanfar, K.; Deberardinis, A.; Pu, L.; Bean, J. C., Dopant passivation and work function tuning through attachment of heterogeneous organic monolayers on silicon in ultrahigh vacuum. *Appl. Surf. Sci.* **2011**, *257*, 6138-6144.
6. Kuo, C. H.; Liu, C. P.; Lee, S. H.; Chang, H. Y.; Lin, W. C.; You, Y. W.; Liao, H. Y.; Shyue, J. J., Effect of surface chemical composition on the work function of silicon substrates modified by binary self-assembled monolayers. *Phys. Chem. Chem. Phys.* **2011**, *13*, 15122-15126.
7. Li, Y.; O'Leary, L. E.; Lewis, N. S.; Galli, G., Combined Theoretical and Experimental Study of Band-Edge Control of Si through Surface Functionalization. *J. Phys. Chem. C* **2013**, *117*, 5188-5194.
8. Oura, K.; Katayama, M.; Zotov, A. V.; Lifshits, V. G.; Saranin, A. A., *Surface Science*; Springer Berlin Heidelberg, 2003.
9. Fall, C. J.; Binggeli, N.; Baldereschi, A., Deriving accurate work functions from thin-slab calculations. *J. Phys. Condens. Matter* **1999**, *11*, 2689-2696.
10. Singh-Miller, N. E.; Marzari, N., Surface energies, work functions, and surface relaxations of low-index metallic surfaces from first principles. *Phys. Rev. B* **2009**, *80*, 235407-235407.
11. Segev, L.; Salomon, A.; Natan, A.; Cahen, D.; Kronik, L.; Amy, F.; Chan, C. K.; Kahn, A., Electronic structure of Si(111)-bound alkyl monolayers: Theory and experiment. *Phys. Rev. B* **2006**, *74*, 165323-6.
12. Hofmann, O. T.; Egger, D. A.; Zojer, E., Work-function modification beyond pinning: When do molecular dipoles count? *Nano Lett.* **2010**, *10*, 4369-4374.
13. Li, Y.; Galli, G., Electronic and spectroscopic properties of the hydrogen-terminated Si(111) surface from ab initio calculations. *Phys. Rev. B* **2010**, *82*, 045321-045321.

14. Kanai, Y.; Selloni, A., Competing mechanisms in the optically activated functionalization of the hydrogen-terminated Si(111) surface. *J. Am. Chem. Soc.* **2006**, *128*, 3892-3.
15. Aliano, A.; Li, Y.; Cicero, G.; Galli, G., Structural and Electronic Properties of the Methyl-Terminated Si(111) Surface. *J. Phys. Chem. C* **2010**, *114*, 11898-11902.
16. Barone, V.; Cacelli, I.; Ferretti, A.; Monti, S.; Prampolini, G., Organic Functionalization and Optimal Coverage of a Silicon(111) Surface in Solvent: A Computational Study. *J. Phys. Chem. C* **2011**, *115*, 4145-4154.
17. Pourtois, G.; Lauwers, A.; Kittl, J.; Pantisano, L.; Soree, B.; De Gendt, S.; Magnus, W.; Heyns, A.; Maex, K., First-principle calculations on gate/dielectric interfaces: On the origin of work function shifts. *Microelectron. Eng.* **2005**, *80*, 272-279.
18. Bocquet, M. L.; Rappe, A. M.; Dai, H. L., A density functional theory study of adsorbate-induced work function change and binding energy: Olefins on Ag(111). *Mol. Phys.* **2005**, *103*, 883-890.
19. Rusu, P. C.; Brocks, G., Surface dipoles and work functions of alkylthiolates and fluorinated alkylthiolates on Au(111). *J. Phys. Chem. B* **2006**, *110*, 22628-22634.
20. Bagus, P.; Staemmler, V.; Wöll, C., Exchangelike Effects for Closed-Shell Adsorbates: Interface Dipole and Work Function. *Phys. Rev. Lett.* **2002**, *89*, 096104-096104.
21. Giannozzi, P.; Baroni, S.; Bonini, N.; Calandra, M.; Car, R.; Cavazzoni, C.; Ceresoli, D.; Chiarotti, G. L.; Cococcioni, M.; Dabo, I.; Dal Corso, A.; de Gironcoli, S.; Fabris, S.; Fratesi, G.; Gebauer, R.; Gerstmann, U.; Gougoussis, C.; Kokalj, A.; Lazzeri, M.; Martin-Samos, L.; Marzari, N.; Mauri, F.; Mazzarello, R.; Paolini, S.; Pasquarello, A.; Paulatto, L.; Sbraccia, C.; Scandolo, S.; Sclauzero, G.; Seitsonen, A. P.; Smogunov, A.; Umari, P.; Wentzcovitch, R. M., QUANTUM ESPRESSO: A modular and open-source software project for quantum simulations of materials. *J. Phys. Condens. Matter* **2009**, *21*, 395502-395521.
22. Bengtsson, L., Dipole correction for surface supercell calculations. *Phys. Rev. B* **1999**, *59*, 12301-12304.
23. Hunger, R.; Jaegermann, W.; Merson, A.; Shapira, Y.; Pettenkofer, C.; Rappich, J., Electronic structure of methoxy-, bromo-, and nitrobenzene grafted onto Si(111). *J. Phys. Chem. B* **2006**, *110*, 15432-15441.
24. Lou, J. L.; Shiu, H. W.; Chang, L. Y.; Wu, C. P.; Soo, Y. L.; Chen, C. H., Preparation and characterization of an ordered 1-dodecylthiol monolayer on bare Si(111) surface. *Langmuir* **2011**, *27*, 3436-3441.
25. Davydov, S. Y., Effect of Adsorption of Group VI Atoms on the Silicon Work Function. *Phys. Solid State* **2005**, *47*, 1779-1779.
26. Papageorgopoulos, A. C.; Kamaratos, M., Adsorption and desorption of Se on Si(100)2×1: surface restoration. *Surf. Sci.* **2000**, *466*, 173-182.

27. Papageorgopoulos, A. C.; Kamaratos, M., Interactions between Se, Cs and Si upon Se adsorption on Cs/Si(111)-7×7 surfaces. *J. Phys. Condens. Matter* **2002**, *14*, 5255-5270.
28. Yoshikawa, S. A.; Nogami, J.; Quate, C. F.; Pianetta, P., Behavior of tellurium on silicon (100). *Surf. Sci.* **1994**, *321*, L183-L188.
29. Yang, L.; Lin, H.; Wang, T.; Ye, S.; Shao, M.; Lee, S.-T., Tellurium-modified silicon nanowires with a large negative temperature coefficient of resistance. *Appl. Phys. Lett.* **2012**, *101*, 133111-133111.
30. Yang, L.; Lin, H. Y.; Zhang, Z. S.; Cheng, L.; Ye, S. Y.; Shao, M. W., Gas sensing of tellurium-modified silicon nanowires to ammonia and propylamine. *Sensor. Actuat. B-Chem.* **2013**, *177*, 260-264.
31. He, T.; Ding, H.; Peor, N.; Lu, M.; Corley, D. A.; Chen, B.; Ofir, Y.; Gao, Y.; Yitzchaik, S.; Tour, J. M., Silicon/molecule interfacial electronic modifications. *J. Am. Chem. Soc.* **2008**, *130*, 1699-1710.

## Chapter 4

# Density Functional Theory with van der Waals Corrections Study of the Adsorption of Alkyl, Alkylthiol, Alkoxy, and Amino-Alkyl Chains on the H:Si(111) Surface

### 4.1. Introduction

In this Chapter we present a first-principles DFT study of a prototypical H:Si(111) surface functionalized with different length alkyl chains that are attached to the surface via four different linkers. We apply DFT, with the inclusion of the van der Waals interaction that is important for inter-chain interactions, to calculate the adsorption energy, structure and chain orientation of a systematic series of SAMs attached to the Si(111) surface, that we can denote as H:Si(111)–X–Alkyl. The SAMs vary in the nature of the linker, namely X = CH<sub>2</sub>, NH, O and S. These linkers are used in experiments for surface modification and we have previously demonstrated that they have a significant impact on the surface properties.<sup>1-2</sup> In addition, these structures allow further functionalization.<sup>3-6</sup> The chain length varies from C<sub>2</sub> to C<sub>12</sub> to provide a wide range of SAM structures which can be used to explain experimentally observed data on alkyl, alkoxy, aminoalkyl and thiolalkylated silicon surfaces.<sup>6-13</sup> We

also predict the properties of new surface-linker-alkyl chain combinations, focusing on adsorption energies, layer thickness, and chain-surface angles.

Organic functionalization of the silicon has been studied thoroughly in both theory<sup>6, 11</sup> and experiment.<sup>14-15</sup> Alkyl monolayers have been always useful for this purpose allowing the surface functionality to be boosted by modifying the head (linker) group or tail group of the SAMs.<sup>5, 16</sup> Apart from carbon itself, O, N and S have been shown to be valuable linker groups. Modification of silicon surfaces using O, N or S alone also has been studied extensively.<sup>4, 12, 17-18</sup>

Oxygen chemisorption on Si(111) surface has been previously studied.<sup>19-20</sup> Reddy *et al.*<sup>21</sup> showed the possibility of methoxy-passivation of the Si(111) surface [Si–OCH<sub>3</sub>] and Haber *et al.*<sup>22</sup> confirmed this surface passivation mode. Michalak *et al.* showed that methanol passivation could be one of the products of the reaction of the H:Si(111) surface with liquid methanol.<sup>23</sup> Their theoretical study predicts the possibility to create full coverage of methoxy-passivated Si(111). However their experimental data shows that the maximum coverage is around 50%. Their later studies using FTIR spectroscopy as a function of solution temperature showed a coverage of *ca.* 30%.<sup>8</sup> More recently they demonstrated that a ‘snap’ surface chemistry can be realized with the readily achieved interchange of Si–F, Si–OH and, more generally, Si–OR (R = alkyl species) species, without any attack of the silicon surface. Consequently, organic self-assembled monolayers and various oxide materials (for example, high- $\kappa$  dielectrics) can be chemically grafted onto an atomically smooth surface.<sup>24</sup> The theoretical results from Solares *et al.*<sup>9</sup> for coverage were consistent with Michalak *et al.* They showed that the Si(111)–OCH<sub>3</sub> surface can, in principle, afford a route to achieve full termination of terrace atop Si sites on an unreconstructed Si(111) surface, offering 100% coverage of functional groups with minimal strain in the alkoxy overlayer. Relative to the Si(111)–CH<sub>3</sub> surface, the chemical and electrical properties of the Si(111)–OCH<sub>3</sub> surface should therefore reflect differences solely arising from changing the Si–C–R bonds into Si–OC–R bonds, as opposed to coverage, packing density, or other major chemical differences arising from residual Si–H bonds, at least on the

terraces of such functionalized surfaces. Using second harmonic generation (SHG) spectroscopy Mitchell *et al.*<sup>25</sup> showed the stability of decyloxy(–O–C<sub>10</sub>H<sub>21</sub>)–terminated Si(111) in air. Other type of modifications, including different aromatic compounds have been investigated.<sup>10</sup>

Juarez *et al.*<sup>6</sup> undertook a comprehensive theoretical investigation of the stability of high coverage structures of small organic and inorganic molecules (–CH<sub>3</sub>, –CCH<sub>3</sub>, –CN, –CH<sub>2</sub>CH<sub>3</sub>, –OCH<sub>3</sub>, –OH, –NH<sub>2</sub>, –NHOH, –ONH<sub>2</sub>) bound to the Si(111) surface via Si–C, Si–N, and Si–O bonds. They investigated the effect of hydrogen bonding interactions between different layers on the structure and stability of OH– and NH<sub>2</sub>–terminated monolayers. Their result showed that intermolecular repulsion is relatively small. However at full coverage on the Si(111) surface there is an intermolecular separation of 3.84 Å which is smaller than the van der Waals diameter of the molecules. They showed that subsurface (backbond) oxidation increases the strength of Si–C bond by 0.78 eV. They found the lowest activation barrier for Si–N bond breaking (0.34 eV) and Si–C bond breaking (0.58 eV). They showed that since the intermolecular repulsion is relatively small for all the molecules investigated a high packing density could be possible.

Hacker<sup>26</sup> investigated various structural and electronic properties of H:Si(111) after formation of Si–O–C, Si–C–C, and Si–S–C bonded alkyl monolayers, and showed almost same contact angle for alkene and thiol functionalized H:Si(111), at 100°. A slightly bigger contact angle of 105° was found for the O linker. A similar study was performed by Ashley *et al.*<sup>27</sup> where they investigated the contact potential difference, work function (WF), change in electron affinity and band bending of a range of phenylacetylene-based molecules (*p*–X–C<sub>6</sub>H<sub>4</sub>≡CH, where X = CF<sub>3</sub>, OCH<sub>3</sub>, and H) covalently bounded onto a hydrogen-terminated silicon surface using scanning Kelvin probe technique. To identify elementary reaction steps and their corresponding energy barriers using DFT Soria *et al.*<sup>12</sup> investigated the reactivity of hydrogenated, chlorinated, and partially chlorinated Si(111) surfaces toward NH<sub>3</sub>, H<sub>2</sub>O, H<sub>2</sub>S, CH<sub>3</sub>NH<sub>2</sub>, CH<sub>3</sub>OH, and CH<sub>3</sub>SH molecules. They found that these molecules have a reaction mechanism with



only one step and an activation barrier around 1.43–1.82 eV. Their activation energy values showed that the H:Si(111) surface is unreactive with these molecules at room temperature. Based on their results the order of reactivity is  $N > O > S$  in term of the headgroup, which shows that while molecular size is important, nucleophilicity also plays a key role.

A desorption energy of 2.04 eV was measured for  $\text{NH}_3$  adsorbed on the Si(100) surface.<sup>28</sup> Theoretical studies for  $\text{NH}_3$  adsorbed on Si(100) predicted bond lengths of 1.75 Å for N–Si and 1.05 Å for N–H and a vertical angle of  $10^\circ$  for the Si–N–**n** (**n** is surface normal vector) angle.<sup>29</sup> Sieval *et al.*<sup>4</sup> developed a method to prepare high density ( $> 50\%$ ) amino-terminated monolayers on silicon surface and confirmed the reactivity of the amine group by further modification. There are other studies of amino terminated monolayers on silicon.<sup>30</sup>  $\text{NH}_3$  adsorption with high coverage was demonstrated<sup>31</sup> on Si(111) and was studied both theoretically and experimentally.<sup>24, 32</sup> Si–N linkages were formed on oxide-free single silicon crystals in the study by Tian *et al.*<sup>17</sup>

Patitsas *et al.*<sup>33</sup> prepared thiophene-based monolayers covalently bonded to a Si(111) surface using a wet chemical approach. They suggested that covalent bonding of thiophenes to the Si surface followed by chemical or electrochemical polymerization would improve electron transport between organic layers and the semiconductor. Lou *et al.*<sup>13</sup> have grown a 1–dodecylthiol (DDT) monolayer on a bare Si(111) surface through ultraviolet-assisted photochemical reaction and an average water contact angle of  $57^\circ$  was found.

Despite the significant body of work on this topic of Si surface functionalization with molecules<sup>15, 34</sup> there are a number of questions that still require further investigation. In particular, there is the question of how structural properties are related to device performance. This can be driven by the type of linker group that anchors the molecule to the Si surface and the chain length. These factors will determine the stability, the coverage, the packing of the chains and ultimately key properties including the WF. To provide a detailed microscopic understanding of the effect of linker and chain length on the structural characteristics of molecule-modified semiconductor surfaces, we present in this

Chapter a first principles density functional theory (DFT), including van der Waals interactions, study of the H:Si(111) surface functionalized with alkyl monolayers and with three different linkers  $X = -NH-, -O-, -S-$ , i.e. amine-alkyl alkoxy, and thiol-alkyl. These are grafted onto the H:Si(111) at half coverage, since this is accepted as the most stable coverage of alkyl monolayers (without linker) in the literature.<sup>35-36</sup> Lacking sufficient experimental data for the other linkers, we worked with this coverage and found that the other alkyl-linker chains do bind to Si(111), even more strongly than alkyl chains linked via carbon. Fixing all calculations to this coverage allowed us to have a meaningful structural comparison between different linkers since the coverage is the same. To examine coverage effects we have calculated the adsorption energy of (X)-hexyl and (X)-dodecyl at H:Si(111) for four other coverages - 25%, 66%, 75% and 100%. This gives a sufficiently large data set for making a judgment about the most stable coverage for different linkers. We find that while the optimal coverage of the alkyl chains on the Si(111) surface is highly sensitive to the type of linker employed, the ordering of stability between linkers is not. The sulfur linker appears to show three regimes of stability as a function of chain length. For the case of alkyl modification there is saturation in the tilt angle but with the other linkers ( $-O-, -NH-, -S-$ ) the tilt angle depends on chain length. This work provides a comprehensive picture of the key structural properties of alkyl functionalized H:Si(111).

This Chapter is organized as follows; In Section 4.2 details of the calculations and structure simulations are explained. Section 4.3 contains the main results of this Chapter. It starts with clarifying the role of van der Waals interactions on the adsorption energy and structural analysis, followed by structural and adsorption energy analysis of different linker-chains. Concluding remarks are presented in Section 4.4.

## 4.2. Computational details

First principles Density Functional Theory (DFT) is a valuable tool for studies of surface modifications of materials such as silicon using organic or inorganic species.<sup>11</sup> Depending on the type of approximate exchange-correlation functional used, DFT can overestimate<sup>37</sup> (mainly for LDA) or underestimate<sup>38</sup> (mainly for GGA) binding energies. Although the binding energies do not coincide with the experiment they reproduce trends and correlate with changes on other properties.<sup>39-40</sup> For example, using DFT-GGA with PW91 functional, Bocquet *et al.*<sup>40</sup> studied the change in the WF of the Ag(111) surface due to physisorption of molecules such as ethylene, vinyl chloride and butadiene. They found optimized adsorption structures consistent with experiment<sup>41</sup> and the trends in the WF changes were the same as experiment. However their calculated binding energies were very small ( $0.03 < BE < 0.07$  eV) compared to experiment.<sup>41</sup> They proposed that the WF changes due to adsorption could be used to calibrate the binding energies. In another theoretical work, Rusu *et al.*<sup>42</sup> investigated  $-CH_3$  and  $-CF_3$  terminated short-chain alkylthiolate monolayers on Au(111). They found that the adsorption energies of alkylthiolates on Au(111) depended on the DFT exchange-correlation functional used but that all functionals gave the same order of stability for the studied binding sites.

Our DFT calculations are carried out using the PWSCF code in the QUANTUM-ESPRESSO (QE) program suite.<sup>43</sup> The Perdew-Burke-Ernzerhof (PBE) functional within the generalized gradient approximation (GGA) and ultrasoft pseudopotentials (USPPs) are used. The number of valence electrons is as follows: Si 4, C 4, N 5, S 5, O 6 and H 1. The kinetic-energy cutoff in the plane wave basis expansion of the valence electron wavefunctions is 35 Ry for the wave function and 400 Ry for the charge density; both are well converged for all elements in our calculations. After inclusion of the vdW-DF2 correction, optimization of the lattice constant yields a value of 3.87 Å for Si(111)-(1×1) which was used in all calculations with van der Waals correction.

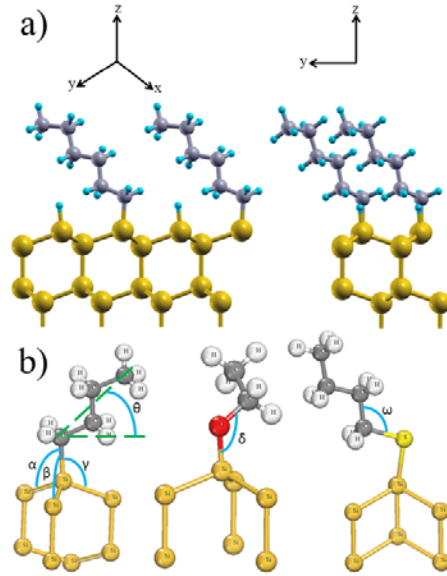


Figure 4.1. (a) H:Si(111) modified by hexyl at 50 % coverage in the  $yz$  (right) and  $[y\cos(60)]z$  (left) planes. (b) Definitions of the different angles characterized in this Chapter:  $\delta = \text{Si-Linker-C}$ ,  $\omega = \text{Linker-C-C}$ ,  $\alpha/\beta/\gamma = \text{Si}_{1,2,3}\text{-Si-Linker}$  and  $\theta =$  the angle of chain axis w.r.t horizontal surface.

We use a 6 atomic layer thick slab<sup>1</sup> of the H terminated unreconstructed silicon (111) surface with appropriate surface supercell expansions for the coverages examined: 25% ( $2\times 2$ ), 50% ( $2\times 1$ ), 66% ( $3\times 1$ ), 75% ( $2\times 2$ ) and 100% ( $1\times 1$ ). Regarding the fact that each ( $1\times 1$ ) surface of the as-cleaved slab possesses one dangling bond on each side, which is either saturated with hydrogen or adsorbate linker (non-functionalized surface is always saturated with hydrogen), these choices of supercell enable us to simulate the target coverage with acceptable computational cost. Functionalized and non-functionalized surfaces are separated by nine equivalent vacuum layers. We performed an ionic relaxation of the top surface fixing the bottom hydrogen atom(s) until the forces on each individual atom are less than  $0.01 \text{ eV/\AA}$ . Depending on the choice of supercell dimensions, Brillouin-zone integrations were performed using ( $8\times 8\times 1$ ), ( $4\times 8\times 1$ ), ( $3\times 8\times 1$ ) and ( $4\times 4\times 1$ ) Monkhorst-Pack  $k$ -points mesh for ionic relaxations. The fixed occupation technique was employed using ten additional bands to ensure convergence of the electronic states. For local density of states (LDOS) and Löwdin charge analysis, four times denser  $k$ -grid and tetrahedron occupation

method was used. The adsorption energy of the molecule at the H:Si(111) surface is defined as:

$$E^{ads} = [E(H:Si - Molecule(s)) + E(H_2)] - [E(Molecule(s)) + E(H:Si)],$$

(eq. 4.1)

where  $E(H:Si-Molecule(s))$  and  $E(H_2)$  are the total energies of the molecule(s) adsorbed at the surface and one, two or three (depending on simulated coverage) free  $H_2$  molecule(s) (which forms since the molecule loses one, two or three H and the surface loses one, two or three terminating H upon adsorption).  $E(Molecule(s))$  and  $E(H:Si)$  are the total energies of the free molecule(s) and the H-terminated Si(111) surface. With this definition, a negative adsorption energy indicates a stable molecule-surface binding configuration.

Since we consider alkyl chains adsorbed at a semiconductor surface, it is important to take account of the dispersion interactions that are not entirely included in the local PBE-GGA functional. In section 4.3, we will first show that including vdW interaction has a significant effect on the adsorption energies at the Si(111) surface. The vdW-DF functional term (DFT-D)<sup>44-45</sup> is available in QE based on a previously developed method<sup>46-48</sup> and it has been applied to many cases.<sup>49</sup> Also a higher-accuracy van der Waals density functional (vdW-DF2) was recently released and shows a better agreement with accurate quantum chemical calculations on 22 diatomic molecules<sup>50</sup>; this however is used in all calculations (unless we are comparing the effect of vdW correction), including those for cut off energies convergence tests and lattice constant optimization.

To compare the effect of the vdW interaction we first calculated the adsorption energies of a series of alkyl chains at Si(111) both with and without including the vdW interaction at half coverage and these results are discussed in section 4.3.1.

## 4.3. Results and discussion

### 4.3.1 Adsorption energies and structures with and without the van der Waals correction

Table 4.1 shows the effect of including the corrected vdW interaction on the adsorption energy and structural properties of a series of alkyl chains adsorbed at 50% coverage at the Si(111) surface (C<sub>2</sub>, C<sub>6</sub> and C<sub>12</sub>, linked to the surface by carbon). It is evident that the inclusion of the vdW interaction has a significant effect, in particular on the adsorption energies. We find that the  $E^{\text{ads}}$  of ethyl, hexyl and dodecyl are all positive when no vdW term is included, indicating no interaction of the molecule with the surface. The inclusion of the vdW term results in the adsorption energies becoming overall less positive and they become negative for hexyl and dodecyl. The effect of the vdW interaction shows no significant dependence on the chain length. With vdW-DF2, the longer chains appear to bind more strongly, but this is a weak effect. The Si–C and C<sub>1</sub>–C<sub>2</sub> distances are not affected by the inclusion of the vdW term. But the angles  $\delta$  and  $\omega$  (see Figure 4.1) are reduced and increased, respectively, when the vdW interaction is included. The change in these angles may indicate a stronger molecule-surface binding effect.

For the O, N and S linkers with a hexyl chain, the inclusion of the vdW interaction makes the adsorption energies significantly more negative, thus enhancing the molecule-surface interaction. Similar to the alkyl chains, there are some modifications to the angles  $\delta$  and  $\omega$  as read from table 4.2. Clearly the inclusion of the vdW interaction in these structures is needed to describe molecule-surface binding. To further explore the role of van der Waals forces in the interaction between chains and between chain and substrate, we performed further calculations and conclude that both interactions increase stability. More results are available in section 4.3.1.1.

Table 4.1. Calculated adsorption energy and structural parameters for Si(111) modified with -  
C<sub>n</sub>H<sub>2n+1</sub> chains to assess the effect of the vdW-DF2 correction.

	<b>Ethyl</b>	
	<i>vdW</i>	<i>No-vdW</i>
<b>Adsorption Energy</b>	+0.09 eV	+0.51 eV
<b>δ (°)</b>	115.68	118.03
<b>d<sub>Si-C1</sub> (Å)</b>	1.94	1.93
<b>d<sub>C1-C2</sub> (Å)</b>	1.55	1.53
<b>Hexyl</b>		
<b>Adsorption Energy</b>	-0.07 eV	+0.49 eV
<b>θ (°)</b>	38.05	61.32
<b>δ (°)</b>	108.99	118.51
<b>ω (°)</b>	118.66	112.78
<b>d<sub>Si-C1</sub> (Å)</b>	1.95	1.93
<b>d<sub>C1-C2</sub> (Å)</b>	1.55	1.53
<b>Dodecyl</b>		
<b>Adsorption Energy</b>	-0.17 eV	+0.46 eV
<b>θ (°)</b>	38.48	63.23
<b>δ (°)</b>	108.88	117.81
<b>ω (°)</b>	117.34	113.16
<b>d<sub>Si-C1</sub> (Å)</b>	1.94	1.92
<b>d<sub>C1-C2</sub> (Å)</b>	1.55	1.53

Table 4.2. Calculated adsorption energy and structural parameters for Si(111) modified with –  
OC<sub>6</sub>H<sub>13</sub>, –SC<sub>6</sub>H<sub>13</sub>, and –NHC<sub>6</sub>H<sub>13</sub> chains to assess the effect of the vdW-DF2 correction.

	<b>Alkoxy-Hexyl</b>	
	<i>vdW</i>	<i>No-vdW</i>
<b>Adsorption Energy</b>	-1.02 eV	-0.39 eV
<b>δ°</b>	129.62	126.99
<b>ω°</b>	106.78	109.11
<b>d<sub>Si-N</sub> (Å)</b>	1.68	1.68
<b>d<sub>N-C1</sub> (Å)</b>	1.47	1.44
<b>Amino-Hexyl</b>		
<b>Adsorption Energy</b>	-0.62 eV	-0.02 eV
<b>δ°</b>	123.35	127.69
<b>ω°</b>	112.14	112.05
<b>d<sub>Si-S</sub> (Å)</b>	1.77	1.75
<b>d<sub>S-C1</sub> (Å)</b>	1.48	1.46
<b>Thiol-Hexyl</b>		
<b>Adsorption Energy</b>	-0.71 eV	-0.27 eV
<b>δ°</b>	104.24	108.28
<b>ω°</b>	112.52	108.61
<b>d<sub>Si-S</sub> (Å)</b>	2.19	2.17
<b>d<sub>S-C1</sub> (Å)</b>	1.88	1.84

### 4.3.1.1 Clarifying the role of vdW interaction

We did a few test calculations to find out more about van der Waals contributions to Chain-Chain vs Chain-Substrate interactions. For this purpose, we created a 3×3 supercell (9 dangling bonds saturated with H) and functionalized it with one hexyl per supercell (typical distance between chains of two neighboring supercells is about 11.52 Å) and next functionalized it with two hexyl per supercell. We allowed the structures to relax and then removed the silicon slab, saturated the linker carbon with hydrogen and calculated the total energy for each case. Chain-Chain interaction can be derived from here by calculating  $\Delta E = [E_{\text{tot}}(2 \times \text{C}_6) - 2 \times E_{\text{tot}}(\text{C}_6)]$ . We did it for both PBE and PBE + (vdW-DF2) cases. The result is presented in the table 4.3.

Table 4.3. Chain-Chain interaction with and without including vdW-DF2 correction  $\Delta E = [E_{\text{tot}}(2 \times \text{C}_6) - 2 \times E_{\text{tot}}(\text{C}_6)]$ .

	$\Delta E$ (eV)
<b>PBE</b>	0.04
<b>PBE+ vdW</b>	-0.19

We also calculated the adsorption energy of hexyl chains as a result of 11% and 66% coverage. For 11% coverage, we can fairly consider the chain interacting only with the substrate, but for 66% (typical distances between chains of two neighboring supercells along  $x$  and  $y$  are about 3.84 Å and 7.68 Å respectively) chain-chain interaction is also involved. The results are shown in the table 4.4.

Table 4.4. Coverage effect on the adsorption energy, with and without including vdW-DF2 correction.

	$E_{\text{ads}}$ (eV)	
	11%	66%
<b>PBE</b>	0.39	1.12
<b>PBE + vdW-DF2</b>	-0.26	0.07

The results highlight some points:



(1) PBE approximation does not predict any chain-chain interaction (in fact it predicts more repulsive interactions). However adding the vdW term produces an attractive vdW force between chains that makes them more stable compared to single chain by -0.2 eV approximately.

(2) As discussed thoroughly in the section 4.3.1, vdW correction does predict a lower adsorption energy compared to PBE. Also considering the difference between  $E_{\text{ads}}(\text{PBE})$  and  $E_{\text{ads}}(\text{PBE}+\text{vdW})$  for 11% and 66% which is 0.7 and 1 eV respectively we conclude that chain-chain interaction makes adsorption more favorable. This is also supported by the observation that for longer alkyl chain length, the adsorption energy decreases, that is, stability increases as shown in Figure 4.3 below. (The fact that 66% coverage seems less stable than 11%, is a separate issue which is related to optimum coverage of alkyl functionalization as discussed in the section 4.3.1.1.)

### **4.3.2 Adsorption energies and structures of H-(X)-alkyl chains at the H:Si(111) surface (X = NH, O, S)**

In this section, we discuss the adsorption energies and structures for the different SAMs adsorbed at the Si(111) surface. Table 4.5 shows the adsorption energies, important bond lengths and angles (defined in Figure 4.1) for the alkyl chains with the different linker groups adsorbed onto the Si(111) surface at half coverage. This coverage has been motivated by the fact that many of the experimental<sup>35</sup> and theoretical works<sup>36</sup> confirm that 50 % coverage is optimal for alkyl monolayers with different thicknesses on Si(111) surface.<sup>3, 36, 51</sup> However we have no indication if the other linkers follow this result or not. Fixing all calculations to half coverage allows us to have a meaningful structural comparison between different linkers that all have the same coverage. At the end of this section, we examine two chains, (X)-hexyl and (X)-dodecyl adsorbed on H:Si(111) at 25%, 66%, 75% and 100% coverage, which allows us to rationalize

why our detailed structural comparison based on 50% coverage is sufficient to understand the key properties of these systems.

#### 4.3.2.1 Effect of Linker

First we compare the adsorption energies for the different atoms binding to the Si surface, that is C, O, N and S. Independent of chain length, the oxygen linker always makes the strongest bond to Si(111) among the linkers studied, with adsorption energies around 1 eV, compared to 0.6 – 0.9 eV for sulfur and 0.3 – 0.6 eV for N (see section 4.3.2.2 for a discussion on the length dependence). The Si-C bond shows the smallest adsorption energy, see table 4.5.

That oxygen makes the strongest bond to silicon could be understood, as a first approximation, from the electronegativity difference compared to silicon among the different linkers (electronegativity for each element: H = 2.2, Si = 1.90, C = 2.55, N = 3.04, O = 3.44 and S = 2.58). The sulfur linker shows the second strongest bond to the H:Si(111) surface, while the nitrogen linked chains show stronger binding than carbon but smaller binding energy values than sulfur and oxygen. However, the electronegativity picture seems to be unable to explain this stability ordering;  $E_{Alkoxy}^{ads} < E_{Thiol-Alkyl}^{ads} < E_{Amine-Alkyl}^{ads} < E_{Alkyl}^{ads}$ .

The oxidation number of the linker may offer an interpretation. Sulfur and oxygen, with oxidation number -2, bind to one silicon from surface and one carbon from the alkyl chain (see Figure 4.2 (a) for the atomic structure of the molecule-surface systems for chain length up to 4 carbons). The valence electron density is shared along these two bonds and due to the electronegativity difference it accumulates closer to O and S. Looking at the Si-S and Si-O distances, table 4.5, the former is the longer, which would indicate a weaker bond between Si and S (although S and O have different atomic radii). However for nitrogen with one additional bond to hydrogen, as well as the bonds to carbon and the surface, and for carbon with two bonds to hydrogens and a bond to the next carbon in the chain, a weaker bond to the surface can be expected (however this might not be the only reason).

### 4.3.2.2 Chain length dependence of stability ordering

Figure 4.3 plots the adsorption energy against chain length for the Si surface modifiers, with the adsorption energies given in table 4.5. It is clear that with the exception of the sulfur linker, convergence in the adsorption energies for chains with four or more carbon atoms is found. Finally, the difference between the adsorption energies of the chains with different linkers is not affected by changing the chain length. Oxygen is always the most stable linker and direct bonding of the alkyl chain the least stable, that is,  $E_{Alkoxy}^{ads} < E_{Thiol-Alkyl}^{ads} < E_{Amine-Alkyl}^{ads} < E_{Alkyl}^{ads}$ . The adsorption energies for chains with the sulfur linker do not appear to follow this convergence. We find three regimes for the adsorption energy versus number of carbons; one regime for  $n \leq 2$ , second for  $2 < n < 8$  and the third regime for  $n > 8$ . This is the result of different structural properties as discussed in the section 4.3.2.3.

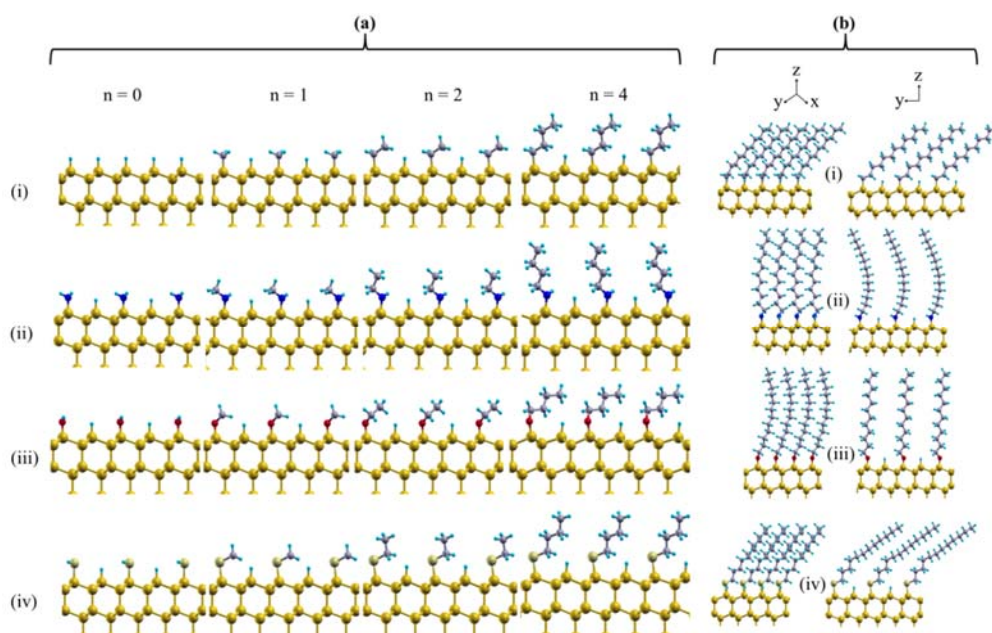


Figure 4.2. (a) Optimized structures of Si(111)-(X)-C<sub>n</sub>H<sub>2n+1</sub> ( $n = 0, 1, 2, 4$ ) for (i) alkyl, (ii) X=NH, (iii) X=O and (iv) X=S. (b) Optimized structures of Si(111)-(X)-dodecyl, for (i) alkyl, (ii) X=NH, (iii) X=O and (iv) X=S from different views. Any apparent bending of the chains appears different from different perspectives.

Table 4.5. The computed adsorption energy, important bond lengths and angles (defined in Figure 4.1) for the four linkers with different alkyl chain lengths. Calculations are carried out including vdW-DF2 term.

<b>H:Si(111)-(C<sub>n</sub>H<sub>2n+1</sub>)</b>							
	<b>E<sup>ads</sup> (eV)</b>	<b>α, β, γ (°)</b>	<b>δ (°)</b>	<b>ω (°)</b>	<b>θ (°)</b>	<b>d<sub>Si-Cl</sub> (Å)</b>	<b>d<sub>Cl-Cl</sub> (Å)</b>
<b>n=1</b>	0.14	109.81,110.11,110.14				1.92	
<b>n=2</b>	0.09	107.5,110.05,113.8	115.68		30.76	1.94	1.55
<b>n=4</b>	-0.06	108.27,109.52,113.4	113.29	114.09	46.78	1.94	1.55
<b>n=6</b>	-0.07	108.61,112.06,112.1	108.99	118.66	38.05	1.95	1.55
<b>n=8</b>	-0.09	108.42,112.05,112.4	108.59	119.05	36.31	1.95	1.55
<b>n=10</b>	-0.10	108.9,111.87,112.33	108.36	119.42	36.62	1.96	1.55
<b>n=12</b>	-0.17	108.88,110.58,111.67	108.88	117.34	36.17	1.94	1.55
<b>H:Si(111)-NH-(C<sub>n</sub>H<sub>2n+1</sub>)</b>							
	<b>E<sup>ads</sup> (eV)</b>	<b>α, β, γ (°)</b>	<b>δ (°)</b>	<b>ω (°)</b>	<b>θ (°)</b>	<b>d<sub>Si-N</sub> (Å)</b>	<b>d<sub>N-Cl</sub> (Å)</b>
<b>n=0</b>	-0.30	107.51,108.32,113.92				1.78	
<b>n=1</b>	-0.48	105.56,110.33,113.86	122.62			1.77	1.49
<b>n=2</b>	-0.53	104.96,110.68,114.05	123.94	111.01		1.77	1.49
<b>n=4</b>	-0.59	104.92,109.99,114.57	123.87	111.62		1.77	1.48
<b>n=6</b>	-0.62	106.93,109.91,112.69	123.35	112.14		1.77	1.48
<b>n=8</b>	-0.63	106.94,109.86,112.79	122.92	112.33		1.77	1.48
<b>n=10</b>	-0.64	103.91,112.17,113.31	128.78	112.43		1.76	1.49
<b>n=12</b>	-0.63	103.01,111.51,114.66	128.94	111.99		1.75	1.48
<b>H:Si(111)-O-(C<sub>n</sub>H<sub>2n+1</sub>)</b>							
	<b>E<sup>ads</sup> (eV)</b>	<b>α, β, γ (°)</b>	<b>δ (°)</b>	<b>ω (°)</b>	<b>θ (°)</b>	<b>d<sub>Si-O</sub> (Å)</b>	<b>d<sub>O-Cl</sub> (Å)</b>
<b>n=0</b>	-0.72	105.13,110.95,112.15				1.71	
<b>n=1</b>	-0.91	103.37,112.22,112.69	124.63			1.69	1.46
<b>n=2</b>	-1.02	105.52,110.78,112.35	123.48	110.81		1.69	1.47
<b>n=4</b>	-1.01	104.63,104.65,120.16	133.58	110.45		1.69	1.47
<b>n=6</b>	-1.02	101.27,112.18,113.88	129.62	106.78		1.68	1.47
<b>n=8</b>	-1.02	109.40,109.62,110.76	113.67	115.50		1.71	1.47
<b>n=10</b>	-1.04	101.55,112.64,113.16	128.17	107.13		1.68	1.47
<b>n=12</b>	-1.05	104.42,109.74,113.51	127.99	108.40		1.69	1.46
<b>H:Si(111)-S-(C<sub>n</sub>H<sub>2n+1</sub>)</b>							
	<b>E<sup>ads</sup> (eV)</b>	<b>α, β, γ (°)</b>	<b>δ (°)</b>	<b>ω (°)</b>	<b>θ (°)</b>	<b>d<sub>Si-S</sub> (Å)</b>	<b>d<sub>S-Cl</sub> (Å)</b>
<b>n=0</b>	-0.58	108.5, 109.68, 109.87				2.21	
<b>n=1</b>	-0.69	102.26, 11.9, 114.89	105.06			2.19	1.86
<b>n=2</b>	-0.79	102.76,111.18,115.32	104.24	109.32		2.19	1.87
<b>n=4</b>	-0.77	104.21,110.88,114.81	100.23	112.53		2.19	1.87
<b>n=6</b>	-0.92	102.98,110.73,115.15	102.56	108.74		2.19	1.88
<b>n=8</b>	-0.80	104.28,111.37,114.37	100.06	112.11		2.20	1.87
<b>n=10</b>	-0.94	103.41,110.91,114.83	101.86	109.46		2.19	1.87
<b>n=12</b>	-0.89	105.99,110.87,114.05	98.28	113.70		2.20	1.87

Now splitting the vdW effect into chain-chain and chain-interface interactions, the first term grows as the chain length grows, however the second term vanishes with distance from the surface with the factor of  $r^{-2}$ . Apparently for chains with 4 carbons and more the term that affects mostly the adsorption energy is the chain-chain interaction. Looking at the adsorption energy formula  $[E(\text{H:Si-Molecule}) + E(\text{H}_2)] - [E(\text{Molecule}) + E(\text{H:Si})]$ , the chain-chain interaction terms cancel with each other for long enough chains. However, it should be noted that the adsorption energy continues to decrease with increasing chain length if the vdW term is neglected in the  $E(\text{Molecule})$ .

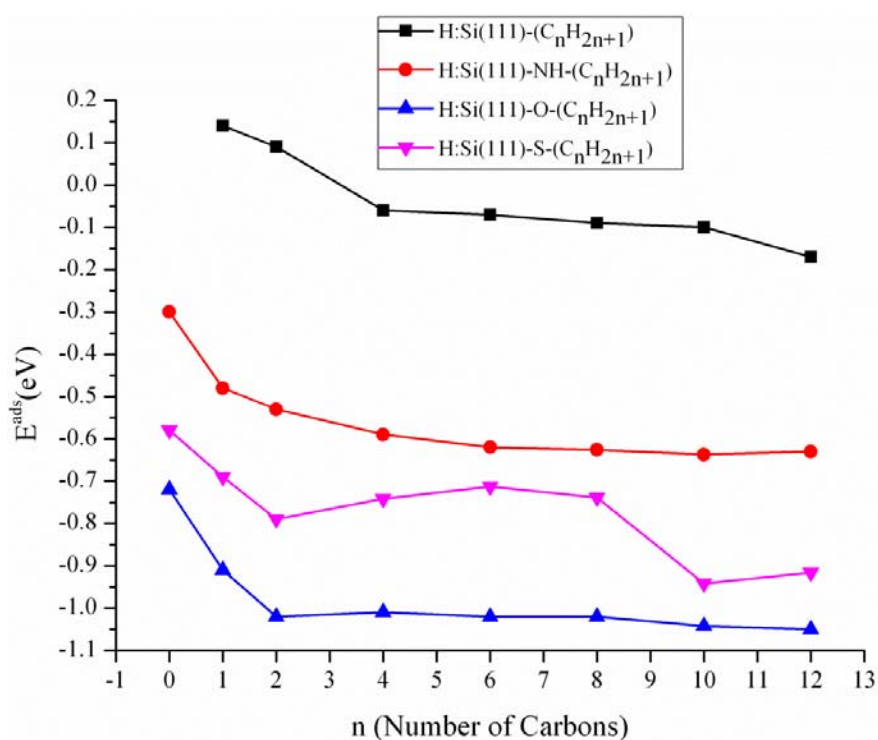


Figure 4.3. Adsorption energy for the alkyl chain ( $n = 0, 1, 2, 4, 6, 8, 10, 12$ ) and linker combinations, O, N, S, studied in this work.

### 4.3.2.3 Structural Analysis

Analysis of the geometry shows that there is a convergence with respect to chain length of the Si-(A=C, N, O, S)-C angle ( $\delta$ ) and the (A)-C-C angle ( $\omega$ ) and for the angle of chain axis with respect to the horizontal surface in the case of alkyl

chains (angles are defined in Figure 4.1; see also Figure 4.4 for definition of “A” as the bridging atom). Figure 4.2 (b) shows the atomic structures for the 12 chain molecules adsorbed at the H:Si(111) surface, while Figure 4.4 and table 4.6 present distances used to characterize the tilting of the chains – a longer distance between  $C_1$  and  $C_{12}$  or between Si and  $C_{12}$  indicates a more upright chain and *vice versa*. The structure of the  $C_{12}$  chains (and similarly for  $C_8$  and  $C_{10}$ ) show a strong dependence on the nature of the linker. The long bond length between Si and S, the largest out of all the linkers, facilitates a wider range of the possible movements (tilt relative to the surface, torsion within the chain leading to greater conformational flexibility) as carbons are added to the chain and for  $n > 8$ . The dodecyl chain lies with an angle of  $36^\circ$  relative to the surface plane, whereas with the O and N linkers, the chains show a tilt that is more upright. This is borne out by the data in table 4.6, showing longer Si– $C_{12}$  and  $C_1$ – $C_{12}$  distances for the more upright chains. The dodecyl chain with the sulfur linker shows a different atomic structure in that there is a change in the torsion angle after the fourth carbon (present also in  $C_8$  and  $C_{10}$  chains). By looking at the molecular structure of the dodecylthiol in Figure 4.4, up until  $C_8$ , the second phase alkyl groups are interacting with the first phase groups (e.g.  $C_8$  with  $C_4$ ) but after this the second phase alkyl groups only interact with each other (e.g.  $C_{10}$  with  $C_6$ ), which is in part responsible for the change in the magnitude of the adsorption energy with chain length.

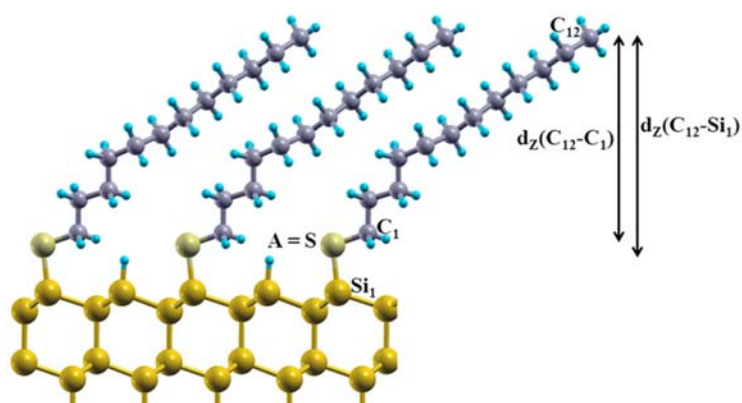


Figure 4.4. Illustration of the parameters presented in table 4.6.

Table 4.6. Thickness of different monolayers along z axis:  $d_z(\text{C}_{12}\text{-C}_1)$ ,  $d_z(\text{C}_{12}\text{-A})$  and  $d_z(\text{C}_{12}\text{-Si}_i)$  as indicated in Figure 4.4 (A denotes the possible bridging atoms to Si surface, that is, C, N, O, S).

	Dodecyl	NH-Dodecyl	OH-Dodecyl	SH-Dodecyl
$d_z(\text{C}_{12}\text{-C}_1)$ Å	8.35	13.56	13.54	8.78
$d_z(\text{C}_{12}\text{-A})$ Å	8.35	14.63	14.54	9.28
$d_z(\text{C}_{12}\text{-Si}_i)$ Å	10.29	16.37	16.22	11.46

We have examined the geometry in the adsorbed chains, in particular lengths of important bonds such as the Si–A, A–C<sub>1</sub> and C<sub>1</sub>–C<sub>2</sub> (for the alkyl chains the latter two correspond to the C<sub>1</sub>–C<sub>2</sub> and C<sub>2</sub>–C<sub>3</sub> bonds) for each structure. Table 4.5 shows these data for the case of each linker as the chain length increases. For a given linker, the results show that these bond distances are independent from increases in the chain length.

The bond lengths involving the linker such as Si–A and A–C and A–H (A = C, N, O, S) do show a notable dependence on the nature of the linker. The longest Si–A bond is found for sulfur with a distance of 2.2 Å. The next longest bond belongs to carbon which is 1.95 Å. Nitrogen and oxygen have the shortest Si–A bonds, at 1.77 Å and 1.68 Å respectively. This is in agreement with the electronegativity picture (O > N > S ~ C), but does not fully follow the trend in the adsorption energies. Considering the bond distances of the linker to the first carbon atom in the free molecule, the longest bond belongs to the S–C bond, at 1.9 Å. For the other linkers the A–C distance is around 1.5 Å, and is 0.1 Å longer for the C–C bond. The same trend is found for any H–A bonds present, and the H–C bond is again 0.1 Å longer than the remaining A–H bonds.

Si–Si bond lengths in the surface are slightly affected by the linkers, with changes ranging from -0.01 Å to +0.03 Å compared to the original Si–Si distance of 2.35 Å for the bare hydrogenated slab, with a stronger effect found for longer chains. The Si–Si distance shows the highest sensitivity with the alkyl functionalization. The first C–C distance is invariant at around 1.54 Å for all linkers; oxygen shows a small increase of 0.1 Å.

We defined important angles in Figure 4.1 to represent the important geometrical characteristics of the structures. The extracted data are shown in

table 4.5. We see that the minimum value of the angles  $\alpha$ ,  $\beta$ ,  $\gamma$  changes by a few degrees upon adding the first carbons to the linker but converges quickly upon lengthening the chains, in a similar fashion to the adsorption energies. In the case of carbon and sulfur linkers, the angle  $\delta$  converges to a value close to the minimum of  $\alpha$ ,  $\beta$ ,  $\gamma$  after adding the third carbon. For oxygen and nitrogen  $\delta$  is almost 20 degrees larger than the minimum of the angles  $\alpha$ ,  $\beta$ ,  $\gamma$  at saturation. No clear trend for the  $\omega$  was observed although its value with respect to the linker shows a weaker dependence than the other angles. The angles of alkyl chains with respect to the surface normal show saturation at  $36^\circ$ , which is consistent with the experimental value for 1-dodecyl on H:Si(111).<sup>51</sup>

We have also used the structure of the C<sub>12</sub> chain with the N linker as an input structure for the oxygen linker and *vice versa* to examine the effect of different chain structures on the structural properties. Upon full relaxation, the A-C<sub>12</sub> chains relax back to their original structures shown in Figure 4.2 (b), indicating a preference for particular chain configurations that depend on the type of linker present in the adsorbed molecule; table 4.7 presents a comparison of energetic and structural data for this case.

Table 4.7. A comparison of energetic and structural parameters for dodecyl chains with O and NH linkers. The original relaxed structures are presented in the columns headed NH-dodecyl and O-dodecyl. The column headed “Exchange O with NH and relax” signifies exchanging oxygen in the O-dodecyl structure with NH and relaxing. The data show a structure very similar to the originally relaxed structure. A similar interpretation holds for the column headed “Exchange NH with O and relax”. vdW-DF2 correction has been included in the calculations.

	NH-Dodecyl	Exchange O with NH and relax	OH-Dodecyl	Exchange NH with O
<b>E<sup>ads</sup> (eV)</b>	-0.63	-0.61	-1.05	-1.06
<b><math>\alpha, \beta, \gamma</math> (°)</b>	103.01,111.51,114.66	103.42,111.40,114.21	104.42,109.74,113.51	102.33,111.73,113.26
<b><math>\delta</math> (°)</b>	128.94	129.24	127.99	127.36
<b><math>\omega</math> (°)</b>	111.99	109.60	108.40	107.43
<b>d<sub>Si-A</sub> (Å°)</b>	1.75	1.76	1.69	1.68
<b>D<sub>A-C2</sub> (Å°)</b>	1.48	1.48	1.46	1.47
<b>d<sub>C-C</sub> (Å°)</b>	1.54	1.54	1.53	1.54



#### ***4.3.2.4 Adsorption Analysis***

To understand the adsorption character of the linkers and compare their stability, we analyze the local density of states and local charge on the interface atoms (which is sufficient to describe the molecule-surface interaction), for H:Si(111) covered with 50% (X)-hexyl (X = NH, O, S) which is sufficient to explain the general adsorption phenomena that occur at all other chain lengths and coverages.

The Local Density of States projected to the interface atoms (LDOS), is depicted in Figure 4.5. There, the LDOS is plotted for the surface silicon bonded to “bridging” atom (A = C, N, O, S), the atom itself (A), the next nearest silicon neighbour to the bridging atom (Si-*nnn*) and the first carbon atom from the alkyl chain bonded to A (C1). From the LDOS plot, the LDOS of A has the largest variation in comparison with the other interface atoms in different panels, which helps to define the stability order. The three linkers have sharp and high intensity electronic states near the HOMO. On the other hand, A = C makes the direct carbon bond to surface silicon the least stable bond. For the two linkers (N, S), nitrogen and sulfur have a large weight and sharp LDOS peak at HOMO states very close to the gap. However, the sulfur linker follows this trend deeper into the valence states overlapping with the surface silicon LDOS. This implies that sulfur linkages would be more stable than those based on nitrogen. In the case of O, although there is quite low intensity of electronic states in the HOMO region close to the gap, the LDOS for valence states far from the gap is quite large over a broad spectrum. This results in significant overlap with the LDOS of the first and second neighbour silicons. Together with a quite sharp and high peak deep in the valence region, oxygen establishes itself as the most stable linker in terms of adsorption energy, even though very close to sulfur.

The results of our Löwdin charge analysis are tabulated in table 4.8. There is considerable change in the charge of top silicon at the surface and the attached linker. However the carbons of the alkyl chain, which are not in direct contact to the surface atoms, seem to be entirely insensitive to functionalization. Charge increments on second nearest silicon atoms that are neighbors to the linker

however fluctuate with attaching (X)-alkyl chains and show slightly bigger change for more electronegative bridging atoms (O and N). The situation is inverse for “A” itself, where a smaller increase occurs for O and N, though the effect is small. The biggest charge difference in general, happens for the directly bonded silicon. Considering the Si-A (A = C, N, O, S) bond, silicon always loses charge. The amount of charge reorganization on the silicon follows the sequence  $\Delta q(\text{O}) > \Delta q(\text{N}) > \Delta q(\text{C}) > \Delta q(\text{S})$ . The withdrawn charge is shared between the slab and the molecule.

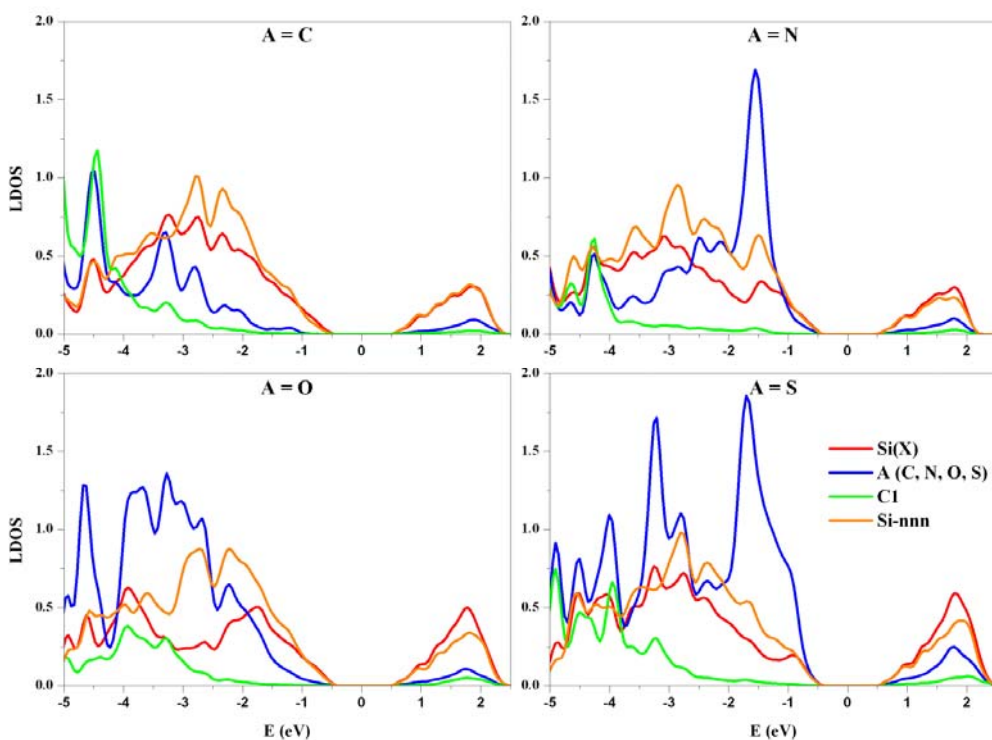


Figure 4.5. Local Density of States projected to the interface atoms (LDOS): surface silicon bonded to linker atom (A = C, N, O, S), linker atom itself (A), next nearest silicon neighbor to the linker atom (Si-*nnn*) and the first carbon atom from the alkyl chain bonded to linker (C1).

The charge analysis can also give us insights into the stability of the linkers. As we can see from the table 4.8, charge reorganization on the linker atoms is not entirely in the same order as the energetic stability (table 4.8).  $\Delta q_A$  alone cannot account for the stability sequence since charge could be transferred from the

chain atoms rather than from silicon to the linker and a larger value does not always signify more stability.  $\Delta q_{Total}$  is therefore a more appropriate quantity (although the variation is small), and this is in agreement with the stability order. For the specific cases of sulfur and nitrogen our results predict a more stable adsorption of the thiol linker compared to amine. Since N has a higher electronegativity than S we may expect the inverse. Charge analysis may offer an explanation here. From table 4.8, we see that  $\Delta q_N$  (0.05) is slightly less than  $\Delta q_S$  (0.07). However due to the longer Si-S bond compared to Si-N (Table 4.5), the resultant dipole ( $a \times \Delta q$ ) will be significantly larger for sulfur and therefore S will have a bond dipole comparable to N. Also from the LDOS plot for NH and S linkers (see Figure 4.6) it is clear that in both valence and conduction regions, sulfur has considerably higher density of states which can directly translate into higher stability.

What is quite obvious here in terms of the amount of reorganized charge is that oxygen and nitrogen stand over sulfur and carbon linkers. However we cannot come to a clear conclusion as the absolute charge values in some cases are so small (a fraction of electron charge). Also there is the fear of DFT-GGA error in charge evaluation. This along with LDOS analysis could be complementary and interpretative.

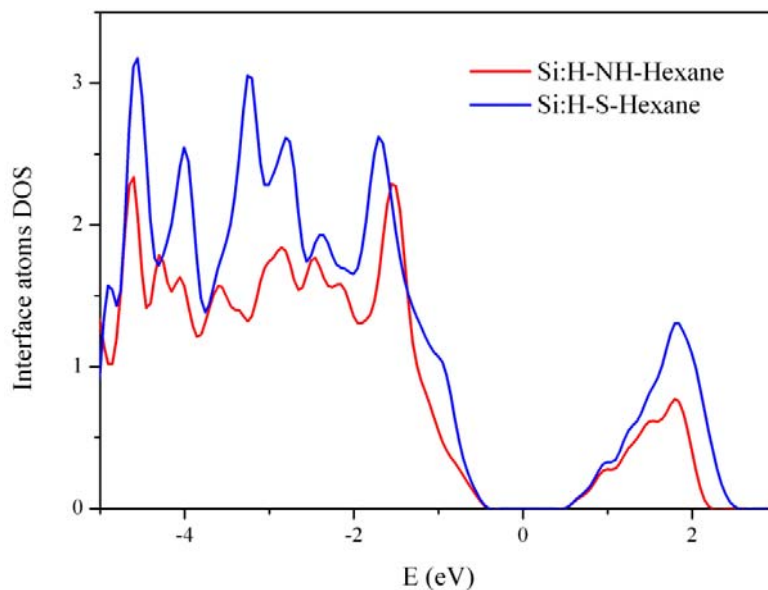


Figure 4.6. Interface DOS for N (red curve) and S (blue curve) linkers. Interface DOS is calculated as summation over Si(X), X, Si-nnn and C1 LDOSs.

Table 4.8. Löwdin charge analysis for H:Si(111)-(X)-Hexyl at 50% coverage:  $\Delta q_{Si(1)} = [q_{Si(1)(Slab-(X)-Hexyl)} - q_{Si(1)(Slab)}]$  and  $\Delta q_{Si(2)} = [q_{Si(2)(Slab-(X)-Hexyl)} - q_{Si(2)(Slab)}]$  stands for charge difference on first and second (averaged over 3 silicons) nearest silicon neighbors to A = N, O, S, respectively.  $\Delta q_A = [q_{A(Slab-(A)-Hexyl)} - q_{A-(Slab)}]$  represents the charge difference on the bridging atom after functionalization.  $\Delta q_{C(1)}$  and  $\Delta q_{C(2)}$  shows the charge difference on first and second nearest carbon w.r.t linker and  $\Delta q_{Total}$  has been calculated as  $[(\Delta q_{Slab-(X)-Hexyl} + \Delta q_{H2}) - (\Delta q_{Slab} + \Delta q_{Molecule})]$ . Negative charge difference represents electron withdrawal and positive values stand for electron gaining.

	Hexyl	NH <sub>2</sub> -Hexyl	OH-Hexyl	SH-Hexyl
$\Delta q_{Si(1)}$	-0.15	-0.31	-0.42	-0.09
$\Delta q_{Si(2)}$	+0.06	+0.15	+0.15	+0.06
$\Delta q_A$	+0.08	+0.05	+0.04	+0.07
$\Delta q_{C(1)}$	-0.02	0.00	0.00	-0.01
$\Delta q_{C(2)}$	0.00	0.00	0.00	0.00
$\Delta q_{Total}$	+0.56	+0.53	+0.50	+0.53

#### 4.3.2.5 Effect of Coverage

We discuss the effect of coverage on adsorption energy of (X)-hexyl and (X)-dodecyl at H:Si(111) for four other coverages - 25% (only hexyl), 66%, 75%,

100%. Together with 50% coverage we can predict the most stable coverage for different linkers.

The adsorption energies from vdW-DF2 have been calculated and are plotted in Figure 4.7. Apart from pure alkyl chains, it appears that 50% is not the most stable coverage for (X)-Alkyl functionalization but in fact around 75%. This would be worthy of experimental verification. The adsorption energy change is very significant for the case of oxygen linker at 75% compared to 50% coverage (about 2 eV more stable). LDOS comparison for interface atoms is made for H:Si-O-Hexyl at 50% and 75% coverage and the plot is available in Figure 4.8. Comparing 75% to 50%, considerable intensity increase in the oxygen linker LDOS at the valence region (around -4 eV) and surface silicons in the conduction region is seen.

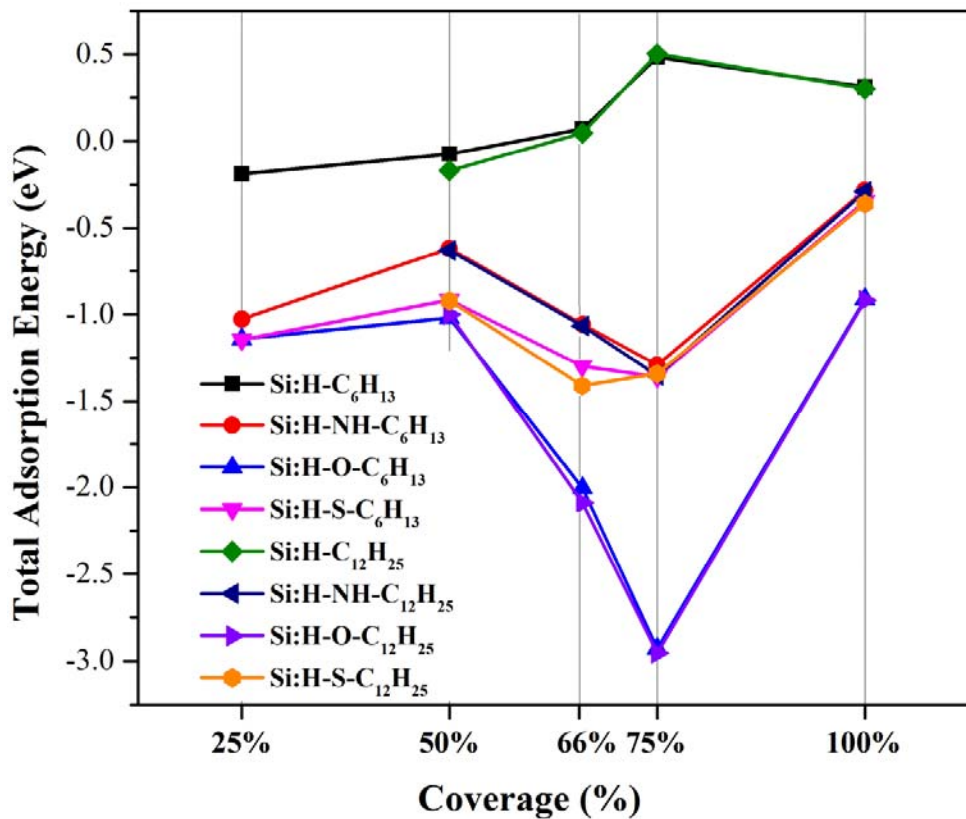


Figure 4.7. Total adsorption energy for different coverage of (X)-Hexyl (25%, 50%, 66%, 75% and 100%) and (X)-Dodecyl (50%, 66%, 75% and 100%) at the H:Si(111) surface. (X = NH, O and S)

It is worth noting that chain with different linkers can have different optimum coverage because linkers with different van der Waals radii have a different steric effect and consequently, different angle of bonding at linker. For example among our linkers here (CH<sub>2</sub>, NH, O and S), C has the biggest van der Waals radius compared to others which implies larger steric repulsion and less packing density.

However it is important to mention that the two major points that we discussed, i.e. the sequence of the stability and the saturation of the adsorption energy with respect to length are independent of the surface coverage (see Figure 4.7). This means that our detailed structural comparison which was based on 50% coverage is sufficient to understand the key properties of these systems.

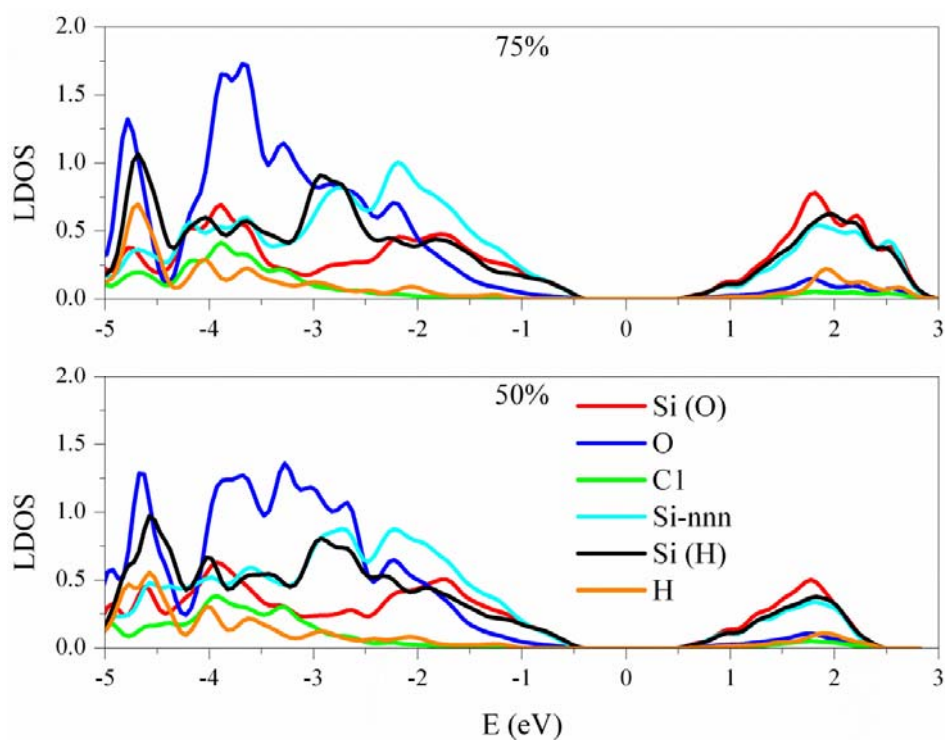


Figure 4.8. Local Density of States projected to the interface atoms (LDOS) for H:Si(111) functionalized with 50% (lower panel) and 75% (top panel) O-Hexyl: surface silicon bonded to linker atom O, O linker itself, next nearest silicon neighbor to the O (Si-nnn) and the first carbon atom from the alkyl chain bonded to O (C1). The LDOSs for surface silicon (Si(H)) saturated with H, are also presented for comparison.

#### 4.3.2.6 Comparison with Experiments

Wallart et al.<sup>55</sup> studied alkyl and alkoxy monolayers directly grafted on atomically flat H-Si(111) surfaces using quantitative X-ray photoelectron spectroscopy (XPS). Their results provide direct evidence that Si-C and Si-O-C linkages are formed, respectively, after reaction with decene and decanol and show that the interface is free of oxide. They found that both kinds of monolayers are very dense, 48% for Si-C linkage and 42%-52% for Si-O-C, however the estimate of the latter coverage is more subject to hypothesis about contaminations and a possible limited oxidation. Without this assumption it shows coverage of 0.97 which is surprisingly high. Quantitative analysis of the satellite peaks in Si2p and C1s core level XPS spectra for both structures shows that the Si-O-C bond is slightly stronger. This is however in agreement with both our predictions of stability ordering for direct alkyl and O-alkyl monolayers attached to silicon surface as well as the possibility of increasing coverage up to 75%, by using oxygen linker instead of direct Si-C bond.

In the pioneer work of Linford and Chidsey<sup>52</sup> the direct reaction of 1-octadecane and H:Si(111) resulted in 50% coverage with a tilt angle around 28-36° detected by IR spectroscopy. From polarized FTIR spectra of C<sub>12</sub>H<sub>25</sub>O-Si(111) and C<sub>18</sub>H<sub>37</sub>O-Si(111) monolayers for s- and p-polarization Zhu *et al.*<sup>53</sup> measured an average tilt angle of 5-15° between the alkyl chain and surface normal. These measurements are in agreement with our calculated 36° tilt angle for alkyl functionalized surface and the up-right tendency of O-alkyl functionalization, respectively. X-ray reflectivity data give a packing density of 85% for n-C<sub>18</sub>H<sub>37</sub>O-monolayer on H:Si(111) surface. In another work by Effenberger et al.<sup>54</sup> 1-octadecanal yielded surprisingly high coverage around 97% and tilt angle of 15° on H:Si(111), comparable with earlier experiment and also our predictions.

Harada *et al.*<sup>55</sup> successfully fabricated aromatic SAMs covalently bonded to Si(111) surfaces through different anchor structures (Si-O-, Si-CH<sub>2</sub>-CH<sub>2</sub>-, and Si-CH=CH-). Current density-voltage measurements of Hg/aromatic SAM-Si(111) sandwiched structures revealed that the "Si(111)-O-Ph" (SAM

from phenol) show higher conductivity compared with the long-chain alkyl (C<sub>12</sub>) SAM on Si(111). Our LDOS/charge analysis indicates a similar result for the oxygen linker in comparison with carbon evidenced by a bigger shift in conduction band states for O and a larger amount of charge transferred to the surface silicon in contact with the oxygen linker. Based on XPS results they also concluded that aromatic SAMs offer similar coverage (~0.5) to long alkyl chain SAMs (C<sub>12</sub>).

In another recent study<sup>56</sup> hydrolytic and thermal stability of 24 different kinds of monolayers on Si(111), Si(100), SiC, SiN, SiO<sub>2</sub>, CrN, Indium Tin Oxide (ITO), Porous Aluminum Oxide (PAO), Au, and stainless steel surfaces were investigated. These surfaces were modified utilizing appropriate organic compounds having a constant alkyl chain length (C<sub>18</sub>), but with different surface-reactive groups, such as 1-octadecene, 1-octadecyne, 1-octadecyltrichlorosilane, 1-octadecanethiol, 1-octadecylamine and 1-octadecylphosphonic acid. The covalently bound alkyne monolayers on Si(111), Si(100), and SiC were shown to be among the most stable monolayers under acidic and neutral conditions.

Using ultraviolet-assisted photochemical reaction, Lou et al.<sup>13</sup> grew a 1-dodecanthiol (DDT) monolayer on a bare Si(111) surface. Their synchrotron radiation-based high-resolution X-ray photoelectron spectroscopy (HRPES) results indicated almost fully covered Si(111) surface with DDT. This is generally in agreement with our result from this point of view that functionalization with linker increases the coverage. Further investigation was made using water contact angle measurement. The initial tilt angle of  $54.8^{\circ} \pm 1.8^{\circ}$  increased up to  $101.5^{\circ} \pm 1.5^{\circ}$  during the reaction and then decreased. The average value of  $57^{\circ}$  was taken as the tilt angle. Although our relaxed calculation for DDT on Si(111) predicted a twisted chain with non-recognizable angle, it is approximately in agreement with this measurement from the structural point of view (our relaxed structure of dodecanethiol shows a twisted chain, approximately between 45 and 65 degree with respect to the surface normal). Using near-edge X-ray absorption fine structure spectroscopy (NEXAFS) they



evaluated the monolayer thickness to be around 15 Å. Our calculation yields the thickness of ~11.5 Å. The Si-S bond length equals 2.14 Å and S-C is 1.81 Å as included in the formula of another work<sup>57</sup>. Both are very close to our calculated bond lengths.

Overall our predicted structural properties for a functionalized silicon (111) surface with linker-alkyl chains are consistent with available experimental results. This indicates that insights from first principle studies such as this work can help to further understand the mechanism of changes in functionalized silicon surfaces at the microscopic level and motivate future experiments. Functionalized surfaces have a broad range of application in bio/opto-electronic devices in which monolayers' stability and dense packing is one of the primary concerns. The predicted improvement in stability by using different linker species rather than carbon in contact with silicon which was shown in this Chapter, offers a new approach to achieve the goal of enhanced stability and dense packing. The role of the linker in inducing various structural effects predicted in this work is also important while dealing with opto-electronic devices, where we showed that for the same length of the alkyl there is a significant difference in thickness for monolayer with sulfur and carbon linkers compared to oxygen and nitrogen head-groups. This can significantly affect optical indices and adsorption spectra in those devices. More importantly, the potential for higher coverages as a result of grafting monolayers via linkers other than carbon, that we systematically investigated for the first time, may motivate the experimentalist to consider it in the future for device design.

## 4.4 Concluding remarks

With the aim to understand the role played by the nature of the linker and the chain length on the adsorption structures and stabilities of H:Si(111) modified with molecular chains with the general formula H:Si-(X)-(CH<sub>2</sub>)<sub>n</sub>-CH<sub>3</sub>, where X = NH, O, S and n = (0, 1, 3, 5, 7, 9, 11), we presented a density functional theory (DFT) study of these assemblies, with the following conclusions:

(1) It is absolutely necessary to take into account the van der Waals interaction between the alkyl chains in order to describe correctly the interaction of a layer of these molecules with the H:Si(111) surface;

(2) The strongest binding is for the oxygen linker, followed by sulfur and nitrogen irrespective of chain length. Direct binding of the alkyl chains to silicon is the least stable. This ordering can be explained by analyzing the bridging bond distances, the electronegativity of the bridging atoms and silicon, and their oxidation state;

(3) For all bridging atoms apart from sulfur structural properties, such as surface-(linker)-chain angles, are converged once  $n > 3$ . For sulfur, there are three regimes, namely  $n = 0 - 3$ ,  $n = 5 - 7$  and  $n = 9 - 11$ , with characteristic adsorption structures.

(4) Including a linker between the alkyl chain and the Si surface influences the optimum surface coverage. Our results predict that NH, O and S linkers allow more packing density up to 75% coverage. However the sequence of the stability order seems to be independent of the coverage.

Where experimental data are available, our results are shown to be consistent with measurements and we demonstrate how the fundamental structural properties of modified Si surfaces can be controlled by the choice of linking group and chain length.

## 4.5 References

1. Arefi, H. H.; Fagas, G., Chemical Trends in the Work Function of Modified Si(111) Surfaces: A DFT Study. *J. Phys. Chem. C* **2014**, *118*, 14346–14354.
2. Nolan, M.; O'Callaghan, S.; Fagas, G.; Greer, J. C.; Frauenheim, T., Silicon Nanowire Band Gap Modification. *Nano Lett.* **2006**, *7*, 34-38.
3. Li, Y.; Calder, S.; Yaffe, O.; Cahen, D.; Haick, H.; Kronik, L.; Zuilhof, H., Hybrids of Organic Molecules and Flat, Oxide-Free Silicon: High-Density Monolayers, Electronic Properties, and Functionalization. *Langmuir* **2012**, *28*, 9920-9.
4. Sieval, A. B.; Linke, R.; Heij, G.; Meijer, G.; Zuilhof, H.; Sudhölter, E. J. R., Amino-Terminated Organic Monolayers on Hydrogen-Terminated Silicon Surfaces. *Langmuir* **2001**, *17*, 7554-7559.
5. Uosaki, K.; Fukumitsu, H.; Masuda, T.; Qu, D., Construction of a Metal-Organic Monolayer-Semiconductor Junction on a Hydrogen-Terminated Si(111)

- Surface via Si-C Covalent Linkage and its Electrical Properties. *Phy. Chem. Chem. Phys.* **2014**, *16*, 9960-9965.
6. Juarez, M. F.; Soria, F. A.; Patrito, E. M.; Paredes-Olivera, P., Influence of Subsurface Oxidation on the Structure, Stability, and Reactivity of Grafted Si(111) Surfaces. *J. Phys. Chem. C* **2008**, *112*, 14867-14877.
  7. Faber, E. J.; de Smet, L. C. P. M.; Olthuis, W.; Zuilhof, H.; Sudhölter, E. J. R.; Bergveld, P.; van den Berg, A., Si-C Linked Organic Monolayers on Crystalline Silicon Surfaces as Alternative Gate Insulators. *ChemPhysChem* **2005**, *6*, 2153-66.
  8. Michalak, D. J.; Amy, S. R.; Estève, A.; Chabal, Y. J., Investigation of the Chemical Purity of Silicon Surfaces Reacted with Liquid Methanol. *J. Phys. Chem. C* **2008**, *112*, 11907-11919.
  9. Solares, S. D.; Michalak, D. J.; Goddard, W. A.; Lewis, N. S., Theoretical Investigation of the Structure and Coverage of the Si(111)-OCH<sub>3</sub> surface. *J. Phys. Chem. B* **2006**, *110*, 8171-5.
  10. Hunger, R.; Jaegermann, W.; Merson, A.; Shapira, Y.; Pettenkofer, C.; Rappich, J., Electronic Structure of Methoxy-, Bromo-, and Nitrobenzene Grafted onto Si(111). *J. Phys. Chem. B* **2006**, *110*, 15432-41.
  11. Segev, L.; Salomon, A.; Natan, A.; Cahen, D.; Kronik, L.; Amy, F.; Chan, C.; Kahn, A., Electronic Structure of Si(111)-Bound Alkyl Monolayers: Theory and Experiment. *Phys. Rev. B* **2006**, *74*, 1-6.
  12. Soria, F. A.; Patrito, E. M.; Paredes-Olivera, P., Tailoring the Surface Reactivity of Silicon Surfaces by Partial Halogenation. *J. Phys. Chem. C* **2013**, *117*, 18021-18030.
  13. Lou, J. L.; Shiu, H. W.; Chang, L. Y.; Wu, C. P.; Soo, Y.-L.; Chen, C.-H., Preparation and Characterization of an Ordered 1-Dodecylthiol Monolayer on Bare Si(111) Surface. *Langmuir* **2011**, *27*, 3436-3441.
  14. Boukherroub, R.; Morin, S.; Bensebaa, F.; Wayner, D. D. M., New Synthetic Routes to Alkyl Monolayers on the Si(111) Surface 1. *Langmuir* **1999**, *15*, 3831-3835.
  15. Wolkow, R. A., Controlled Molecular Adsorption on Silicon: Laying a Foundation for Molecular Devices. *Annu. Rev. Phys. Chem.* **1999**, *50*, 413-41.
  16. Bierbaum, K.; Kinzler, M.; Woell, C.; Grunze, M.; Haehner, G.; Heid, S.; Effenberger, F., A Near Edge X-ray Absorption Fine Structure Spectroscopy and X-ray Photoelectron Spectroscopy Study of the Film Properties of Self-Assembled Monolayers of Organosilanes on Oxidized Si(100). *Langmuir* **1995**, *11*, 512-518.
  17. Tian, F.; Teplyakov, A. V., Silicon Surface Functionalization Targeting Si-N Linkages. *Langmuir* **2013**, *29*, 13-28.
  18. Böcking, T.; Salomon, A.; Cahen, D.; Gooding, J. J., Thiol-Terminated Monolayers on Oxide-Free Si: Assembly of Semiconductor-Alkyl-S-Metal Junctions. *Langmuir* **2007**, *23*, 3236-41.
  19. Ciraci, S.; Ellialtıođlu, S.; Erkoç, S., Interpretation of the Spectra Obtained from Oxygen-Adsorbed and Oxidized Silicon Surfaces. *Phys. Rev. B* **1982**, *26*, 5716-5729.
  20. Engel, T., The Interaction of Molecular and Atomic Oxygen with Si(100) and Si(111). *Surf. Sci. Rep.* **1993**, *18*, 93-144.
  21. Reddy, A. J.; Chan, J. V.; Burr, T. A.; Mo, R.; Wade, C. P.; Chidsey, C. E. D.; Michel, J.; Kimerling, L. C., Defect States at Silicon Surfaces. *Physica B* **1999**, *273*, 468-472.
  22. Haber, J. A.; Lauermann, I.; Michalak, D.; Vaid, T. P.; Lewis, N. S., Electrochemical and Electrical Behavior of (111)-Oriented Si Surfaces Alkoxyated through Oxidative Activation of Si-H Bonds. *J. Phys. Chem. B* **2000**, *104*, 9947-9950.

23. Michalak, D. J.; Rivillon, S.; Chabal, Y. J.; Estève, A.; Lewis, N. S., Infrared Spectroscopic Investigation of the Reaction of Hydrogen-Terminated, (111)-Oriented, Silicon Surfaces with Liquid Methanol. *J. Phys. Chem. B* **2006**, *110*, 20426-34.
24. Michalak, D. J.; Amy, S. R.; Aureau, D.; Dai, M.; Estève, A.; Chabal, Y. J., Nanopatterning Si(111) Surfaces as a Selective Surface-Chemistry Route. *Nat. Mater.* **2010**, *9*, 266-71.
25. Mitchell, S. A.; Boukherroub, R.; Anderson, S., Second Harmonic Generation at Chemically Modified Si(111) Surfaces. *J. Phys. Chem. B* **2000**, *104*, 7668-7676.
26. Hacker, C. a., Modifying Electronic Properties at the Silicon–Molecule Interface Using Atomic Tethers. *Solid-State Electron.* **2010**, *54*, 1657-1664.
27. Cooper, A. J.; Keyvanfar, K.; Deberardinis, A.; Pu, L.; Bean, J. C., Dopant Passivation and Work Function Tuning through Attachment of Heterogeneous Organic Monolayers on Silicon in Ultrahigh Vacuum. *Appl. Sur. Sci.* **2011**, *257*, 6138-6144.
28. Dresser, M. J.; Taylor, P. A.; Wallace, R. M.; Choyke, W. J.; Yates, J. T., The Adsorption and Decomposition of NH<sub>3</sub> ON Si(100)—Detection of the NH<sub>2</sub>(a) Species. *Surf. Sci.* **1989**, *218*, 75-107.
29. Miotto, R.; Ferraz, A. C.; Srivastava, G. P., Dissociative Adsorption of NH<sub>3</sub> on Si(001)-(2×1). *Phys. Rev. B* **1998**, *58*, 7944-7949.
30. Bowler, D.; Owen, J., Molecular Interactions and Decomposition Pathways of NH<sub>3</sub> on Si(001). *Phys. Rev. B* **2007**, *75*, 155310.
31. Cho, I.; Kim, Y.; Yeom, H., Temperature-Dependent Adsorption and Dissociation Behaviors of NH<sub>3</sub> on Si(111)7×7: A High-Resolution Core-Level Photoemission Study. *Phys. Rev. B* **2006**, *73*, 115328.
32. Dai, M.; Wang, Y.; Kwon, J.; Halls, M. D.; Chabal, Y. J., Nitrogen Interaction with Hydrogen-Terminated silicon Surfaces at the Atomic Scale. *Nat. Mater.* **2009**, *8*, 825-30.
33. He, J.; Patitsas, S. N.; Preston, K. F.; Wolkow, R. A.; Wayner, D. D. M., Covalent Bonding of Thiophenes to Si(111) by a Halogenation/Thienylation Route. *Chem. Phys. Lett.* **1998**, *286*, 508-514.
34. Koch, N., Organic Electronic Devices and their Functional Interfaces. *ChemPhysChem* **2007**, *8*, 1438-55.
35. Wallart, X.; Henry de Villeneuve, C.; Allongue, P., Truly Quantitative XPS Characterization of Organic Monolayers on Silicon: Study of Alkyl and Alkoxy Monolayers on H–Si(111). *J. Am. Chem. Soc.* **2005**, *127*, 7871-7878.
36. Sieval, A. B.; van den Hout, B.; Zuilhof, H.; Sudhölter, E. J. R., Molecular Modeling of Covalently Attached Alkyl Monolayers on the Hydrogen-Terminated Si(111) Surface. *Langmuir* **2001**, *17*, 2172-2181.
37. Cohen, A. J.; Mori-Sanchez, P.; Yang, W. T., Insights into Current Limitations of Density Functional Theory. *Science* **2008**, *321*, 792-794.
38. Zhao, Y.; Truhlar, D. G., How Well Can New-Generation Density Functional Methods Describe Stacking Interactions in Biological Systems? *Phys. Chem. Chem. Phys.* **2005**, *7*, 2701-2705.
39. Li, Y.; O’Leary, L. E.; Lewis, N. S.; Galli, G., Combined Theoretical and Experimental Study of Band-Edge Control of Si through Surface Functionalization. *J. Phys. Chem. C* **2013**, *117*, 5188-5194.
40. Bocquet, M.-L.; Rappe, a. M.; Dai, H.-L., A Density Functional Theory Study of Adsorbate-Induced Work Function Change and Binding Energy: Olefins on Ag(111). *Mol. Phys.* **2005**, *103*, 883-890.
41. Pursell, D. P.; Bocquet, M.-L.; Vohs, J. M.; Dai, H.-L., Adsorption Structure, Energetics, and Thermal Reactions of Vinyl Chloride on Ag(111). *Surf. Sci.* **2003**, *522*, 90-104.

42. Rusu, P. C.; Brocks, G., Surface Dipoles and Work Functions of Alkylthiolates and Fluorinated Alkylthiolates on Au(111). *J. Phys. Chem. B* **2006**, *110*, 22628-34.
43. Giannozzi, P.; Baroni, S.; Bonini, N.; Calandra, M.; Car, R.; Cavazzoni, C.; Ceresoli, D.; Chiarotti, G. L.; Cococcioni, M.; Dabo, I.; Dal Corso, A.; de Gironcoli, S.; Fabris, S.; Fratesi, G.; Gebauer, R.; Gerstmann, U.; Gougoussis, C.; Kokalj, A.; Lazzeri, M.; Martin-Samos, L.; Marzari, N.; Mauri, F.; Mazzarello, R.; Paolini, S.; Pasquarello, A.; Paulatto, L.; Sbraccia, C.; Scandolo, S.; Sclauzero, G.; Seitsonen, A. P.; Smogunov, A.; Umari, P.; Wentzcovitch, R. M., QUANTUM ESPRESSO: A Modular and Open-Source Software Project for Quantum Simulations of Materials. *J. Phys. Condens. Matter* **2009**, *21*, 395502.
44. Grimme, S., Semiempirical GGA-type Density Functional Constructed with a Long-Range Dispersion Correction. *J. Comput. Chem.* **2006**, *27*, 1787-99.
45. Barone, V.; Casarin, M.; Forrer, D.; Pavone, M.; Sambri, M.; Vittadini, A., Role and Effective Treatment of Dispersive Forces in Materials: Polyethylene and Graphite Crystals as Test Cases. *J. Comput. Chem.* **2009**, *30*, 934-939.
46. Dion, M.; Rydberg, H.; Schröder, E.; Langreth, D. C.; Lundqvist, B. I., Van der Waals Density Functional for General Geometries. *Phys. Rev. Lett.* **2004**, *92*, 246401.
47. Thonhauser, T.; Cooper, V. R.; Li, S.; Puzder, A.; Hyldgaard, P.; Langreth, D. C., Van der Waals Density Functional: Self-Consistent Potential and the Nature of the van der Waals Bond. *Phys. Rev. B* **2007**, *76*, 125112.
48. Román-Pérez, G.; Soler, J., Efficient Implementation of a van der Waals Density Functional: Application to Double-Wall Carbon Nanotubes. *Phys. Rev. Lett.* **2009**, *103*, 096102.
49. Langreth, D. C.; Lundqvist, B. I.; Chakarova-Käck, S. D.; Cooper, V. R.; Dion, M.; Hyldgaard, P.; Kelkkanen, A.; Kleis, J.; Kong, L.; Li, S.; Moses, P. G.; Murray, E.; Puzder, A.; Rydberg, H.; Schröder, E.; Thonhauser, T., A Density Functional for Sparse Matter. *J. Phys. Condens. Matter* **2009**, *21*, 084203.
50. Lee, K.; Murray, É. D.; Kong, L.; Lundqvist, B. I.; Langreth, D. C., Higher-Accuracy van der Waals Density Functional. *Phys. Rev. B* **2010**, *82*, 081101.
51. Scheres, L.; Giesbers, M.; Zuilhof, H., Organic Monolayers onto Oxide-Free Silicon with Improved Surface Coverage: Alkynes versus Alkenes. *Langmuir* **2010**, *26*, 4790-4795.
52. Linford, M. R.; Chidsey, C. E. D., Alkyl Monolayers Covalently Bonded to Silicon Surfaces. *J. Am. Chem. Soc.* **1993**, *115*, 12631-12632.
53. Zhu, X. Y.; Boiadjev, V.; Mulder, J. A.; Hsung, R. P.; Major, R. C., Molecular Assemblies on Silicon Surfaces via Si-O Linkages. *Langmuir* **2000**, *16*, 6766-6772.
54. Effenberger, F.; Götz, G.; Bidlingmaier, B.; Wezstein, M., Photoactivated Preparation and Patterning of Self-Assembled Monolayers with 1-Alkenes and Aldehydes on Silicon Hydride Surfaces. *Angew. Chem. Int. Ed.* **1998**, *37*, 2462-2464.
55. Harada, Y.; Koitaya, T.; Mukai, K.; Yoshimoto, S.; Yoshinobu, J., Spectroscopic Characterization and Transport Properties of Aromatic Monolayers Covalently Attached to Si(111) Surfaces. *J. Phys. Chem. C* **2013**, *117*, 7497-7505.
56. Bhairamadgi, N. S.; Pujari, S. P.; Trovela, F. G.; Debrassi, A.; Khamis, A. A.; Alonso, J. M.; Al Zahrani, A. A.; Wennekes, T.; Al-Turaif, H. A.; van Rijn, C.; Alhamed, Y. A.; Zuilhof, H., Hydrolytic and Thermal Stability of Organic Monolayers on Various Inorganic Substrates. *Langmuir* **2014**, *30*, 5829-5839.
57. Gibbs, G. V.; D'Arco, P.; Boisen, M. B., Molecular Mimicry of Bond Length and Angle Variations in Germanate and Thiogermanate Crystals: A Comparison with Variations Calculated for Carbon-, Silicon-, and Tin-Containing Oxide and Sulfide Molecules. *J. Phys. Chem.* **1987**, *91*, 5347-5354.

# Chapter 5

## **Role of the Head- and/or Tail-groups on Controlling the Work Function of SAM-Functionalized H:Si(111) Surface**

### **5.1 Introduction**

Although some studies have highlighted that the interfacial bonding between the Si surface and the organic chain is chiefly responsible for the alteration of the interface electronic properties,<sup>1-2</sup> these studies have primarily focussed on alkyl chains linked to the surface by carbon (Si-C).<sup>3-6</sup> There are few studies of other chains in the literature, such as ref. 11 in which Si was modified with an alkyl chain with 10 and 18 carbons, linked to Si by C, O, S and the electronic structure was discussed experimentally through different spectroscopic techniques, including X-ray and ultraviolet photoemission spectroscopy and this showed changes in the WF, compared to unmodified Si, of up to ~0.4 eV. In the metal functionalized surfaces the focus is on the SAM attachment via thiolated bonds. The modification of Si with alkyl chains that have different chain lengths, other linker (head)-groups such as nitrogen or oxygen and terminating (tail) groups such as -NH<sub>2</sub> or -SH has not been studied with respect to electronic properties. This is an area of great interest because surface tuning by chemistry variation (head or tail groups) is an attractive approach to modify the interface electronic structure.<sup>7-10</sup> Although sulfur and nitrogen radicals are very often used for

different purposes in SAM technology such as creating fibre surfaces either for analyte interaction or further modification,<sup>11-19</sup> it is therefore imperative to understand how the modification of Si with alkyl chains with different head- and/or tail-groups as well as different alkyl chain lengths can be used to modify the WF of Si in a well understood manner. Achieving this understanding is the subject of the present Chapter.

In Chapter 3,<sup>20</sup> using density functional theory we provided a microscopic explanation on how simple surface modifications of the H-terminated Si(111) surface can change the surface WF in different ways by adsorption of terminal-groups such as -BH<sub>2</sub>, -CH<sub>3</sub>, -NH<sub>2</sub>, -OH, chalcogenides and halides. Subsequently in Chapter 4, we studied the adsorption and structural properties of alkyl chains assembled on H:Si(111) via different head-groups at three different coverages showing also that vdW interactions are required to properly describe Si surfaces functionalized by alkyl-based SAMs.<sup>21</sup> Using the same first-principles framework we now show how the presence of different head- and/or tail-groups plays a dominant role in determining the WF of H:Si(111) surface modified with alkyl chains up to 14 carbons. The possibility to tune the WF of H:Si(111) using different chemical groups at either extreme of the alkyl chain is studied and described based on electronic and structural changes at the interface.

After introducing the computational details in Section 5.2, the main results of the Chapter follow in Section 5.3. The Chapter concludes with some remarks.

## 5.2 Computational Details

We use Density Functional Theory (DFT) with inclusion of vdW interactions to model modified H:Si(111) and calculate the WF; this allows us to separate the various contributions to the change in WF after surface modification.<sup>22</sup> DFT produces trends in the adsorbate-modified substrate WF in qualitative agreement with experiment.<sup>23-25</sup> We perform periodic supercell calculations using a plane wave basis set within the PWSCF code of the QUANTUM-ESPRESSO distribution,<sup>26</sup> with the PBE gradient corrected functional.<sup>27</sup> The electron-ion

interaction is described by ultrasoft pseudopotentials (USPPs) with the following number of valence electrons for each element: Si:4, C:4, N:5, O:6, S:6 and a one electron potential for hydrogen. The kinetic-energy cutoff for the plane wave basis was 35 Ry for the wave function and 400 Ry for the charge density. Starting from bulk lattice constant (5.43 Å), we built a six layer slab of silicon (111), with two dangling bonds on each surface separated by nine equivalent vacuum layers (i.e., unreconstructed (2×1) surface supercell expansion that allows us to simulate 50% coverage<sup>21</sup>).

The dangling bonds are saturated with hydrogen on both surfaces. Full ionic relaxation with the bottom hydrogens fixed was performed until the forces on all atoms were less than 0.01 eV/Å. The Brillouin-zone was sampled using a (4×8×1) Monkhorst-Pack k-point sampling mesh with zero offset. The fixed occupation technique was employed using ten additional bands to ensure convergence of the electronic states. A dipole correction<sup>28</sup> as well as the semi-empirical dispersion term (DFT-D)<sup>29-30</sup> including vdW interactions,<sup>31-35</sup> was used as in Chapter 4, where we showed that including the vdW interaction is required to describe even qualitatively the adsorption properties of these structures.<sup>21</sup>

## 5.3 Results and Discussion

The general structure of H:Si(111) modified with  $-[X^{\text{head-group}}]-(\text{CH}_2)_n-[X^{\text{tail-group}}]$  adsorbates is presented in Figure 5.1 with the example of  $X = \text{NH}_2$ ; as a head-group (-NH-decane, left panel: bonds to Si surface with loss of H), as a tail-group (-decane-NH<sub>2</sub>, middle panel: at non-bonding end of chain) and as both head- and tail-groups (-NH-decane-NH<sub>2</sub>, right panel) allowing us to study the effect of the surface modifiers and extract trends in the change of the H:Si(111) WF. Figure 5.2 (page 101) shows the computed WF of modified H:Si(111) as a function of chain length for the case of  $-[X]$ -Alkyl functionalization with  $X = \text{NH}$ , O and S head-groups. In Figure 5.3 (page 104) we present the effect of tail-group functionalization  $-(\text{CH}_2)_n-[X]$ , focusing on sulfur and nitrogen, on the



WF of H:Si(111). The combined effect of head- and tail-groups on the WF is shown in Figure 5.6 (page 109).

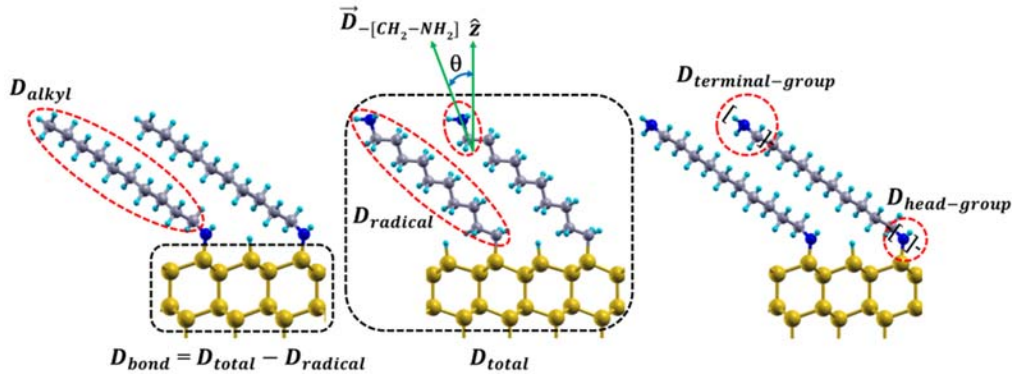


Figure 5.1. Schematic of dipole contributions for different fragments of the adsorbate (adsorbate radical, alkyl chain, head-group and terminal-group), for the case of nitrogen as head- and/or tail-groups. Black-dashed rectangles indicate the area in which the total (middle panel) and bond (left panel) dipole moments are involved.

### ***5.3.1 The effect of the Head-Group on the alkyl- and (O, S, NH)-alkyl-modified H:Si(111) work function***

First we discuss the effect of the head-group on the work function (WF). The computed WF of the unmodified H:Si(111) surface is 4.55 eV. From Figure 5.2 and similar to Chapter 3 and our previous work<sup>20</sup> modifying the surface with the head-group atoms, without any alkyl chains, decreases the WF for N, C, and O and increases for S; the origin of this was discussed in terms of radical dipole, bond dipole, the electronegativity and interatomic distance of the adsorbed species.<sup>24, 36-39</sup> The radical dipole component along the surface normal causes a shift in the WF and the direction of the shift is determined by the sign of radical dipole moment of the adsorbate. On the other hand, the bond dipole which arises from charge reorganization at the silicon-linker (head-group) bond creates a dipole layer which affects the electron acceleration toward the vacuum and

subsequently the WF. The direction and amount of the charge that transfers at the interface directly affects the sign and strength of the surface dipole layer. This can be determined by the valency and electronegativity of the head-group and for this simple case chemical concepts are sufficient to explain the changes.

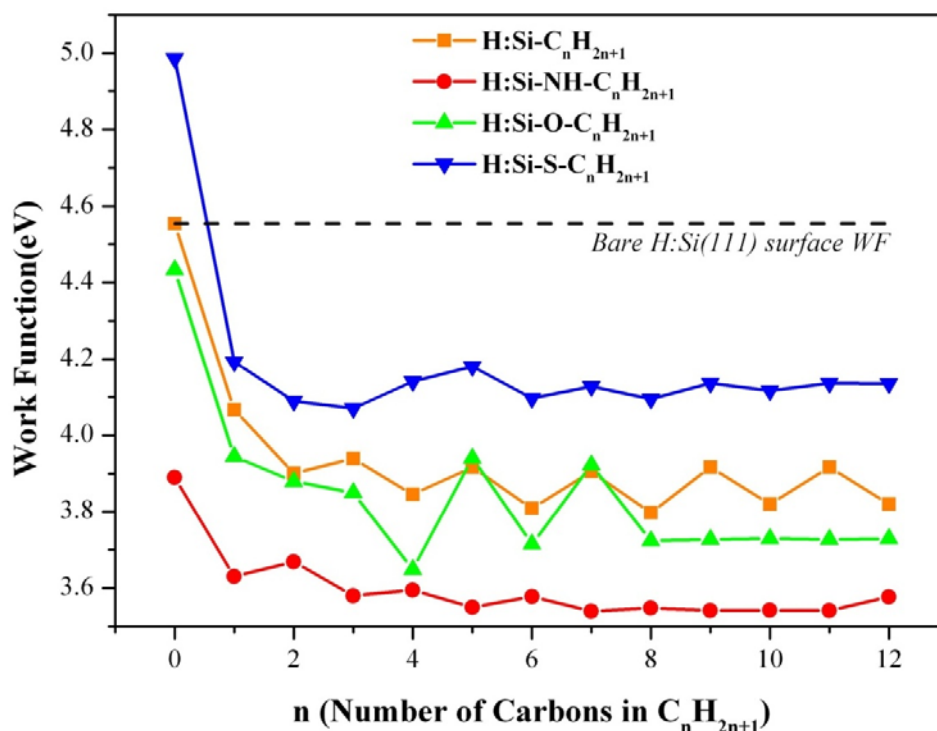


Figure 5.2. WF changes due to variation in the length of the alkyl chain for  $-\text{[X]}-\text{C}_n\text{H}_{2n+1}$  [ $\text{X} = \text{O}, \text{S}, \text{NH}$ ] at half coverage. The black dashed line represents the work function of bare  $\text{H}:\text{Si}(111)$ .

When alkyl chains are adsorbed (i.e. direct Si-C), we see that irrespective of the nature of the head-group, the WF always decreases compared to the unmodified surface. The nitrogen head-group shows the largest decrease in the WF compared to  $\text{H}:\text{Si}(111)$ , irrespective of chain length. However, the largest single WF change is upon adsorption of  $-\text{NH}_2$  ( $\sim 1$  eV) and with addition of alkyl chains, this head-group then shows the smallest shift in the WF ( $\sim 0.1$  eV) as a function of chain length among all the linker-chain structures, potentially limiting the ability to tune the WF over a wide range. The  $-\text{O}-$ ,  $-\text{CH}_2-$  and  $-\text{S}-$  linked chains show larger variations in  $\text{WF}^{20}$  of up to 0.9 eV (for sulfur),

allowing a relatively large range over which the WF can be tuned simply by changing the chemistry. It is worth noting that while the sign of the work function shift compared to the bare surface is the same as that found in theoretical<sup>23, 40-44</sup> and experimental<sup>45-47</sup> studies for organic monolayers on metallic substrates, the magnitudes differ significantly. Also the measured effective WF shift for thiolalkyl chains of different lengths on a gold substrate is qualitatively in agreement with our saturation picture in Figure 5.2.<sup>46</sup>

The result of Ref. 11 is consistent with our results in Figure 5.2 since in that study C<sub>10</sub> monolayers attached by sulfur, oxygen and carbon linkers show similar surface dipoles and work functions as the C<sub>18</sub> monolayers, which reveals that surface chemistry dominates over electronic effects for long chains. Here we extend these studies by examining in detail the effects of the alkyl chain length (C<sub>1</sub>-C<sub>16</sub>) and nitrogen linker group.

It is clear that the WF is most sensitive to chain length for the shortest alkyl chains and despite the small variations of *ca.* 0.1 eV and 0.2 eV for the carbon and oxygen head-groups respectively that gives an apparent odd-even effect, it otherwise tends to saturate for chains with  $n > 6$  carbons. The reason that the WF is sensitive to chain length for short alkyls is that the adsorbed monolayer undergoes a considerable change in structural properties by adding -(CH<sub>2</sub>)- units to the alkyl chain. In general the -[X]-Alkyl chain gains considerable freedom to move by increasing the number of carbons for short alkyls ( $n < 5$ )<sup>21</sup> and consequently this affects the radical dipole moment (see table 5.1). But once the head-group's structure is converged (i.e., remains unchanged by adding -(CH<sub>2</sub>)- units) and the direction of radical dipole moment's vector has no significant change, the WF appears to saturate.

In understanding the shifts in the WF of modified H:Si(111) due to the head-groups, the total dipole moment, bond dipole and radical dipole have been analyzed.<sup>23-24, 36-39</sup> Considering sulfur as the head-group, the total dipole moment due to sulfur functionalization changes sign from negative to positive when the alkyl chain is added (see table 5.1). This switches the direction of the change in the WF compared to having only sulfur termination considered, that is, the WF

becomes smaller compared to the bare surface instead of being larger for just -SH functionalization. Sulfur also shows the smallest dipole moment of all head-groups irrespective of chain length which results in the smallest change in the WF relative to H:Si(111). The largest dipole moment is for adsorbed -NH<sub>2</sub> and -NH-Alkyl chains which is consistent with the largest shift in the WF compared to the bare H:Si(111) surface. But the change in dipole on adding alkyls to the head-group is smallest for -NH-Alkyls, consistent with the smallest WF change amongst the linkers studied. The radical dipole also shows the same behavior as the total dipole: for chain lengths  $0 \leq n \leq 4$ ,  $N > O > C > S$  and for chain lengths  $n > 4$ ,  $O < N < C < S$ . The bond dipole and the electronegativity do not appear, however, to correlate with the change in WF.

Table 5.1. Total dipole moment (Debye) along z (as indicated in schematic of Figure 5.1) for different length -[X]-Alkyl chains. n shows the number of carbons in the alkyl fragment.

	n=0	n=1	n=2	n=3	n=4	n=5	n=6	n=10	n=12
-(C <sub>n</sub> H <sub>2n+1</sub> )	0.00	0.33	0.44	0.42	0.48	0.43	0.51	0.51	0.51
-[NH]-(C <sub>n</sub> H <sub>2n+1</sub> )	0.44	0.61	0.58	0.65	0.64	0.66	0.65	0.67	0.66
-[O]-(C <sub>n</sub> H <sub>2n+1</sub> )	0.08	0.40	0.45	0.46	0.60	0.41	0.57	0.56	0.56
-[S]-(C <sub>n</sub> H <sub>2n+1</sub> )	-0.30	0.24	0.31	0.31	0.28	0.25	0.31	0.28	0.27

### ***5.3.2 The effect of the Tail-Group on the alkyl-modified H:Si(111) work function***

We now consider adsorption of alkyl chains with -NH<sub>2</sub> and -SH tail-groups, which have been used by experimentalists in preparation of different SAMs that facilitate further functionalization.<sup>11-19</sup> Figure 5.3 shows the WF versus number of carbons in the chain and Figure 5.4 shows the atomic structure of the H:Si(111)-C<sub>n</sub>H<sub>2n</sub>-NH<sub>2</sub> systems studied. Interestingly the WF behaves completely differently compared to the case where only head-groups are present. Both tail-groups show large odd-even oscillations with respect to the number of carbons in the chains. The WF converges (to oscillating values) for odd and even number

of carbons at  $n \geq 9$  for nitrogen and at  $n \geq 7$  for sulfur. The peak-to-peak amplitude of the WF with respect to  $n$  at saturation is 1.3 eV and 1.7 eV for sulfur and nitrogen tail-groups with a maximum 0.7 eV and 1.5 eV downward shift from H:Si(111) WF, respectively. For an even number of carbons there is a 0.5 eV difference between alkyls with -NH<sub>2</sub> and -SH tail-groups and this is 0.9 eV for the case of odd number of carbons. Compared to the -NH- and -S- head-groups the WF order remains unchanged with the largest change overall resulting from -NH<sub>2</sub> (tail-group) functionalization.

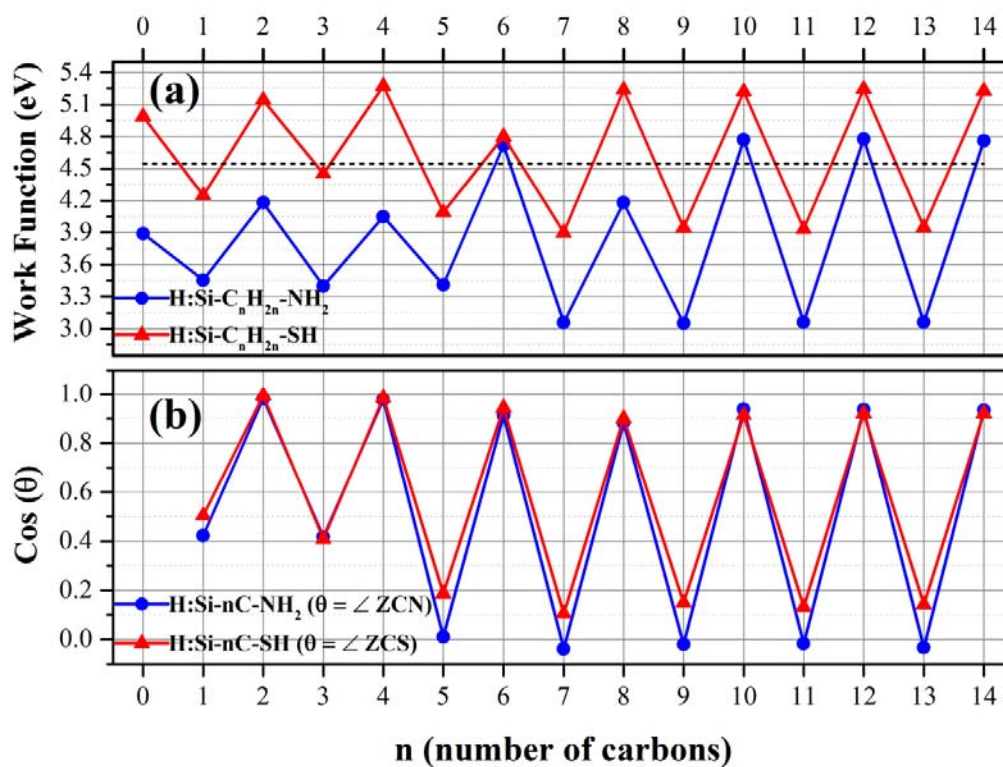


Figure 5.3. (a) WF changes due to variation in the length of the alkyl chain for -C<sub>n</sub>H<sub>2n</sub>-SH and -C<sub>n</sub>H<sub>2n</sub>-NH<sub>2</sub>. (b) The cosine variation of the angle between -[CH<sub>2</sub>-NH<sub>2</sub>] or -[CH<sub>2</sub>-SH] dipole vectors with the z-axis. The black dashed line in (a) indicates the work function of bare H:Si(111).

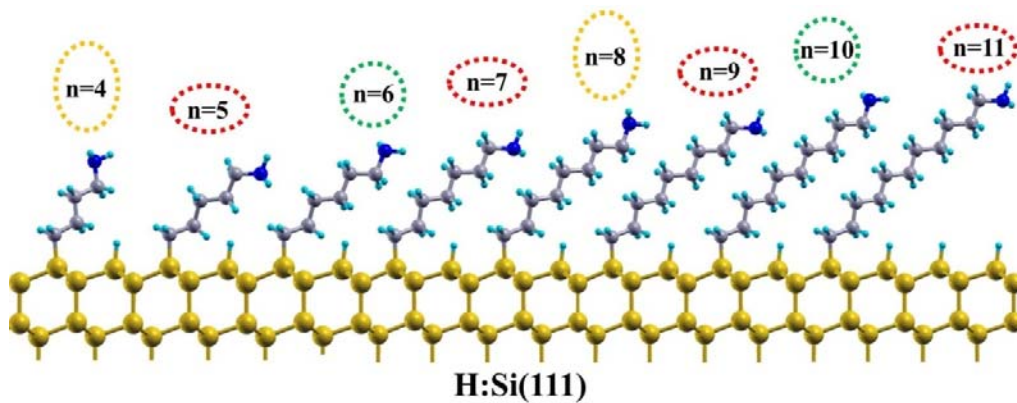


Figure 5.4. Structural variation  $-C_nH_{2n}-NH_2$  for  $4 \leq n \leq 11$ . The dashed ellipsoids with the same color represent the same structural orientation of the tail-group.

Odd-even effects on the structural and electronic properties of SAMs have been reported before<sup>48</sup> particularly for alkyl chains grafted on gold and silver.<sup>49-53</sup> There are no odd-even results on silicon surfaces to our knowledge. In fact, the oscillations observed here for the modified semiconductor are nearly ten times larger than for modified metal surfaces, with magnitudes up to 1.7 eV. Hence, this effect can be a valuable option in tuning the various electronic devices based on silicon-organic interfaces which are currently studied intensively.<sup>54-58</sup>

To fully understand oscillatory behavior of the WF in Figure 5.3, we consider the WF definition and analyze the contributions of the dipoles allocated to different fragments of the SAM, based on ideal molecular monolayer picture which has previously been derived for an infinite, defect-free, two-dimensional periodic array of molecules.<sup>37, 40, 59-63</sup> For a molecular fragment (Figure 5.1) considered as a point dipole (Figure 5.5, a) with electric dipole moment  $\vec{D} = (qd)\hat{r}$  where the opposite charges ( $\pm q$ ) are separated by distance  $d$  from each other, the electric potential ( $V$ ) at any arbitrary point ( $r$ ) and far from the center of the dipole (Figure 5.5, b) can be formulated as:<sup>64</sup>

$$V = \frac{\vec{D} \cdot \vec{r}}{r^3} \text{ (eq. 5.1)}$$

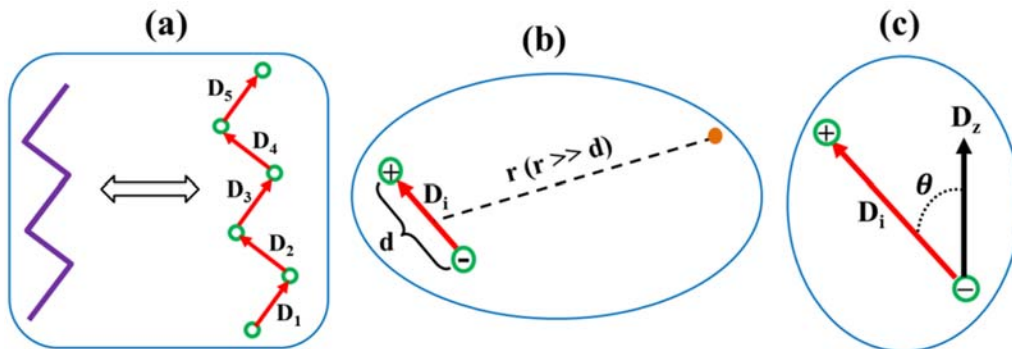


Figure 5.5. (a) Schematic of a molecular fragment as point dipoles, (b) the electrostatic potential for an individual fragment somewhere far from the center of the dipole and (c) the dipole component along surface normal with definition of the angle between them.

Based on superposition principle, the individual fragments potentials will sum up to give the total potential. The average potential outside the monolayer quickly converges to the vacuum level ( $V_{vac}$ ) and this is essential for the determination of the WF:<sup>20</sup>

$$WF = V_{vac} - E_f \text{ (eq. 5.2)}$$

Considering the WF equation and bearing in mind that the Fermi energy is a bulk property, we expect that changes in the vacuum potential directly translate into changes in the WF. Now assuming our surface lies in the  $x$ - $y$  plane and we attach an infinite 2D periodic array of monolayers with finite length, the lateral component of the generated field cancels out due to symmetry and a constant potential is expected. Therefore the average potential which decays to the vacuum level far from the surface is mainly affected by the  $z$ -component of each single-point dipole. Therefore:

$$V_{vac} \propto \frac{D \cos \theta}{r^2}. \text{ (eq. 5.3)}$$

Since  $D_z = D \cos \theta$  (See Figure 5.1) and this equation highlights the dependence of the vacuum potential on each dipole component along the surface normal, with insignificant effect from inner dipoles in a thick monolayer. Considering the superposition principle, an adsorbed alkyl chain with head- and/or tail-groups affects the surface by the contribution of multiple dipoles (Figure 5.1).

Thus the numerator can be written as the summation over dipoles of different fragments (i) along the surface normal:

$$D \cos \theta = \sum_i D_i \cos(\theta_i) \text{ (eq. 5.4)}$$

Therefore the terminal-group (see Figure 5.1 and Figure 5.5 c) is the only dipole that can have an effect when a  $-(\text{CH}_2)-$  unit is added. It should be noted that in a densely packed monolayer the situation is much more complicated than this simple picture we used here to qualitatively explain the oscillations in the WF as a result of chain length. In fact, molecular polarizability, molecule-molecule and molecule-substrate interaction along with structural changes all must be considered for deriving a more accurate formula.<sup>22, 37, 42-43, 63, 65-69</sup> Deriving an exact formula which includes these effects is beyond our scope, however, this simplified approach gives a qualitative account of the origin of the oscillations, as follows.

Figure 5.3 (b) shows the cosine variation of the angle ( $\theta$ ) between the z-axis and the  $-\text{[CH}_2\text{-NH}_2\text{]}$  ( $-\text{[CH}_2\text{-SH]}$ ) dipole vector ( $\theta$  is indicated in the middle panel of Figure 5.1). The WF oscillations match the  $\cos \theta$  variation for both tail-groups. Therefore, we attribute the odd-even effect to the varying dipole alignment of the  $-\text{[CH}_2\text{-CH}_3\text{]}$  terminal-group as a result of adding carbons to the alkyl chain. The value of  $\cos \theta$  is the same to within 0.01 for  $-\text{NH}_2$  and  $-\text{SH}$  tail-groups for even number of carbons and has a shift of about 0.17 for the odd numbers (Figure 5.3, b). This implies a larger component of  $-\text{[CH}_2\text{-NH}_2\text{]}$  dipole moment at odd number of carbons and explains the larger WF shift in Figure 5.3.

Another interesting observation here is that the magnitude of the WF for H:Si(111) functionalized with alkyl-nitrogen is lower than the WF value for alkyl-sulfur functionalized surface. This sequence is the same as when sulfur and nitrogen was used as head-groups only. The stronger bond-dipole<sup>20</sup> in the case of head-group explains the bigger downward shift for nitrogen. However in the case of tail-group both have similar effect in that regard by having Si-C bond at the silicon-chain interface. The terminal-group dipole then determines the magnitude and direction of the WF shift. Table 5.2 presents the z-component of



the terminal-group dipole for the nitrogen and sulfur tail-groups and different length of the alkyl chain up to ten carbons. The data explain both the WF sequence for nitrogen and sulfur (due to larger dipole moment for -Alkyl-NH<sub>2</sub> functionalization) and odd-even effects as a result of adding -(CH<sub>2</sub>)- units to the chain. Also it is worth noting that WF oscillations for the sulfur tail-group at saturation have a symmetrical behavior around that of the bare H:Si(111) surface, which might be potentially applicable as an alternative switch.

Table 5.2: Terminal-Group dipole component (in Debye units) along z (as indicated in schematic of Figure 5.1) for -Alkyl-[X] (X= NH<sub>2</sub>, SH) chains. n shows the number of carbons in the alkyl fragment.

n	1	2	3	4	5	6	7	8	9	10
-(C <sub>n</sub> H <sub>2n</sub> )-[NH <sub>2</sub> ]	1.23	0.71	1.21	0.60	0.87	-0.06	1.19	0.26	1.19	0.01
-(C <sub>n</sub> H <sub>2n</sub> )-[SH]	0.81	0.17	0.71	-0.03	0.74	-0.24	0.74	-0.31	0.73	-0.30

### ***5.3.3 The effect of the Head- and Tail-Groups [-NH-C<sub>n</sub>H<sub>2n</sub>-NH<sub>2</sub>] on the alkyl-modified H:Si(111) work function***

We also examined the case when both head- and tail-groups are present. We calculated the WF (Figure 5.6 a) and decomposed the dipole contributions for different fragments (total, bond, head- and terminal-group) of -NH-C<sub>n</sub>H<sub>2n</sub>-NH<sub>2</sub>, adsorbed on H:Si(111) (Figure 5.8).

In the Figure 5.6 (a) the WF is compared with the WFs of -NH-C<sub>n</sub>H<sub>2n+1</sub> and -C<sub>n</sub>H<sub>2n</sub>-NH<sub>2</sub> functionalization: The WF is plotted as a function of total and radical dipole moments for each case and this shows that the WF is exactly a linear function of the total dipole moment in all cases (Figure 5.6 b). This extends to the radical dipole within reasonable approximation (with a near-linear fit for radical dipoles). This is fully consistent with the Helmholtz-equation<sup>70</sup> used commonly to determine experimentally the molecular tilt angle and the surface coverage based on calculated radical dipoles.<sup>71-72</sup>

Figure 5.6 (a) compares the WF versus number of carbons in the alkyl chain for -NH- head-group, -NH<sub>2</sub> tail-group and -NH/-NH<sub>2</sub> head/tail-groups. For the same reason as before, the odd-even effect is still present in the case of head and tail-groups implementation. However for short chains (n < 6) the oscillations can be thought of as being 'out of phase' between -NH-C<sub>n</sub>H<sub>2n</sub>-NH<sub>2</sub> and -C<sub>n</sub>H<sub>2n</sub>-NH<sub>2</sub> functionalization. After a transition length between n=7 and n=10 both functionalizations show in-phase oscillations with even carbon chains exhibiting the larger WF.

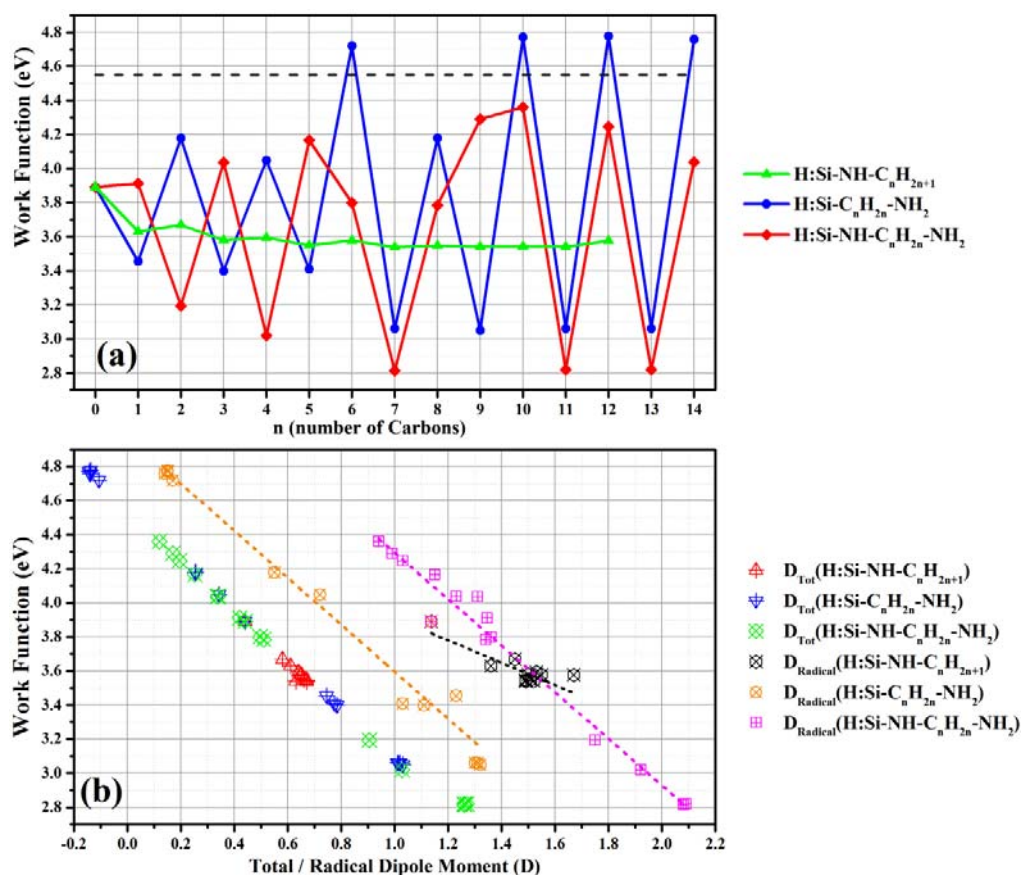


Figure 5.6. (a) WF plotted as a function of number of carbons in the alkyl chain and (b) total/radical dipole moments for H:Si(111)-[NH]-C<sub>n</sub>H<sub>2n</sub>-[NH<sub>2</sub>] (The dashed lines stand for linear fit to the radical dipole points).

OH- and COOH-terminated alkanethiol SAMs have been successfully created on a gold substrate<sup>73</sup> and for alkyl functionalization on gold with both head- and tail-group present, three regimes are distinguishable in term of dipole interaction between head and tail: strong dipole coupling for  $n \leq 4$ , intermediate coupling for  $5 \leq n \leq 13$  and weak coupling for  $n \geq 14$ .<sup>42-43</sup> These three regimes have not been reported for silicon functionalized surfaces to the best of our knowledge. What is visible from Figure 5.6 (a) for head- and tail-group functionalization is the clear distinction between regimes at  $n=5$  and  $n=10$ . The oscillatory behavior for only tail-group functionalization seems to follow closer the regimes identified for the gold functionalized surface, although we do not have data for  $n > 14$ .

For the same length of the alkyl chains with odd number of carbons at saturation, when both head- and tail-groups are present, the WF is 0.2 eV lower than when only the tail-group is present (Figure 5.6 (a)). This is the constructive effect of the bond dipole Si-N which causes further decrease of the WF and allows a WF reduction of up to 1.73 eV compared to the bare hydrogenated silicon surface. In addition, there is a significant reduction in peak-to-peak amplitude of the WF oscillations (1.43 eV) in comparison with the tail-group case (1.7 eV). This is attributed to the smaller oscillation of the terminal-group dipole angle with respect to z-axis ( $\theta$ ) for odd-even variation. This will cause a smaller dipole component change along the surface normal and consequently smaller WF change interval. We expect that 1.73 eV is the maximum tuning we can get from the combination of the studied species as tail- and/or head-groups. Apart from the possibility of further tuning, as we showed earlier, a correct choice of the head-group can guarantee the structure stability and creation of a densely packed monolayer.<sup>21</sup>

In order to understand further the effect of head- and tail-groups on the WF, we decomposed the -NH-Alkyl-NH<sub>2</sub> chain into several fragments as shown in Figure 5.1 and we calculated the dipole moments of each part, separately. Subtracting the calculated radical dipole from the total dipole moment also yields the bond dipole which is determined by the bond strength between the

head-group and surface silicon. Figure 5.8 shows the calculated data for nitrogen-based head and tail-groups. It is clear that the total dipole, radical dipole and terminal-group dipole have similar oscillatory behavior to the work function; a higher dipole causes a lower WF and the inverse is true. The head-group and alkyl chain dipoles are well converged at long chain length. Together with the insignificant role of the carbon bond dipole, this explains why having only the head-group causes saturation of the WF for long ( $n > 6$ ) chains. Three different phases are distinguishable in the WF's behavior; in the  $n=1-5$  it oscillates similar to the case of tail-group but in opposite phase, region  $n=6-9$  which marks a change in phase and  $n=10-14$  in which odd-even oscillations are the same as the nitrogen tail-group. Structural changes in the transition region are mainly responsible for the change in behavior to that of the tail-group mode as the alkyl chain grows (see Figure 5.7).

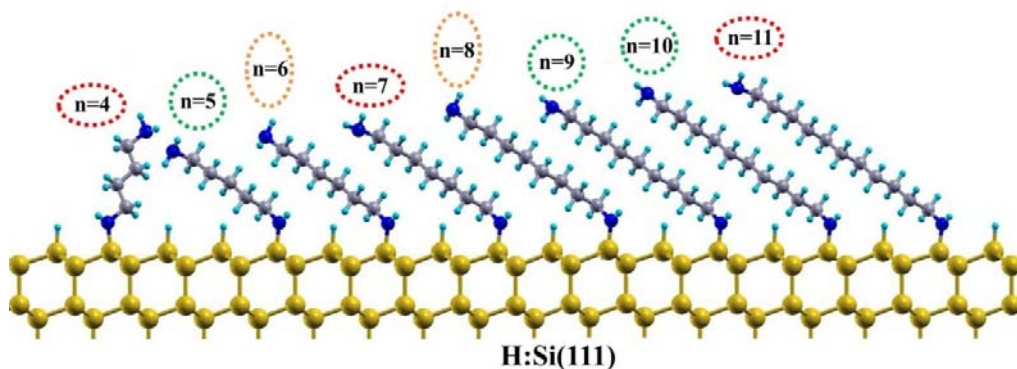


Figure 5.7. Structural variation  $-\text{NH}-\text{C}_n\text{H}_{2n}-\text{NH}_2$  for  $4 \leq n \leq 11$ . The dashed ellipsoids with the same color represent the same structural orientation of the tail-group.

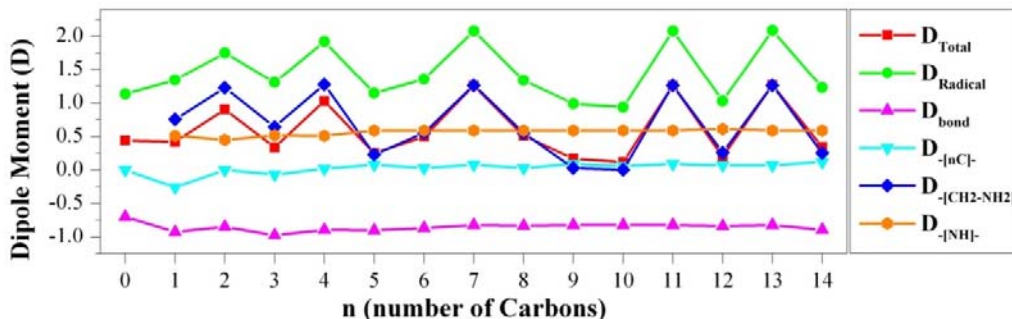


Figure 5.8. Dipole moments of different fragments versus length of the alkyl chain for  $-\text{NH}-\text{C}_n\text{H}_{2n}-\text{NH}_2$ .

### ***5.3.4 Comparison with experiment***

To the best of our knowledge, the investigations in this Chapter, especially the effect of tail and head/tail-group combinations on the WF of H:Si(111), has not been studied before and we have not found relevant experimental results to compare with. In one of the few related experimental works<sup>11</sup> only the effect of linker on the WF of silicon (111) was studied and the results revealed that C<sub>10</sub> monolayers attached by sulfur, oxygen and carbon linkers show similar surface dipole moments and WFs as the C<sub>18</sub> monolayers with the same linker respectively. This indicates the domination of surface chemistry over electronic effects at long alkyl chain length. This is however consistent with our findings in section 5.3.1 that WF converges for various linkers for alkyl chains longer than 8 carbons.

Oscillations in structural and electronic properties of SAMs have been seen before,<sup>48</sup> to date for alkyl chains attached to gold and silver<sup>49-53</sup> and to our knowledge this has not been reported for silicon surfaces. For example, alkanethiol SAMs with OH- and COOH- terminal groups have been created on a gold surface.<sup>73</sup> Following this study and using the same head- and tail-group it was shown that there are three regimes distinguishable in terms of dipole interaction between head and tail: strong dipole coupling regime for  $n \leq 4$ , intermediate coupling regime for  $5 \leq n \leq 13$  and weak coupling regime for  $n \geq 14$ .<sup>42-43</sup> For functionalized silicon surfaces, such regimes have not been reported. Our results for nitrogen as both head- and tail-group shows that there is a clear distinction between regimes at  $n=5$  and  $n=10$ . Although we do not have data for  $n > 14$ , odd-even oscillations for only tail-group functionalization appears to be more consistent with the identified regimes from the previously mentioned study on gold.

The computed oscillations for the modified H:Si(111) in this study are one order of magnitude larger (up to 1.7 eV) than on the metal surfaces.<sup>50</sup> Therefore, this large tuning interval can be a valuable option in modifying various silicon-organic based devices.<sup>54-58</sup> For example, to get higher sensitivity in FET-based nanowire sensors it is important to keep the threshold voltage around zero, as

close as possible.<sup>78</sup> It is shown that alkyl monolayers are capable of modifying the threshold voltage<sup>56</sup> and including this large odd-even tuning interval predicted here can substantially improve our control of the threshold voltage or sensor sensitivity in the next generation of organic-inorganic devices. Considering the large predicted peak-to-peak amplitude of oscillations this can also be implemented in the future as an alternative molecular switch with application in nanosensors or as an option for reaction monitoring and control of the monolayer thickness.

## 5.4. Concluding remarks

In summary, our results show that the WF of the H:Si(111) surface can be modified by up to 1.73 eV by adsorption of organic chains with judicious choice of head groups for strong surface binding and tail-groups for WF modulation. No matter which combination of head- or tail-groups is used, for short chains the WF depends on chain length with pronounced effects arising from the choice of head and tail groups as well as displaying a weak odd-even effect. With different head-groups the WF converges quickly showing no significant odd-even effects at long chain lengths and the WF shifts compared to bare H:Si(111) are determined by the head-group.

For functionalization with different tail-groups or with both head and tail-groups a strong oscillatory behavior of the work function is observed, with WF changes of up to 1.73 eV compared to bare H:Si(111). For the types of functionalized alkyl chains employed experimentally,<sup>2, 74-77</sup> namely with 12 or more carbons in the alkyl chain and terminated with -SH and -NH<sub>2</sub>, the WF change is dominated by the nature of the tail-group. The number of carbons in the alkyl chain plays a role in controlling the WF through the odd-even effect.

Thus SAMs of high stability with maximum tunability in the WF can be achieved by functionalizing with both head and tail-groups, in which the head-group determines the stability of the SAM and the tail-group is able to induce large shifts in the surface WF. In addition, the WF can also be controlled by

exploiting the odd-even effect in long alkyl chains. These results give important microscopic insights into work function tuning of H:Si(111) by modification with functionalized alkyl chains.

## 5.5. References

1. Vilan, A.; Yaffe, O.; Biller, A.; Salomon, A.; Kahn, A.; Cahen, D., Molecules on Si: Electronics with Chemistry. *Adv. Mater.* **2010**, *22*, 140-159.
2. Hacker, C. A., Modifying Electronic Properties at the Silicon-Molecule Interface Using Atomic Tethers. *Solid-State Electron.* **2010**, *54*, 1657-1664.
3. Faber, E. J.; de Smet, L. C.; Olthuis, W.; Zuilhof, H.; Sudholter, E. J.; Bergveld, P.; van den Berg, A., Si-C Linked Organic Monolayers on Crystalline Silicon Surfaces as Alternative Gate Insulators. *ChemPhysChem* **2005**, *6*, 2153-2166.
4. Lavi, A.; Cohen, H.; Bendikov, T.; Vilan, A.; Cahen, D., Si-C-Bound Alkyl Chains on Oxide-Free Si: Towards Versatile Solution Preparation of Electronic Transport Quality Monolayers. *Phys. Chem. Chem. Phys.* **2011**, *13*, 1293-1296.
5. Uosaki, K.; Fukumitsu, H.; Masuda, T.; Qu, D., Construction of a Metal-Organic Monolayer-Semiconductor Junction on a Hydrogen-Terminated Si(111) Surface Via Si-C Covalent Linkage and its Electrical Properties. *Phys. Chem. Chem. Phys.* **2014**, *16*, 9960-9965.
6. Wong, K. T.; Lewis, N. S., What a Difference a Bond Makes: The Structural, Chemical, and Physical Properties of Methyl-Terminated Si(111) Surfaces. *Acc. Chem. Res.* **2014**, *47*, 3037-3044.
7. Vilan, A.; Shanzer, A.; Cahen, D., Molecular Control over Au/GaAs Diodes. *Nature* **2000**, *404*, 166-168.
8. Selzer, Y.; Cahen, D., Fine Tuning of Au/SiO<sub>2</sub>/Si Diodes by Varying Interfacial Dipoles Using Molecular Monolayers. *Adv. Mater.* **2001**, *13*, 508-511.
9. Hunger, R.; Jaegermann, W.; Merson, A.; Shapira, Y.; Pettenkofer, C.; Rappich, J., Electronic Structure of Methoxy-, Bromo-, and Nitrobenzene Grafted onto Si(111). *J. Phys. Chem. B* **2006**, *110*, 15432-15441.
10. He, T.; Ding, H.; Peor, N.; Lu, M.; Corley, D. A.; Chen, B.; Ofir, Y.; Gao, Y.; Yitzchaik, S.; Tour, J. M., Silicon/Molecule Interfacial Electronic Modifications. *J. Am. Chem. Soc.* **2008**, *130*, 1699-1710.
11. Wagner, P.; Nock, S.; Spudich, J. A.; Volkmuth, W. D.; Chu, S.; Cicero, R. L.; Wade, C. P.; Linford, M. R.; Chidsey, C. E., Bioreactive Self-Assembled Monolayers on Hydrogen-Passivated Si(111) as a New Class of Atomically Flat Substrates for Biological Scanning Probe Microscopy. *J. Struct. Biol.* **1997**, *119*, 189-201.
12. Zhao, Y. D.; Pang, D. W.; Hu, S.; Wang, Z. L.; Cheng, J. K.; Dai, H. P., DNA-Modified Electrodes; Part 4: Optimization of Covalent Immobilization of DNA on Self-Assembled Monolayers. *Talanta* **1999**, *49*, 751-756.
13. Strother, T.; Cai, W.; Zhao, X.; Hamers, R. J.; Smith, L. M., Synthesis and Characterization of DNA-Modified Silicon (111) Surfaces. *J. Am. Chem. Soc.* **2000**, *122*, 1205-1209.
14. Frutos, A. G.; Brockman, J. M.; Corn, R. M., Reversible Protection and Reactive Patterning of Amine- and Hydroxyl-Terminated Self-Assembled Monolayers on Gold Surfaces for the Fabrication of Biopolymer Arrays. *Langmuir* **2000**, *16*, 2192-2197.

15. Yang, Z.; Frey, W.; Oliver, T.; Chilkoti, A., Light-Activated Affinity Micropatterning of Proteins on Self-Assembled Monolayers on Gold. *Langmuir* **2000**, *16*, 1751-1758.
16. Li, H. L.; Fu, A. P.; Xu, D. S.; Guo, G. L.; Gui, L. L.; Tang, Y. Q., In Situ Silanization Reaction on the Surface of Freshly Prepared Porous Silicon. *Langmuir* **2002**, *18*, 3198-3202.
17. Harant, A. W.; Khire, V. S.; Thibodaux, M. S.; Bowman, C. N., Thiol-Ene Photopolymer Grafts on Functionalized Glass and Silicon Surfaces. *Macromolecules* **2006**, *39*, 1461-1466.
18. Goddard, J. M.; Hotchkiss, J. H., Polymer Surface Modification for the Attachment of Bioactive Compounds. *Prog. Polym. Sci.* **2007**, *32*, 698-725.
19. Campos, M. A.; Paulusse, J. M.; Zuilhof, H., Functional Monolayers on Oxide-Free Silicon Surfaces Via Thiol-Ene Click Chemistry. *Chem. Commun.* **2010**, *46*, 5512-5514.
20. Arefi, H. H.; Fagas, G., Chemical Trends in the Work Function of Modified Si(111) Surfaces: A Dft Study. *J. Phys. Chem. C* **2014**, *118*, 14346-14354.
21. Arefi, H. H.; Nolan, M.; Fagas, G., Density Functional Theory with van der Waals Corrections Study of the Adsorption of Alkyl, Alkylthiol, Alkoxy, and Amino-Alkyl Chains on the H:Si(111) Surface. *Langmuir* **2014**, *30*, 13255-13265.
22. Segev, L.; Salomon, A.; Natan, A.; Cahen, D.; Kronik, L.; Amy, F.; Chan, C. K.; Kahn, A., Electronic Structure of Si(111)-Bound Alkyl Monolayers: Theory and Experiment. *Phys. Rev. B* **2006**, *74*, 165323-6.
23. Rusu, P. C.; Brocks, G., Surface Dipoles and Work Functions of Alkylthiolates and Fluorinated Alkylthiolates on Au(111). *J. Phys. Chem. B* **2006**, *110*, 22628-22634.
24. Bocquet, M. L.; Rappe, A. M.; Dai, H. L., A Density Functional Theory Study of Adsorbate-Induced Work Function Change and Binding Energy: Olefins on Ag(111). *Mol. Phys.* **2005**, *103*, 883-890.
25. Pourtois, G.; Lauwers, A.; Kittl, J.; Pantisano, L.; Soree, B.; De Gendt, S.; Magnus, W.; Heyns, A.; Maex, K., First-Principle Calculations on Gate/Dielectric Interfaces: On the Origin of Work Function Shifts. *Microelectron. Eng.* **2005**, *80*, 272-279.
26. Giannozzi, P., et al., Quantum Espresso: A Modular and Open-Source Software Project for Quantum Simulations of Materials. *J. Phys. Condens. Matter.* **2009**, *21*, 395502-39521.
27. Perdew, J.; Burke, K.; Ernzerhof, M., Generalized Gradient Approximation Made Simple. *Phys. Rev. Lett.* **1996**, *77*, 3865-3868.
28. Bengtsson, L., Dipole Correction for Surface Supercell Calculations. *Phys. Rev. B* **1999**, *59*, 12301-12304.
29. Grimme, S., Semiempirical GGA-Type Density Functional Constructed with a Long-Range Dispersion Correction. *J. Comput. Chem.* **2006**, *27*, 1787-1799.
30. Barone, V.; Casarin, M.; Forrer, D.; Pavone, M.; Sambri, M.; Vittadini, A., Role and Effective Treatment of Dispersive Forces in Materials: Polyethylene and Graphite Crystals as Test Cases. *J. Comput. Chem.* **2009**, *30*, 934-939.
31. Dion, M.; Rydberg, H.; Schröder, E.; Langreth, D.; Lundqvist, B., van der Waals Density Functional for General Geometries. *Phys. Rev. Lett.* **2004**, *92*, 246401.
32. Thonhauser, T.; Cooper, V.; Li, S.; Puzder, A.; Hyldgaard, P.; Langreth, D., van der Waals Density Functional: Self-Consistent Potential and the Nature of the van der Waals Bond. *Phys. Rev. B* **2007**, *76*, 125112.
33. Langreth, D. C., et al., A Density Functional for Sparse Matter. *J. Phys. Condens. Matter* **2009**, *21*, 084203.



34. Román-Pérez, G.; Soler, J., Efficient Implementation of a van der Waals Density Functional: Application to Double-Wall Carbon Nanotubes. *Phys. Rev. Lett.* **2009**, *103*, 096102.
35. Lee, K.; Murray, É.; Kong, L.; Lundqvist, B.; Langreth, D., Higher-Accuracy van der Waals Density Functional. *Phys. Rev. B* **2010**, *82*, 081101.
36. Cahen, D.; Kahn, A., Electron Energetics at Surfaces and Interfaces: Concepts and Experiments. *Adv. Mater.* **2003**, *15*, 271-277.
37. Natan, A.; Zidon, Y.; Shapira, Y.; Kronik, L., Cooperative Effects and Dipole Formation at Semiconductor and Self-Assembled-Monolayer Interfaces. *Phys. Rev. B* **2006**, *73*, 193310-4.
38. Hofmann, O. T.; Egger, D. A.; Zojer, E., Work-Function Modification Beyond Pinning: When Do Molecular Dipoles Count? *Nano Lett.* **2010**, *10*, 4369-4374.
39. Li, Y.; O'Leary, L. E.; Lewis, N. S.; Galli, G., Combined Theoretical and Experimental Study of Band-Edge Control of Si through Surface Functionalization. *J. Phys. Chem. C* **2013**, *117*, 5188-5194.
40. Heimel, G.; Romaner, L.; Zojer, E.; Bredas, J. L., Toward Control of the Metal-Organic Interfacial Electronic Structure in Molecular Electronics: A First-Principles Study on Self-Assembled Monolayers of Pi-Conjugated Molecules on Noble Metals. *Nano Lett.* **2007**, *7*, 932-940.
41. Heimel, G.; Romaner, L.; Zojer, E.; Bredas, J. L., The Interface Energetics of Self-Assembled Monolayers on Metals. *Acc. Chem. Res.* **2008**, *41*, 721-729.
42. Sushko, M. L.; Shluger, A. L., Dipole-Dipole Interactions and the Structure of Self-Assembled Monolayers. *J. Phys. Chem. B* **2007**, *111*, 4019-4025.
43. Sushko, M. L.; Shluger, A. L., Intramolecular Dipole Coupling and Depolarization in Self-Assembled Monolayers. *Adv. Funct. Mater.* **2008**, *18*, 2228-2236.
44. Rusu, P. C.; Brocks, G., Work Functions of Self-Assembled Monolayers on Metal Surfaces by First-Principles Calculations. *Phys. Rev. B* **2006**, *74*, 073414-4.
45. Zehner, R. W.; Parsons, B. F.; Hsung, R. P.; Sita, L. R., Tuning the Work Function of Gold with Self-Assembled Monolayers Derived from X-[C<sub>6</sub>H<sub>4</sub>-C(C)-]NC<sub>6</sub>H<sub>4</sub>-SH (N= 0, 1, 2; X = H, F, CH<sub>3</sub>, CF<sub>3</sub>, and OCH<sub>3</sub>). *Langmuir* **1999**, *15*, 1121-1127.
46. Alloway, D. M.; Hofmann, M.; Smith, D. L.; Gruhn, N. E.; Graham, A. L.; Colorado, R.; Wysocki, V. H.; Lee, T. R.; Lee, P. A.; Armstrong, N. R., Interface Dipoles Arising from Self-Assembled Monolayers on Gold: UV-Photoemission Studies of Alkanethiols and Partially Fluorinated Alkanethiols. *J. Phys. Chem. B* **2003**, *107*, 11690-11699.
47. Beebe, J. M.; Engelkes, V. B.; Miller, L. L.; Frisbie, C. D., Contact Resistance in Metal-Molecule-Metal Junctions Based on Aliphatic SAMs: Effects of Surface Linker and Metal Work Function. *J. Am. Chem. Soc.* **2002**, *124*, 11268-9.
48. Lu, H.; Terfort, A.; Zharnikov, M., Bending Potential as an Important Factor for the Structure of Monomolecular Thiolate Layers on GaAs Substrates. *J. Phys. Chem. Lett.* **2013**, *4*, 2217-2222.
49. Azzam, W.; Cyganik, P.; Witte, G.; Buck, M.; Woll, C., Pronounced Odd-Even Changes in the Molecular Arrangement and Packing Density of Biphenyl-Based Thiol SAMs: A Combined Stm and LEED Study. *Langmuir* **2003**, *19*, 8262-8270.
50. Tao, F.; Bernasek, S. L., Understanding Odd-Even Effects in Organic Self-Assembled Monolayers. *Chem. Rev.* **2007**, *107*, 1408-1453.
51. Stoliar, P.; Kshirsagar, R.; Massi, M.; Annibale, P.; Albonetti, C.; de Leeuw, D. M.; Biscarini, F., Charge Injection Across Self-Assembly Monolayers in Organic Field-Effect Transistors: Odd-Even Effects. *J. Am. Chem. Soc.* **2007**, *129*, 6477-6484.

52. Heimel, G.; Romaner, L.; Bredas, J. L.; Zojer, E., Odd-Even Effects in Self-Assembled Monolayers of Omega-(Biphenyl-4-yl)Alkanethiols: A First-Principles Study. *Langmuir* **2008**, *24*, 474-482.
53. Alloway, D. M.; Graham, A. L.; Yang, X.; Mudalige, A.; Colorado, R.; Wysocki, V. H.; Pemberton, J. E.; Randall Lee, T.; Wysocki, R. J.; Armstrong, N. R., Tuning the Effective Work Function of Gold and Silver Using  $\Omega$ -Functionalized Alkanethiols: Varying Surface Composition through Dilution and Choice of Terminal Groups. *J. Phys. Chem. C* **2009**, *113*, 20328-20334.
54. Cui, Y.; Wei, Q.; Park, H.; Lieber, C. M., Nanowire Nanosensors for Highly Sensitive and Selective Detection of Biological and Chemical Species. *Science* **2001**, *293*, 1289-1292.
55. Kobayashi, S.; Nishikawa, T.; Takenobu, T.; Mori, S.; Shimoda, T.; Mitani, T.; Shimotani, H.; Yoshimoto, N.; Ogawa, S.; Iwasa, Y., Control of Carrier Density by Self-Assembled Monolayers in Organic Field-Effect Transistors. *Nat. Mater.* **2004**, *3*, 317-322.
56. He, T.; He, J.; Lu, M.; Chen, B.; Pang, H.; Reus, W. F.; Nolte, W. M.; Nackashi, D. P.; Franzon, P. D.; Tour, J. M., Controlled Modulation of Conductance in Silicon Devices by Molecular Monolayers. *J. Am. Chem. Soc.* **2006**, *128*, 14537-14541.
57. Ito, Y.; Virkar, A. A.; Mannsfeld, S.; Oh, J. H.; Toney, M.; Locklin, J.; Bao, Z., Crystalline Ultrasoother Self-Assembled Monolayers of Alkylsilanes for Organic Field-Effect Transistors. *J. Am. Chem. Soc.* **2009**, *131*, 9396-9404.
58. Cummings, S. P.; Savchenko, J.; Ren, T., Functionalization of Flat Si Surfaces with Inorganic Compounds-Towards Molecular CMOS Hybrid Devices. *Coord. Chem. Rev.* **2011**, *255*, 1587-1602.
59. Lennard-Jones, J. E.; Dent, B. M., Cohesion at a Crystal Surface. *J. Chem. Soc. Faraday Trans.* **1928**, *24*, 92-108.
60. Macdonald, J. R.; Barlow, C. A., Work Function Change on Monolayer Adsorption. *J. Chem. Phys.* **1963**, *39*, 412-422.
61. De Renzi, V.; Rousseau, R.; Marchetto, D.; Biagi, R.; Scandolo, S.; del Pennino, U., Metal Work-Function Changes Induced by Organic Adsorbates: A Combined Experimental and Theoretical Study. *Phys. Rev. Lett.* **2005**, *95*, 046804-4.
62. Cornil, D.; Olivier, Y.; Geskin, V.; Cornil, J., Depolarization Effects in Self-Assembled Monolayers: A Quantum-Chemical Insight. *Adv. Funct. Mater.* **2007**, *17*, 1143-1148.
63. Natan, A.; Kronik, L.; Haick, H.; Tung, R. T., Electrostatic Properties of Ideal and Non-Ideal Polar Organic Monolayers: Implications for Electronic Devices. *Adv. Mater.* **2007**, *19*, 4103-4117.
64. Jackson, J. D., *Classical Electrodynamics*, 3rd ed.; Wiley, 1998.
65. Gershevit, O.; Sukenik, C. N.; Ghabboun, J.; Cahen, D., Molecular Monolayer-Mediated Control over Semiconductor Surfaces: Evidence for Molecular Depolarization of Silane Monolayers on Si/SiO<sub>x</sub>. *J. Am. Chem. Soc.* **2003**, *125*, 4730-4731.
66. Gershevit, O.; Grinstein, M.; Sukenik, C. N.; Regev, K.; Ghabboun, J.; Cahen, D., Effect of Molecule-Molecule Interaction on the Electronic Properties of Molecularly Modified Si/SiO<sub>x</sub> Surfaces. *J. Phys. Chem. B* **2004**, *108*, 664-672.
67. Perebeinos, V.; Newton, M., Electronic Structure of S-C<sub>6</sub>H<sub>5</sub> Self-Assembled Monolayers on Cu(111) and Au(111) Substrates. *Chem. Phys.* **2005**, *319*, 159-166.
68. Fukagawa, H.; Yamane, H.; Kera, S.; Okudaira, K.; Ueno, N., Experimental Estimation of the Electric Dipole Moment and Polarizability of Titanyl Phthalocyanine Using Ultraviolet Photoelectron Spectroscopy. *Phys. Rev. B* **2006**, *73*, 041302-4.

69. Deutsch, D.; Natan, A.; Shapira, Y.; Kronik, L., Electrostatic Properties of Adsorbed Polar Molecules: Opposite Behavior of a Single Molecule and a Molecular Monolayer. *J. Am. Chem. Soc.* **2007**, *129*, 2989-2997.
70. G. A. Somorjai; Y. Li, *Introduction to Surface Chemistry and Catalysis*, 2nd ed.; Wiley: Hoboken, NJ, 2010.
71. Weber, R.; Winter, B.; Hertel, I. V.; Stiller, B.; Schrader, S.; Brehmer, L.; Koch, N., Photoemission from Azobenzene Alkanethiol Self-Assembled Monolayers. *J. Phys. Chem. B* **2003**, *107*, 7768-7775.
72. Lange, I., et al., Tuning the Work Function of Polar Zinc Oxide Surfaces Using Modified Phosphonic Acid Self-Assembled Monolayers. *Adv. Funct. Mater.* **2014**, *24*, 7014-7024.
73. Himmel, H. J.; Weiss, K.; Jäger, B.; Dannenberger, O.; Grunze, M.; Wöll, C., Ultrahigh Vacuum Study on the Reactivity of Organic Surfaces Terminated by OH and COOH Groups Prepared by Self-Assembly of Functionalized Alkanethiols on Au Substrates. *Langmuir* **1997**, *13*, 4943-4947.
74. Sano, H.; Maeda, H.; Ichii, T.; Murase, K.; Noda, K.; Matsushige, K.; Sugimura, H., Alkyl and Alkoxy Monolayers Directly Attached to Silicon: Chemical Durability in Aqueous Solutions. *Langmuir* **2009**, *25*, 5516-5525.
75. Sano, H.; Ohno, K.; Ichii, T.; Murase, K.; Sugimura, H., Alkanethiol Self-Assembled Monolayers Formed on Silicon Substrates. *Jpn. J. Appl. Phys.* **2010**, *49*, 01AE09.
76. Lou, J. L.; Shiu, H. W.; Chang, L. Y.; Wu, C. P.; Soo, Y. L.; Chen, C. H., Preparation and Characterization of an Ordered 1-Dodecylthiol Monolayer on Bare Si(111) Surface. *Langmuir* **2011**, *27*, 3436-3441.
77. Pujari, S. P.; van Andel, E.; Yaffe, O.; Cahen, D.; Weidner, T.; van Rijn, C. J.; Zuilhof, H., Mono-Fluorinated Alkyne-Derived Sams on Oxide-Free Si(111) Surfaces: Preparation, Characterization and Tuning of the Si Work Function. *Langmuir* **2013**, *29*, 570-580.
78. Buitrago, E.; Fagas, G.; Badia, M. F. B.; Georgiev, Y. M.; Berthome, M.; Ionescu, A. M., Junctionless silicon nanowire transistors for the tunable operation of a highly sensitive, low power sensor. *Sensor Actuat. B-Chem.* **2013**, *183*, 1-10.
79. Wang, B.; Cancelli, J. C.; Torrecilla, J. S.; Haick, H., Artificial sensing intelligence with silicon nanowires for ultrasensitive detection in the gas phase. *Nano Lett.* **2014**, *14*, 933-8.
3. Bratschitsch, R., Optoelectronic devices: Monolayer diodes light up. *Nat. Nano* **2014**, *9*, 247-248.

# Chapter 6

## Binary Functionalization

### 6.1 Introduction

So far we have studied the effect of functionalization on the H:Si(111) surface with different linkers between the surface and SAM structure, focusing on the electronic and structural properties. We showed that different surface terminations can induce a variety of effects.<sup>1</sup> Alkyl chain attachment to Si through Si-[N, O, S] linkers rather than the usual Si-C bond<sup>2-9</sup> can be used to control the WF tuning of the SAM-Si system as well as the stability of the SAM. Therefore, depending on the nature of the linking atom, different structural characteristics are possible. We also analyzed the optimum coverage which exhibits a strong dependence on the nature of the linker. From this, we propose the possibility to gain finer control in WF adjustment and an improvement in SAM stability and coverage density by using a mixture of functionalizations. The optimum choice of components, based on their performance in functionalization with a single linker, can assist in realizing this idea.

From the literature,<sup>10-13</sup> we start from the possibility that the shift of the WF from different linking atoms will be an average of the individual WFs and study how this is affected by coverage. A higher density of the grafted monolayers, as a result of enhanced stability, means more ordered SAMs and consequently fewer defects. This will therefore improve the efficiency of the solid-molecule systems by eliminating the negative impact of the defects and create a uniform interface. Binary functionalization can also prepare a platform for secondary

functionalization which is important in terms of fabricating those structures with desired functionalities. Figure 6.1 shows a schematic view of this idea.

One should notice that mixed functionalization needs to be distinguished from binary functionalization. The former indicates two or more separate components that create spatially patterned distributed islands, each consisting of one type of termination surrounded by a matrix of a second type of functionalization. However binary functionalization consists of only two types of components and ideally homogeneous-like SAMs extended up to the nanoscale. The latter is the focus of this Chapter.

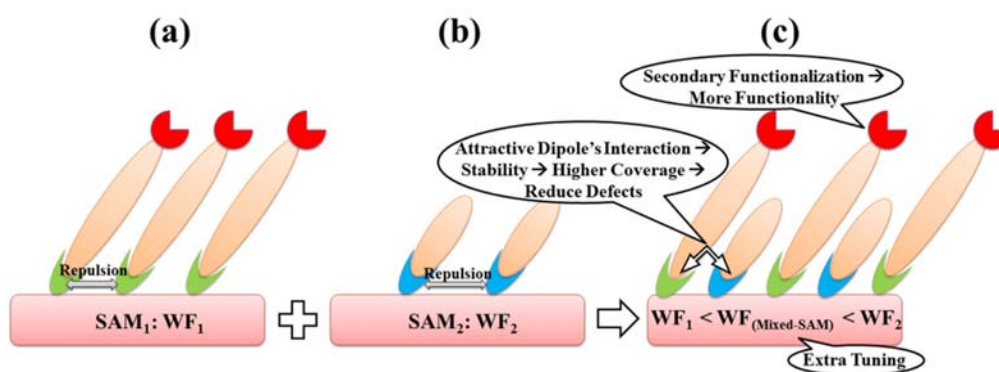


Figure 6.1. Conceptual demonstration of binary functionalization and its potential abilities: Single functionalization of each component has an absolute value of the surface WF with an optimum SAM coverage. See (a) and (b). With the careful choice of components, a mixed monolayer (c) may accommodate a higher coverage of SAMs as a result of attractive dipole interaction between each individual linker and as a result, stability enhancement of the final SAMs. Higher coverage is favorable since it helps reducing the defects by saturation of the adsorption sites and delivers a uniform space charge layer at the interface. In addition, binary functionalization makes it possible to tune the WF within the interval of the WF of single functionalization and controlling the coverage of each SAM can further increase the tuning. Keeping the option of secondary functionalization via tail-groups open is also another advantage of the mixed monolayers.

Similar to functionalization for single type of SAM, as we discussed in previous chapters, it has been shown that surface tuning via binary functionalization on the molecular level also impacts nanoscopic surface ordering properties and thus the macroscopic phenomena of particle accumulation behaviour such as

adhesion and wettability.<sup>12, 14-17</sup> The possibility of mixing functionalities in defined proportions for precise adjustment of surface properties has been realized before<sup>18</sup>; however compared to their fabrication and characterization, potential applications have not been discussed. To date gold has been the most popular choice of inorganic solid in hybrid devices. Most of the binary SAMs use Au-S anchoring and this is due to the ease of fabrication and relatively simple substrate-adsorbate interaction, so that only the intrinsic dipole of the adsorbate layer needs to be counted. However the mechanism of the electronic structure changes at the interface of the solid-SAMs is different for metals and semiconductors. Therefore semiconductor-SAMs require a detailed analysis.

We propose that applying more than one anchoring chemistry can boost the WF tuning in a controllable manner and just as importantly secure the monolayer stability. Considering the ability of silicon to create strong covalent bonds with many potential linkers, this gives us more options compared to gold surfaces which have known problems in surface bonding with linkers other than sulfur. Silicon, as the most widely used material in semiconductor technology and the building block of electronic devices, is the most promising solid substrate for mixed functionalization. Tuning and controlling surface properties in FET-based devices at the nanoscale is vital since it directly influences the device performance and binary functionalization is an interesting approach to achieve further flexibility compared to the effect of a single type surface functionalization.<sup>19-20</sup> In addition, it could help in establishing a platform for enhanced biosensors<sup>21</sup> and efficient optoelectronics.<sup>22-23</sup>

### **6.1.1 Motivation for binary functionalization**

While single-component SAM functionalization is capable of tuning certain properties such as WF or wettability, applying a mixed monolayer with two different components allows a range of surface properties to be tuned in a continuous-like manner simply by adjusting the composition in the mixed monolayer. It has been shown that, for example, the wetting characteristics of

gold surfaces are tunable by mixed monolayers which contain both hydrophobic and hydrophilic components.<sup>24</sup> In another work, the use of different ratio of two types of SAMs, such as n-alkanephosphonic and fluorinated phosphonic acid which are known to decrease and increase the WF respectively, can tune the WF of indium-tin-oxide (ITO) over a range of 5-5.75 eV while the bare ITO WF in that study was  $\sim$ 5.65 eV.<sup>25</sup> Chen et al. showed that wetting and WF can be modified at the same time by using a mixed functionalization of fluorinated alkanethiol and a carboxyl-terminated alkanethiol of various chain lengths on a silver substrate. Their investigation revealed that while changing the composition ratio can yield an interval of 4.3-5.3 eV in the WF, adjusting wettability is dependent on the relative chain length of the individual components.<sup>26</sup> Applying two types of carboranethiol isomer SAMs Jaemyung et al.<sup>19</sup> showed that the WF of gold and silver can be systematically tuned over a wide range of  $\sim$ 0.8 eV with no sizeable change in the surface energy, which provides control of dipole moments without introducing any additional chemical functionalities. Another study by Yong et al.<sup>20</sup> of a gold substrate in an organic-field-effect-transistor (OFETs) structure with an emphasis on regulating charge injection by use of mixed SAMs of 1-decanethiol (1DT) and perfluorodecanethiol (PFDT) at different ratios achieved an interval of 4.4-5.6 eV in the WF. The ratios of 1DT:PFDT were chosen like 10:0, 8:2, 5:5, 3:7, 2:8, 1:9 and 0:10 which resulted the WF values of 5.0, 4.5, 4.7, 5.0, 5.2, 5.3, 5.5 and 5.7 eV respectively.

Mixed functionalization commenced mainly in the early 1980s when organic functionalized silicon-based compounds were fabricated and characterized.<sup>27-33</sup> Soon attention was drawn toward functionalized gold surfaces mainly with mixed thiolated SAMs, by variation of the SAM's mixture, head group, tail group or chain length.<sup>34-41</sup> The most common methods to prepare such a monolayer were either substrate exposure to a multi component solution (usually two components) or exchanging the terminal groups (in definite proportions based on need) of an initially fabricated single-type SAM, which was also called

sequential adsorption (more detailed report on various methods for preparing binary SAMs can be found here<sup>42</sup>).<sup>17, 24, 43-44</sup> This popular method was based on competitive chemisorption. Via these approaches many binary monolayers such as aryl / alkyl<sup>28, 45-46</sup>, alkyl / alkyl<sup>27, 29-31</sup>, fluoroalkyl / alkyl<sup>47-49</sup>, ester / alkyl<sup>32</sup>, haloalkyl / alkyl<sup>32</sup>, phthalimidoalkyl / alkyl<sup>50</sup> and diphenylphosphino / alkyl<sup>28</sup> have been successfully fabricated on various types of silicon and silicon-dioxide substrates using organosilane mixtures. Uniformity of the mixed monolayer is however an important issue as it directly affects the adjustment purpose. Contact angle measurement, X-ray photoelectron spectroscopy (XPS), atomic force microscopy (AFM) and ellipsometric thickness measurements have been used as the main tools for the purpose of characterizing fabricated SAMs.<sup>51-52</sup>

Exploring the details of composition and phase separation of the monolayers was one of the main concerns in early works.<sup>34-38</sup> A mixture of SAMs was presumed to create macroscopic islands; however later studies showed the phase separation up to nanoscale level for various binary n-alkanethiols with long and short chains.<sup>53-58</sup> In general, the distribution of each component in the mixed SAM can be distinguished as phase-separated or homogeneously mixed, even at the nanoscale. This is determined by the type of functional group, chain length and the fabrication process.<sup>55, 59-62</sup> Apart from indications of phase separation up to the microscopic level, the study of combination of short and long alkyl chain functionalization suggested the stability order as long-long > short-short > long-short.<sup>37</sup> This clearly demonstrates the key role of mixed functionalization in determining the stability of the SAMs on metals. It has also been proven that mixed monolayers are suitable for DNA deposition<sup>63-64</sup> and are therefore very important for biological and health studies. In one interesting application Frederix et al.<sup>21</sup> studied a biosensor interface consisting of mixed SAMs of thiols with carboxylic and hydroxyl or poly(ethylene glycol) on gold. Their analysis based on surface plasmon resonance measurements showed that these mixed SAMs improve the sensitivity, stability, and selectivity in comparison with those of commercially available affinity biosensor interfaces.



In terms of electronic structure tuning, binary monolayers of n-alkanethiol (HDT) together with the fluorinated analogue (FDT) attached to silver surface is shown to tune the WF in a continuous-like manner over a wide range of 4.1-5.8 eV, simply by varying the ratio of the components.<sup>10</sup> The extreme of the WFs derive from single-type functionalization of n-alkanethiol and n-flourinated-alkanethiol, while the WF of the silver surface was 4.67 eV after measurement. The ratios of FDT:HDT were selected as 1:0, 4:1, 2:1, 1:1, 1:2, 1:4, 0:1 which gave values of 5.83, 5.53, 5.25, 4.89, 4.65, 4.40, 4.10 eV for the WF. The same experiment for a gold surface resulted in a WF 4.4-5.9 eV interval which was described as being near-linear with respect to component's ratio variation. In order to test the effect of binary functionalization on Fermi-level-pinning and consequently charge injection, they designed a hole-only diode with the Ag/SAM/HTLs/Ag (HTLs:hole-transporting layers) and investigated the I-V characteristics of the device subject to different composition of the binary SAM and hole-transporting layers (HTLs). The maximum current among all investigated ratios of FDT:HDT were obtained for Ag modified with a ratio of 2:1 indicating an efficiency improvement by applying binary SAMs compared to the single functionalization.

A similar study with alkanethiol SAMs deposited on gold with two different terminal groups, carboxylic acid and amine, also reported a linear dependence between composition and the surface WF which varies within the boundary values of single component functionalization.<sup>13</sup> Furthermore, it has been shown that both incomplete SAMs<sup>65</sup> and substituting functional groups<sup>66</sup> can produce tuneable net dipole moment and consequently tailor the WF, but this was highly dependent on controlling the reaction. Whereas mixed functionalization can afford even finer electronic tuneability on both metal and semiconductor substrates,<sup>11, 13, 67-68</sup> its reproducible structure and characteristics as a result of being independent of reaction evolution is another extra advantage of co-deposition.

Applying various characterization methods such as water contact-angle measurements, X-ray photoelectron spectroscopy (XPS), atomic force

microscopy (AFM), and sum frequency generation (SFG) vibrational spectroscopy Tong et al.<sup>52</sup> investigated binary mixed SAMs of 3-aminopropyltriethoxysilane (APS,  $\text{NH}_2(\text{CH}_2)_3\text{Si}(\text{OCH}_2\text{CH}_3)_3$ ) and octadecyltrimethoxysilane (ODS,  $\text{CH}_3(\text{CH}_2)_{17}\text{Si}(\text{OCH}_3)_3$ ) on a silicon oxide surface. Their study revealed substantial structural and electronic effects in the binary functionalization. As a result APS induced a conformation disordering in the ODS molecules at the binary level. The mixed-SAM modified surface was positively charged at  $\text{pH} < 5$  and negatively charged at  $\text{pH} > 7$ . Similar investigation of Au nanoparticles modified by SAMs with mixed carboxylic acid and amine functional groups was done by Lin et al.<sup>69</sup> Their experimental analysis showed the possibility of tailoring surface potential and the iso-electric point (IEP) of the nanoparticles by the ratio of these functional groups. This would achieve an IEP interval between 3.2 and 7.3, the extremes defined by amine and carboxylic acid functional groups. Based on electrostatic interactions, molecules can adsorb/desorb simply by pH variation around this tunable IEP and therefore immobilization can be enhanced.

O'Leary et al.<sup>70</sup> formed mixed methyl/allyl monolayers via two-step halogenation/alkylation reaction process on Si(111) surfaces. Their investigation concludes that there is the possibility to keep the favourable properties of the  $\text{CH}_3\text{-Si}(111)$  such as effective passivation and the rich electrical properties<sup>71</sup>, while incorporating a significant fraction of functional groups to allow secondary functionalization with high total surface coverages and low surface recombination velocities. Later by applying mixed monolayer techniques on H:Si(111) functionalized with methyl and thienyl groups they showed how sequential secondary functionalization can produce high-quality surfaces for tethering small molecules to silicon photoelectrodes and minimizes the residual electronic traps.<sup>72</sup>

Up to the device level Johansson et al.<sup>73</sup> studied the open-circuit potentials of p-Si/(( $\text{MV}^{2+}/\text{MV}^+$ )(aq)) junctions with Si(111) surfaces functionalized with H-,  $\text{CH}_3$ -,  $\text{CH}_2\text{CHCH}_2$ -, or mixed  $\text{CH}_3$ -/ $\text{CH}_2\text{CHCH}_2$ - monolayers while the solution pH was varied from 2.5 to 11. They found out that the pH sensitivity of

the open-circuit potentials, and therefore the band-edge positions, was not correlated with the total fraction of Si atop sites terminated by Si–C bonds. Metal-semiconductor junctions between Hg and CH<sub>3</sub>-, CH<sub>2</sub>CHCH<sub>2</sub>-, or mixed CH<sub>3</sub>-/CH<sub>2</sub>CHCH<sub>2</sub>-terminated n-Si(111) surfaces created rectifying Hg/Si Schottky junctions and yielded mutually similar barrier-heights (~0.9 V). This suggests that the magnitude and direction of the surface dipoles on all of these functionalized surfaces is similar. Later, hybrid Schottky junction solar cell based on methyl/allyl groups terminated silicon nanowire arrays (SiNWs) and poly(3,4-ethylenedioxythiophene)/poly(styrenesulfonate) with a power conversion efficiency (PCE) of 10.2% was demonstrated by Zhang et al.<sup>22</sup> where they showed that devices based on methyl/allyl passivated SiNWs exhibit improved stable electrical output over those based on either methyl or allyl passivated ones. In one of the recent studies Barnea-Nehoshtan et al.<sup>23</sup> applied silane-based binary molecular monolayers on a pentacene/SiC junction and showed that it could be a pathway to decoupling the interface energetics and the morphology of the ingredient phases. In particular, their investigation revealed how use of binary alkyl-silane monolayers with buried dipoles preserves the dipole of the free functionalized surface via the deposition of the organic overlayer, and improves the tunability of the open circuit voltage in a hybrid organic/inorganic solar cell.

Considering the tuneable character of aliphatic SAMs grafted on the substrate and electrical conduction properties of aromatic conjugated molecules, applying a mixture of aliphatic-aromatic binary SAMs was also taken into account. In a study by Smith et al.<sup>74</sup> they highlighted the homogeneity of the surface, nanoscale phase separation and high tunability of the compositions in a mixed fabricated aromatic-aliphatic trichlorinated SAM. Later Patrone et al.<sup>75</sup> fabricated mixed aliphatic/aromatic trichlorosilane molecules on silicon covered by its native oxide and studied the phase separation.

Computational studies on the subject of binary functionalization however are less prominent. In one of the early works, Rissner et al.<sup>76</sup> by the aid of DFT investigated biphenylthiolate-based SAMs adsorbed on the Au(111) surface to

explain the properties of binary adsorbed SAMs with  $-NH_2$  and  $-CN$  tail-groups. Their investigation along with other computational studies on single-type functionalization on gold<sup>77-90</sup> conclude that there is a sizable difference between the electronic structure of binary SAMs compared to the single-component functionalized surface, which they attributed to electrostatic interaction between the sublattices of the mixed-SAM components. Qualitative analysis of band-alignment and variation in the work function by altering each component's ratio showed different dependence in comparison with the coverage effect in single-type SAMs. This was associated with the absence of depolarization in binary SAMs and consequently was responsible for the linear behaviour of the work function and band alignment with respect to variation of the component's ratio. In another work by Kuo et al.<sup>11</sup> a combined theoretical and experimental study of binary siloxane-anchored SAMs with various ratios of 3-aminopropyltrimethoxysilane (APTMS) and 3-mercaptopropyltrimethoxysilane (MPTMS) allowed fine-tuning of the WF to desired values. They conclude that the WF of silicon modified with these binary SAMs shows linear behaviour with changes in chemical composition, which allows gradual tuning between extremes of single type functionalization (up to  $\sim 1.6$  eV). They focused on two functional tail-groups namely amine and thiol, however, in our work we investigate the effect of binary functionalization with different linkers and length of the alkyl chain. Furthermore, we emphasize the stability and coverage enhancement by applying suitable combination of the binary components.

## 6.1.2 Our approach

With this background, we investigate binary functionalization of the silicon (111) surface with alkyl monolayers with different anchoring chemistry (C, O, N, S) to examine if they offer further flexibility for tuning WF and stability. To this end, first we recall from Chapter 5 that alkyl SAMs assembled via nitrogen linker cause the biggest shift in the WF of bare H:Si(111) among all our considered linking atoms. This is followed by oxygen, carbon and finally sulfur.

Thus, as the first step we fix the total coverage to 50% and study mixed functionalization of H:Si(111) surface with the NH<sub>2</sub>, OH and SH terminations, each at 25% coverage. We use different length of alkyl chains namely hexyl and dodecyl. Combination of H:Si-X termination plus H:Si-X-hexyl functionalization will also be considered (X= NH, O, S).

Alkyl functionalization with linking atom other than carbon shows enhanced stability compared to Si-C bonding. In addition, direct alkyl-silicon attachment is not able to accommodate coverages more than 50%, as mentioned in Chapter 4 which has also been shown from both theory and experiment. However alkyl functionalization through a direct Si-C bond has been widely used and there are many established methods to create such a surface. Therefore, instead of creating alkyl-functionalized surface with a different linking atom to obtain higher coverages, which is not straight forward in terms of experimental preparation, increasing the Si-alkyl coverage by adding a few percent of X-alkyl (X = O, S, NH) to the Si-alkyl system can be a more convenient approach. Coverage enhancement is important in surface functionalization as a more densely-packed monolayer is closer to an ordered crystal and is more controllable in terms of characteristics.

The properties at the surface can still be comparable to the uniform Si-alkyl functionalized surface but the new linking atom can help accommodate more alkyl chains through direct Si-C bonds. This can be further investigated while we decompose the lateral interactions between binary linking groups as follows: (i) van der Waals interaction as a result of correlated charge fluctuations. However this is less significant for covalently attached monolayers. (ii) Dipole interactions either due to permanent (radical) dipoles and/or bond dipoles. Regarding the repulsion/attraction for parallel/antiparallel dipoles, obtaining the desired properties is highly dependent on the correct choice of the binary components. (iii) Overlapping orbitals of neighbouring components can have a significant share in lateral interactions depending on how dense the monolayer is packed. (iv) The substrate-mediated interaction has two origins: (a) Charge reorganization at the interface (accumulation/depletion) as a result of strong

covalent bonding between surface atoms and the adsorbate which can penetrate a few Å into the substrate. This creates an indirect interaction between neighbouring adsorbates that depends on the types of components, either repulsive or attractive. (b) The adsorbate's strong covalent bond with the substrate can induce strain at the surface. Therefore depending on the elastic properties of the substrate, a similar interaction to (a) can occur. The substrate mediated effect (indirect) is normally less strong than the direct dipole-dipole interaction. A qualitative local density of states analysis can clarify the contribution of each and this is suitable for future work.

## 6.2 Results and discussion

### 6.2.1 Binary functionalization at fixed coverage— Tuning the WF

A schematic of the supercell for different coverages is shown in Figure 6.2. The coverage was first fixed to 50% and the (2×2) cell (red-dashed parallelogram) applied in all cases in which two out of the four terminating hydrogens are replaced with the new terminations or linker-chains.

Similar to Chapter 3, there are three single terminations, namely SH, OH, NH<sub>2</sub> and we study combinations of NH<sub>2</sub> with OH or SH; NH<sub>2</sub> causes the biggest shift in the work function of these linkers. The WF and adsorption energy were calculated for each system. This is also done for two alkyl chain lengths, hexyl and dodecyl, with the above mentioned linkers on H:Si(111). The results are shown in Figure 6.3 in which the horizontal axis represents the linker-(chain) while the vertical axis shows the corresponding WF (a, b, c) and adsorption energy (d, e, f) of the simulated structures.

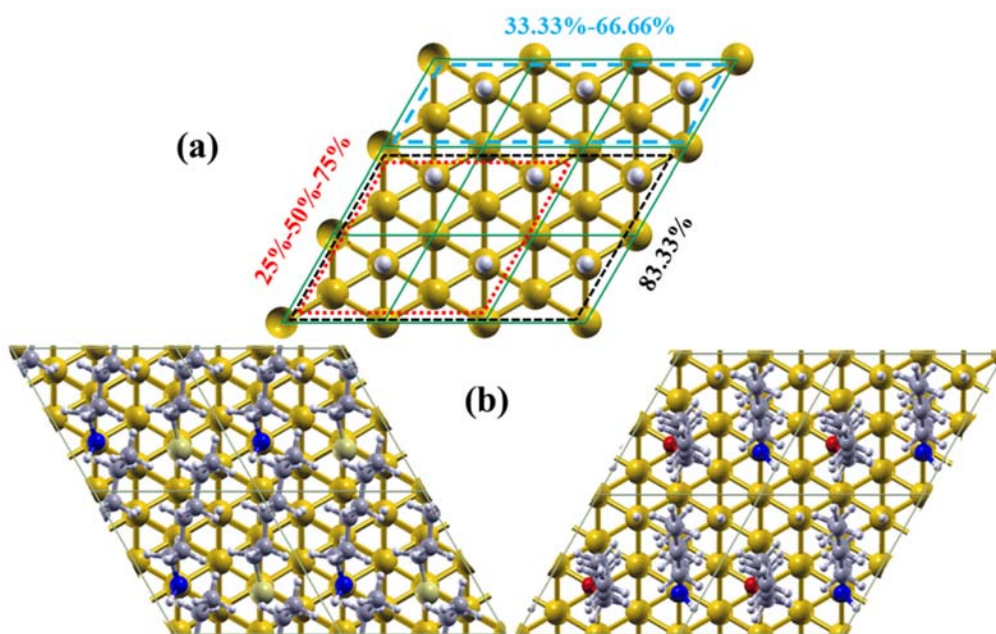


Figure 6.2. (a) Supercell definition for simulate different coverages: Si(111)-1×3 with three adsorption sites was applied for total coverage of 66.6% (33.3% of each component). Si(111)-2×2 cell with four adsorption sites was used to simulate total coverage of 50% (25% for each component) and 75% (25% plus 50% and vice versa). Si(111)-2×3 cell with six adsorption sites implemented to simulate 83.33% (66.7% alkyl plus 16.7% another component) and full coverage (83.33% alkyl plus 16.7% other component) (b) Half covered binary SAMs with –NH–Hexyl/–S–Hexyl (left) and –NH–Hexyl/–O–Hexyl (right) simulated using a H:Si(111)-2×2 cell after geometry optimization. Different coloured spheres stand for following atoms: Si = orange, H = white, C = grey, N = blue, O = red and S = yellow.

**Work function behaviour:** The top panel of Figure 6.3 (a, b, c) shows that the WF of binary functionalized species, with 25% coverage of each, lies between the individual linker WF values at half coverage. The additive nature of the dipole moments has been shown for an individual linker-chain-terminal in previous studies which directly influences the WF shift. Considering that 50% -X termination causes a shift of  $d_x$  in the WF of bare H:Si(111) surface and 50% -Y results in a shift of  $d_y$ , this additive picture suggests that mixed functionalization of (25%X+25%Y) results in a shift of approximately  $(d_x + d_y)/2$  in the WF, which qualitatively explains the average-like behaviour of the resulting WF from binary functionalization, compared with a single linker. Since

the electronic properties at the interface are largely determined by the nature of the silicon-linker bond, this average-like behaviour of the WF is unchanged by adding alkyl chains. Recalling results from Chapter 5, applying different tail-group or increasing the coverage might completely change this linear picture. The coverage effect will be discussed in the next section.

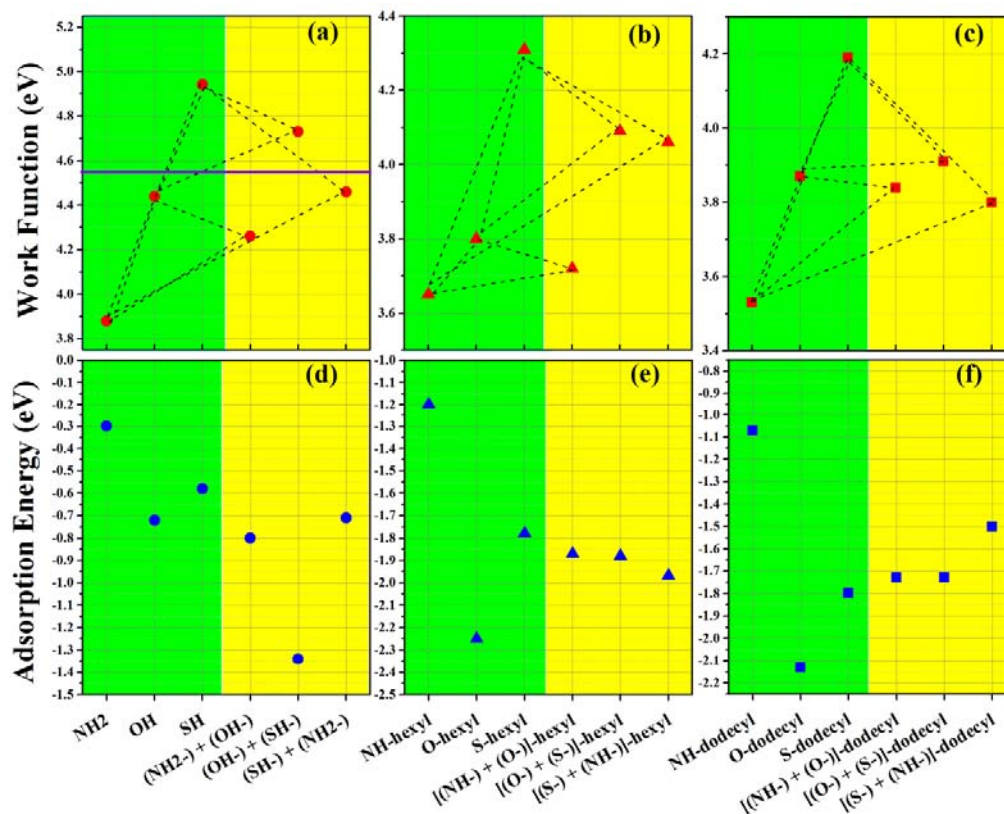


Figure 6.3. (a, b, c) Work function and (d, e, f) Total adsorption energy for binary functionalized linker-(Chain)s (shades of yellow) at fixed coverage (50%); single functionalization (at 50% coverage) is also presented for comparison (shades of green). The horizontal purple line in (a) represents the WF of bare H:Si(111). [(X-) + (Y-)]-alkyl illustrates binary mixture of X-alkyl and Y-alkyl, here at 25% coverage of each.

**Adsorption energy:** The trend in adsorption energy seems to be more complicated than that of the WF when mixed functionalization is applied. For the case of termination groups without alkyl chain, the adsorption energy for the binary case is close to the value of the single termination that is the most stable



and is also slightly stronger. For example, as it can be seen in Figure 6.3 (d), the adsorption energy of [(NH<sub>2</sub>-) + (OH-)] binary functionalized surface ( $E^{\text{ads}} = -0.8$  eV) is close to the component with most stability, OH ( $E^{\text{ads}} = -0.72$  eV), while being more stable.

Adding the alkyl chain to the linker, the (NH-S)-Hexyl monolayer behaves similarly to the binary linker-termination in that the adsorption energy is slightly enhanced over S-Hexyl. However (NH-O)-Hexyl seems to follow an average-like behaviour and for the longer chain (Dodecyl), this picture is seen for both linker combinations.

As we discussed before, adsorption energy is affected by linker electronegativity and therefore by charge transfer at the interface of the H:Si-[linker-(chain)]. Compared to Chapter 3, here we also include vdW-DF2 correction into the DFT-PBE calculations for further enhancing the accuracy, especially for long alkyl chains. In terms of electronegativity we know that the sequence is  $\text{Si} < \text{S} < \text{N} < \text{O}$ . However while the H:Si(111) surface is terminated by -NH<sub>2</sub>, -OH, -SH or a mixture of the terminations, the single molecule electronegativity picture is not enough for assessing the stability. In this case, the charge transfer could be completely distorted by the surface effects, attached hydrogens for saturation of the dangling bonds or by an alkyl chain which is attached through an Si-X(H)-C bond (X = S, O, N). Structural properties appear to play a dominant role on adsorption energy as the chain length is increased. The nature of the linker can have a strong effect on the orientation of the chain and consequently on the adsorption energy. The optimized structure of H:Si-(NH-O/S)-hexyl/dodecyl at half coverage is provided in Figure 6.4. The binary monolayers with the shorter alkyl chain, hexyl (a), seem less distorted. However the longer chain, dodecyl (b), shows more bending/twisting. This indicates that, while the Si-Linker interaction seems to be the main factor in determining the WF shift for short chain alkyls and follows an average-like trend, the chain-chain interaction can strongly affect adsorption energy picture for the long alkyl chains. This was also described in more details in Chapter 4.

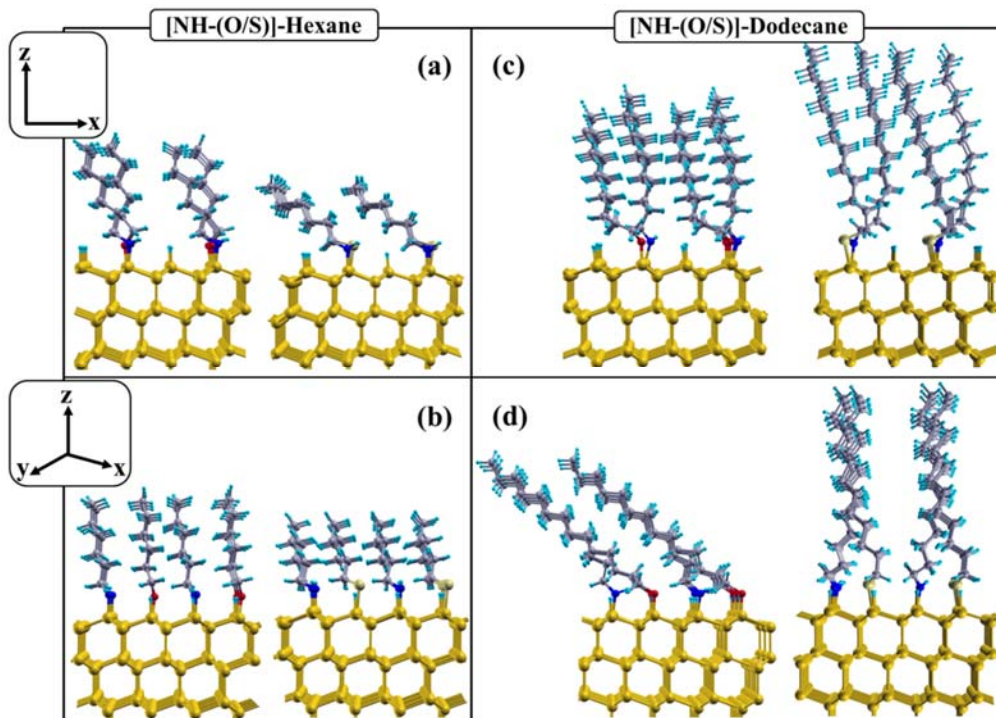


Figure 6.4. (a, b) Binary functionalized [(O-/S-) + (NH-)]-hexyl and (c, d) [(O-/S-) + (NH-)]-dodecyl for 50% coverage presented at two different views along x and xy plane. Coloured spheres stand for following atoms: Si = orange, H = white, C = grey, N = blue, O = red and S = yellow.

## 6.2.2 Binary functionalization for different coverage—Stability and packing

In the previous section we investigated the effect of binary functionalization for combinations of -linker-(chains) with NH<sub>2</sub>, SH and OH linkers and two lengths of alkyl chains -C<sub>6</sub>H<sub>13</sub> and -C<sub>12</sub>H<sub>25</sub> at a total coverage of 50% and compared the result with single functionalization at half coverage. In this section we want to see if variation of the coverage in mixed-functionalization allows extra control to further tune the WF values within the extremes of single linker-chain functionalization and increase coverage on the surface. For this purpose, we use alkyl chains with fixed length up to six carbons that attached through direct Si-C bonds combined with Si-NH-C or Si-O-C.

We start with 25% coverage of each linker, then 33%. Next we consider Si-C at 50% and Si-(NH/O)-hexyl at 25% of each. Fixing the Si-(NH/O)-hexyl to 16.66% we further test 33%, 66.66% and 83.33% Si-hexyl coverages. The latter case indicates full coverage of H:Si(111) surface.

Looking at Figure 6.5 (a,b) we realize that compared to pure Si-C linker, the WF for the case of Si-C/Si-N is lower and with Si-C/Si-O the WF is larger at the same overall coverage.

For adsorption energy, the pure Si-C layer at all coverages is less stable than in combination with another linker. Figure 6.3 (d, e, f) also shows that adding the oxygen linker makes the structure more stable compared to adding nitrogen. However Figure 6.3 (a, b, c) indicates the ability of nitrogen to induce bigger shifts in the WF (for most cases) compared to oxygen. Both findings are in agreement with our previous results for single type functionalization.

Regardless of the precision of the predicted values via DFT, these results clearly show the effect of binary functionalization with N or O linkers in enhancing the stability of these layers on the H:Si(111) surface relative to pure Si-C linked alkyl layers. Furthermore, given that the WF for oxygen linkers combined with Si-C is close to that for pure alkylation (in most cases), this indicates the possibility of using O linkers for enhancing stability while preserving the original electronic properties of the Si-Alkyl SAMs.

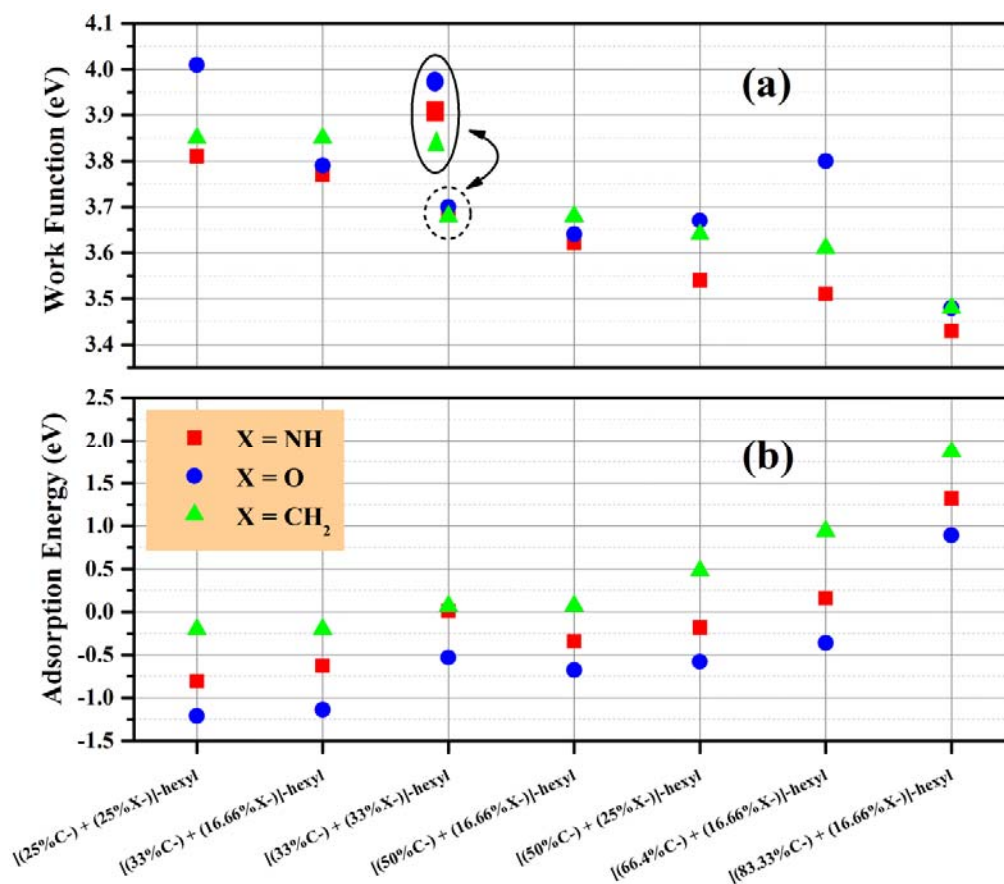


Figure 6.5. (a) Work function and (b) Total adsorption energy for binary functionalized linker-(Chain)s for different ratio of (Si-C/Si-X)-hexyl at half coverage [X= NH, O]. Inset in (a) shows expanded view for the 33%C-33%X-Hexyl to highlight the ordering of N, O, C linkers.

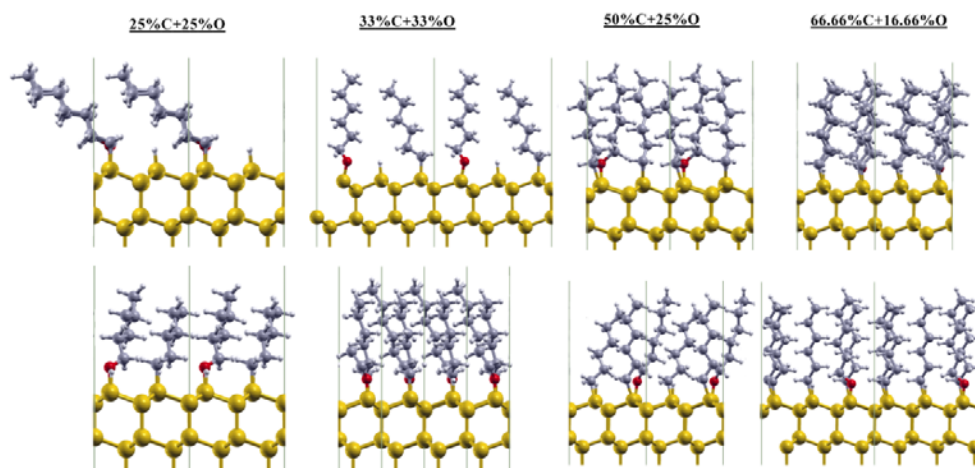


Figure 6.6. Optimized Binary SAMs of O-Hexyl/Hexyl with different ratio of each component, 25%, 33%, 50%, 66% for hexyl and 25%, 33%, 25%, 16.66% for O-Hexyl respectively, presented at two different views along x and xy plane.

## 6.3 Concluding remarks and future outlook

Bringing together the understanding gained from studying single type functionalization of H:Si(111) with different alkyl chains and bearing in mind how utilizing head-group, tail-group or both as well as monolayer coverage affects the electronic and structural properties, we studied in this Chapter functionalized H:Si(111) with binary SAMs. Aiming for enhanced WF adjustment together with SAM stability and coverage, we chose a range of terminations and linker-chains denoted as  $-X-(\text{Alkyl})$  with  $X = \text{CH}_3, \text{O}(\text{H}), \text{S}(\text{H}), \text{NH}_2$  and investigated the stability and WF of various binary components grafted onto the H:Si(111) surface.

In the first part we fixed the total coverage to 50% and applied different terminations of linker-alkyl chains with the same alkyl length (each at 25% coverage) and calculated the WF and adsorption energy. We compared the results with the corresponding single type functionalization for each component at 50% coverage. The result clearly shows the possibility to obtain further WF tuning, with WF values within the extremes of single functionalization. For binary mixtures of linkers, the WF is nearly the average value of the single type functionalization. However this picture seems to be distorted by chain-chain interactions when alkyl chains are included, especially for chains with more than six carbons.

In the second part, we studied hexyl monolayers with direct Si-C bonds to H:Si(111) combined with either  $-\text{NH}-\text{hexyl}$  or  $-\text{O}-\text{hexyl}$ . This is a model of H:Si-C-alkyl mixed with small amount of second linker, H:Si-(NH/O)-alkyl. We have shown that irrespective of the ratio, the binary monolayer is always more stable compared to pure alkyl functionalization. The results also indicate that even using a small percentage of other linkers in combination with alkyl SAM

allows coverages larger than 50%, which is the optimum coverage for the case of pure alkyl monolayers.

In summary:

- 1) Using binary functionalization with two different terminations or linker-chains (linkers were chosen out of NH, O, S and two lengths of chain hexyl and dodecyl were used) we showed that WF can be further tuned within the interval of single type functionalization.
- 2) Binary functionalization can enhance the SAM stability. Although adsorption of direct Si-C grafted SAMs is less favourable compared to their counterparts with O, N or S linkage, regardless of the ratio, binary functionalized alkyl monolayers with X-alkyl (X = NH, O) is always more stable than single type Si-C alkyl functionalization with the same coverage.
- 3) Our results indicate that it is possible to go beyond the optimum coverage of pure alkyl functionalized SAMs (50%) by adding a linker with the correct choice of the linker. This is very important since dense packed monolayers have fewer defects and deliver higher efficiency.

The results obtained here from studies of binary functionalization on Si (111) are consistent with binary functionalization behaviour on metals and semiconductors in that functionalization with two types of chain can tune the WF. However, we have not found any relevant experimental results for binary functionalized surfaces with different linkers which are the focus of this Chapter. In Chapter 4, we showed that single type functionalization with linkers other than carbon can increase the stability and monolayer coverage. With this background we showed in this Chapter that binary functionalized silicon (111) surface with different ratios of Si-C bonds combined with Si-(N/O) is able to enhance the stability of the monolayer over that with pure Si-alkyl chains. We know that direct Si-alkyl monolayers are suffering from poor stability and low coverage over Si-linker-alkyl SAMs (with linkers such as S, O and N) but still the most known monolayer among different types of organic SAMs with established preparation methods. Considering the latter fact, the strategy that is proposed here for the

first time, can help experimentalists to improve the stability and increase the coverage of alkyl functionalization.

## 6.4 References

1. Zhang, Z.; Yates, J. T., Band Bending in Semiconductors: Chemical and Physical Consequences at Surfaces and Interfaces. *Chem. Rev.* **2012**, *112*, 5520-5551.
2. Linford, M. R.; Chidsey, C. E. D., Alkyl Monolayers Covalently Bonded to Silicon Surfaces. *J. Am. Chem. Soc.* **1993**, *115*, 12631-12632.
3. Linford, M. R.; Fenter, P.; Eisenberger, P. M.; Chidsey, C. E. D., Alkyl Monolayers on Silicon Prepared from 1-Alkenes and Hydrogen-Terminated Silicon. *J. Am. Chem. Soc.* **1995**, *117*, 3145-3155.
4. Sieval, A. B.; Demirel, A. L.; Nissink, J. W. M.; Linford, M. R.; van der Maas, J. H.; de Jeu, W. H.; Zuilhof, H.; Sudhölter, E. J. R., Highly Stable Si-C Linked Functionalized Monolayers on the Silicon (100) Surface. *Langmuir* **1998**, *14*, 1759-1768.
5. Buriak, J. M., Organometallic Chemistry on Silicon Surfaces: Formation of Functional Monolayers Bound through Si-C Bonds. *Chem. Commun.* **1999**, 1051-1060.
6. Faber, E. J.; de Smet, L. C.; Olthuis, W.; Zuilhof, H.; Sudholter, E. J.; Bergveld, P.; van den Berg, A., Si-C Linked Organic Monolayers on Crystalline Silicon Surfaces as Alternative Gate Insulators. *ChemPhysChem* **2005**, *6*, 2153-2166.
7. Ciampi, S.; Harper, J. B.; Gooding, J. J., Wet Chemical Routes to the Assembly of Organic Monolayers on Silicon Surfaces Via the Formation of Si-C Bonds: Surface Preparation, Passivation and Functionalization. *Chem. Soc. Rev.* **2010**, *39*, 2158-83.
8. Lavi, A.; Cohen, H.; Bendikov, T.; Vilan, A.; Cahen, D., Si-C-Bound Alkyl Chains on Oxide-Free Si: Towards Versatile Solution Preparation of Electronic Transport Quality Monolayers. *Phys. Chem. Chem. Phys.* **2011**, *13*, 1293-1296.
9. Uosaki, K.; Fukumitsu, H.; Masuda, T.; Qu, D., Construction of a Metal-Organic Monolayer-Semiconductor Junction on a Hydrogen-Terminated Si(111) Surface Via Si-C Covalent Linkage and Its Electrical Properties. *Phys. Chem. Chem. Phys.* **2014**, *16*, 9960-9965.
10. Wu, K.-Y.; Yu, S.-Y.; Tao, Y.-T., Continuous Modulation of Electrode Work Function with Mixed Self-Assembled Monolayers and Its Effect in Charge Injection. *Langmuir* **2009**, *25*, 6232-8.
11. Kuo, C.-H.; Liu, C.-P.; Lee, S.-H.; Chang, H.-Y.; Lin, W.-C.; You, Y.-W.; Liao, H.-Y.; Shyue, J.-J., Effect of Surface Chemical Composition on the Work Function of Silicon Substrates Modified by Binary Self-Assembled Monolayers. *Phys. Chem. Chem. Phys.* **2011**, *13*, 15122-15126.
12. Feichtenschlager, B.; Pabisch, S.; Peterlik, H.; Kickelbick, G., Nanoparticle Assemblies as Probes for Self-Assembled Monolayer Characterization: Correlation between Surface Functionalization and Agglomeration Behavior. *Langmuir* **2011**, *28*, 741-750.
13. Lee, S.-H., et al., Effect of the Chemical Composition on the Work Function of Gold Substrates Modified by Binary Self-Assembled Monolayers. *Phys. Chem. Chem. Phys.* **2011**, *13*, 4335-4339.

14. Vilt, S. G.; Leng, Z.; Booth, B. D.; McCabe, C.; Jennings, G. K., Surface and Frictional Properties of Two-Component Alkylsilane Monolayers and Hydroxyl-Terminated Monolayers on Silicon. *J. Phys. Chem. C* **2009**, *113*, 14972-14977.
15. Capadona, J. R.; Collard, D. M.; García, A. J., Fibronectin Adsorption and Cell Adhesion to Mixed Monolayers of Tri(Ethylene Glycol)- and Methyl-Terminated Alkanethiols†. *Langmuir* **2002**, *19*, 1847-1852.
16. Chang, H.-Y.; Huang, C.-C.; Lin, K.-Y.; Kao, W.-L.; Liao, H.-Y.; You, Y.-W.; Lin, J.-H.; Kuo, Y.-T.; Kuo, D.-Y.; Shyue, J.-J., Effect of Surface Potential on NiH<sub>3</sub>T<sub>3</sub> Cell Adhesion and Proliferation. *J. Phys. Chem. C* **2014**, *118*, 14464-14470.
17. Jia, X.; McCarthy, T. J., Controlled Growth of Silicon Dioxide from “Nanoholes” in Silicon-Supported Tris(Trimethylsiloxy)Silyl Monolayers: Rational Control of Surface Roughness at the Nanometer Length Scale. *Langmuir* **2003**, *19*, 2449-2457.
18. Ulman, A., Formation and Structure of Self-Assembled Monolayers. *Chem. Rev.* **1996**, *96*, 1533-1554.
19. Kim, J.; Rim, Y. S.; Liu, Y.; Serino, A. C.; Thomas, J. C.; Chen, H.; Yang, Y.; Weiss, P. S., Interface Control in Organic Electronics Using Mixed Monolayers of Carboranethiol Isomers. *Nano Lett.* **2014**, *14*, 2946-2951.
20. Xu, Y.; Baeg, K.-J.; Park, W.-T.; Cho, A.; Choi, E.-Y.; Noh, Y.-Y., Regulating Charge Injection in Ambipolar Organic Field-Effect Transistors by Mixed Self-Assembled Monolayers. *ACS Appl. Mater. Interfaces* **2014**, *6*, 14493-14499.
21. Frederix, F.; Bonroy, K.; Laureyn, W.; Reekmans, G.; Campitelli, A.; Dehaen, W.; Maes, G., Enhanced Performance of an Affinity Biosensor Interface Based on Mixed Self-Assembled Monolayers of Thiols on Gold. *Langmuir* **2003**, *19*, 4351-4357.
22. Zhang, F.; Liu, D.; Zhang, Y.; Wei, H.; Song, T.; Sun, B., Methyl/Allyl Monolayer on Silicon: Efficient Surface Passivation for Silicon-Conjugated Polymer Hybrid Solar Cell. *ACS Appl. Mater. Interfaces* **2013**, *5*, 4678-4684.
23. Barnea-Nehoshtan, L.; Nayak, P. K.; Shu, A.; Bendikov, T.; Kahn, A.; Cahen, D., Enhancing the Tunability of the Open-Circuit Voltage of Hybrid Photovoltaics with Mixed Molecular Monolayers. *ACS Appl. Mater. Interfaces* **2014**, *6*, 2317-2324.
24. Folkers, J. P.; Laibinis, P. E.; Whitesides, G. M.; Deutch, J., Phase Behavior of Two-Component Self-Assembled Monolayers of Alkanethiolates on Gold. *J. Phys. Chem.* **1994**, *98*, 563-571.
25. Yu, S.-Y.; Huang, D.-C.; Chen, Y.-L.; Wu, K.-Y.; Tao, Y.-T., Approaching Charge Balance in Organic Light-Emitting Diodes by Tuning Charge Injection Barriers with Mixed Monolayers. *Langmuir* **2011**, *28*, 424-430.
26. Chen, C.-Y.; Wu, K.-Y.; Chao, Y.-C.; Zan, H.-W.; Meng, H.-F.; Tao, Y.-T., Concomitant Tuning of Metal Work Function and Wetting Property with Mixed Self-Assembled Monolayers. *Org. Electron.* **2011**, *12*, 148-153.
27. Erard, J. F.; Kovats, E. S., Determination of the Composition of Organic Layers Chemically Bonded on Silicon Dioxide. *Anal. Chem.* **1982**, *54*, 193-202.
28. Erard, J.-F.; Nagy, L.; Kovats, E. s., The Preparation of Mixed Organic Layers Chemically Bonded on Silicon Dioxide. *Colloids Surf.* **1984**, *9*, 109-132.
29. Wirth, M. J.; Fatunmbi, H. O., Horizontal Polymerization of Mixed Trifunctional Silanes on Silica: A Potential Chromatographic Stationary Phase. *Anal. Chem.* **1992**, *64*, 2783-2786.
30. Fatunmbi, H. O.; Bruch, M. D.; Wirth, M. J., Silicon-29 and Carbon-13 Nmr Characterization of Mixed Horizontally Polymerized Monolayers on Silica Gel. *Anal. Chem.* **1993**, *65*, 2048-2054.



31. Offord, D. A.; Griffin, J. H., Kinetic Control in the Formation of Self-Assembled Mixed Monolayers on Planar Silica Substrates. *Langmuir* **1993**, *9*, 3015-3025.
32. Fryxell, G. E.; Rieke, P. C.; Wood, L. L.; Engelhard, M. H.; Williford, R. E.; Graff, G. L.; Campbell, A. A.; Wiacek, R. J.; Lee, L.; Halverson, A., Nucleophilic Displacements in Mixed Self-Assembled Monolayers. *Langmuir* **1996**, *12*, 5064-5075.
33. Chartier, A.; Gonnet, C.; Morel, D.; Rocca, J. L.; Serpinet, J., Mixed Bonded Phases for High-Performance Liquid Chromatography : I. Synthesis and Physico-Chemical Characterization. *J. Chromatogr. A* **1988**, *438*, 263-271.
34. Bain, C. D.; Evall, J.; Whitesides, G. M., Formation of Monolayers by the Coadsorption of Thiols on Gold: Variation in the Head Group, Tail Group, and Solvent. *J. Am. Chem. Soc.* **1989**, *111*, 7155-7164.
35. Bain, C. D.; Troughton, E. B.; Tao, Y. T.; Evall, J.; Whitesides, G. M.; Nuzzo, R. G., Formation of Monolayer Films by the Spontaneous Assembly of Organic Thiols from Solution onto Gold. *J. Am. Chem. Soc.* **1989**, *111*, 321-335.
36. Laibinis, P. E.; Fox, M. A.; Folkers, J. P.; Whitesides, G. M., Comparisons of Self-Assembled Monolayers on Silver and Gold: Mixed Monolayers Derived from HS(CH<sub>2</sub>)<sub>21</sub>X and HS(CH<sub>2</sub>)<sub>10</sub>Y (X, Y = CH<sub>3</sub>, CH<sub>2</sub>OH) Have Similar Properties. *Langmuir* **1991**, *7*, 3167-3173.
37. Folkers, J. P.; Laibinis, P. E.; Whitesides, G. M., Self-Assembled Monolayers of Alkanethiols on Gold: Comparisons of Monolayers Containing Mixtures of Short- and Long-Chain Constituents with Methyl and Hydroxymethyl Terminal Groups. *Langmuir* **1992**, *8*, 1330-1341.
38. Carey, R. I.; Folkers, J. P.; Whitesides, G. M., Self-Assembled Monolayers Containing .Omega.-Mercaptoalkyl Boronic Acids Adsorbed onto Gold Form a Highly Cross-Linked, Thermally Stable Borate Glass Surface. *Langmuir* **1994**, *10*, 2228-2234.
39. Ballav, N.; Terfort, A.; Zharnikov, M., Mixing of Nonsubstituted and Partly Fluorinated Alkanethiols in a Binary Self-Assembled Monolayer. *J. Phys. Chem. C* **2009**, *113*, 3697-3706.
40. Silien, C.; Räisänen, M. T.; Buck, M., A Supramolecular Network as Sacrificial Mask for the Generation of a Nanopatterned Binary Self-Assembled Monolayer. *Small* **2010**, *6*, 391-394.
41. Kang, J. F.; Liao, S.; Jordan, R.; Ulman, A., Mixed Self-Assembled Monolayers of Rigid Biphenyl Thiols: Impact of Solvent and Dipole Moment. *J. Am. Chem. Soc.* **1998**, *120*, 9662-9667.
42. Fadeev, A. Y.; McCarthy, T. J., Binary Monolayer Mixtures: Modification of Nanopores in Silicon-Supported Tris(Trimethylsiloxy)Silyl Monolayers. *Langmuir* **1999**, *15*, 7238-7243.
43. Chen, S.; Li, L.; Boozer, C. L.; Jiang, S., Controlled Chemical and Structural Properties of Mixed Self-Assembled Monolayers of Alkanethiols on Au(111). *Langmuir* **2000**, *16*, 9287-9293.
44. Kumar, N.; Maldarelli, C.; Steiner, C.; Couzis, A., Formation of Nanometer Domains of One Chemical Functionality in a Continuous Matrix of a Second Chemical Functionality by Sequential Adsorption of Silane Self-Assembled Monolayers. *Langmuir* **2001**, *17*, 7789-7797.
45. Mathauer, K.; Frank, C. W., Binary Self-Assembled Monolayers as Prepared by Successive Adsorption of Alkyltrichlorosilanes. *Langmuir* **1993**, *9*, 3446-3451.
46. Lochmuller, C. H.; Hunnicutt, M. L., Solvent-Induced Conformational Changes on Chemically Modified Silica Surfaces. *J. Phys. Chem.* **1986**, *90*, 4318-4322.

47. Ge, S.; Takahara, A.; Kajiyama, T., Phase Separated Morphology of an Immobilized Organosilane Monolayer Studied by a Scanning Probe Microscope. *Langmuir* **1995**, *11*, 1341-1346.
48. Lagutchev, A. S.; Song, K. J.; Huang, J. Y.; Yang, P. K.; Chuang, T. J., Self-Assembly of Alkylsiloxane Monolayers on Fused Silica Studied by Xps and Sum Frequency Generation Spectroscopy. *Chem. Phys.* **1998**, *226*, 337-349.
49. Huang, J. Y.; Song, K. J.; Lagoutchev, A.; Yang, P. K.; Chuang, T. J., Molecular Conformation and Nanomechanics of Self-Assembled Alkylsiloxane Monolayers. *Langmuir* **1997**, *13*, 58-64.
50. Heid, S.; Effenberger, F.; Bierbaum, K.; Grunze, M., Self-Assembled Mono- and Multilayers of Terminally Functionalized Organosilyl Compounds on Silicon Substrates. *Langmuir* **1996**, *12*, 2118-2120.
51. Mansueto, M.; Sauer, S.; Butschies, M.; Kaller, M.; Baro, A.; Woerner, R.; Hansen, N. H.; Tovar, G.; Pflaum, J.; Laschat, S., Triphenylene Silanes for Direct Surface Anchoring in Binary Mixed Self-Assembled Monolayers. *Langmuir* **2012**, *28*, 8399-407.
52. Tong, Y.; Tyrode, E.; Osawa, M.; Yoshida, N.; Watanabe, T.; Nakajima, A.; Ye, S., Preferential Adsorption of Amino-Terminated Silane in a Binary Mixed Self-Assembled Monolayer. *Langmuir* **2011**, *27*, 5420-6.
53. Imabayashi, S.-i.; Hobara, D.; Kakiuchi, T.; Knoll, W., Selective Replacement of Adsorbed Alkanethiols in Phase-Separated Binary Self-Assembled Monolayers by Electrochemical Partial Desorption. *Langmuir* **1997**, *13*, 4502-4504.
54. Tamada, K.; Hara, M.; Sasabe, H.; Knoll, W., Surface Phase Behavior of N-Alkanethiol Self-Assembled Monolayers Adsorbed on Au(111): An Atomic Force Microscope Study. *Langmuir* **1997**, *13*, 1558-1566.
55. Stranick, S. J.; Parikh, A. N.; Tao, Y. T.; Allara, D. L.; Weiss, P. S., Phase Separation of Mixed-Composition Self-Assembled Monolayers into Nanometer Scale Molecular Domains. *J. Phys. Chem.* **1994**, *98*, 7636-7646.
56. Bertilsson, L.; Liedberg, B., Infrared Study of Thiol Monolayer Assemblies on Gold: Preparation, Characterization, and Functionalization of Mixed Monolayers. *Langmuir* **1993**, *9*, 141-149.
57. Imabayashi, S.-i.; Gon, N.; Sasaki, T.; Hobara, D.; Kakiuchi, T., Effect of Nanometer-Scale Phase Separation on Wetting of Binary Self-Assembled Thiol Monolayers on Au(111). *Langmuir* **1998**, *14*, 2348-2351.
58. Fan, F.; Maldarelli, C.; Couzis, A., Fabrication of Surfaces with Nanoislands of Chemical Functionality by the Phase Separation of Self-Assembling Monolayers on Silicon. *Langmuir* **2003**, *19*, 3254-3265.
59. Takiue, T.; Matsuo, T.; Ikeda, N.; Motomura, K.; Aratono, M., Thermodynamic Study on Phase Transition in Adsorbed Films of Fluoroalkanol at the Hexyl/Water Interface. 5. Miscibility in the Adsorbed Film of an Alkanol and Fluoroalkanol Mixture. *J. Phys. Chem. B* **1998**, *102*, 5840-5844.
60. Chen, S.; Li, L.; Boozer, C. L.; Jiang, S., Controlled Chemical and Structural Properties of Mixed Self-Assembled Monolayers by Coadsorption of Symmetric and Asymmetric Disulfides on Au(111). *J. Phys. Chem. B* **2001**, *105*, 2975-2980.
61. Tielens, F.; Costa, D.; Humblot, V.; Pradier, C.-M., Characterization of  $\Omega$ -Functionalized Undecanethiol Mixed Self-Assembled Monolayers on Au(111): A Combined Polarization Modulation Infrared Reflection–Absorption Spectroscopy/X-Ray Photoelectron Spectroscopy/Periodic Density Functional Theory Study. *J. Phys. Chem. C* **2007**, *112*, 182-190.

62. Lüssem, B.; Müller-Meskamp, L.; Karthäuser, S.; Waser, R.; Homberger, M.; Simon, U., Stm Study of Mixed Alkanethiol/Biphenylthiol Self-Assembled Monolayers on Au(111). *Langmuir* **2006**, *22*, 3021-3027.
63. Martin, P.; Marsaudon, S.; Thomas, L.; Desbat, B.; Aimé, J.-P.; Bennetau, B., Liquid Mechanical Behavior of Mixed Monolayers of Amino and Alkyl Silanes by Atomic Force Microscopy. *Langmuir* **2005**, *21*, 6934-43.
64. Kao, W.-L.; Chang, H.-Y.; Yen, G.-J.; Kuo, D.-Y.; You, Y.-W.; Huang, C.-C.; Kuo, Y.-T.; Lin, J.-H.; Shyue, J.-J., Adsorption Behavior of Plasmid DNA on Binary Self-Assembled Monolayers Modified Gold Substrates. *J. Colloid Interface Sci.* **2012**, *382*, 97-104.
65. Gozlan, N.; Haick, H., Coverage Effect of Self-Assembled Polar Molecules on the Surface Energetics of Silicon. *J. Phys. Chem. C* **2008**, *112*, 12599-12601.
66. Puniredd, S. R.; Platzman, I.; Tung, R. T.; Haick, H., Bidirectional Control of Silicon's Surface Potential by Means of Molecular Coverage. *J. Phys. Chem. C* **2010**, *114*, 18674-18678.
67. Kuo, C.-H.; Chang, H.-Y.; Liu, C.-P.; Lee, S.-H.; You, Y.-W.; Shyue, J.-J., Effect of Surface Chemical Composition on the Surface Potential and Iso-Electric Point of Silicon Substrates Modified with Self-Assembled Monolayers. *Phys. Chem. Chem. Phys.* **2011**, *13*, 3649-3653.
68. Lin, W.-C.; Lee, S.-H.; Karakachian, M.; Yu, B.-Y.; Chen, Y.-Y.; Lin, Y.-C.; Kuo, C.-H.; Shyue, J.-J., Tuning the Surface Potential of Gold Substrates Arbitrarily with Self-Assembled Monolayers with Mixed Functional Groups. *Phys. Chem. Chem. Phys.* **2009**, *11*, 6199-6204.
69. Lin, Y.-C.; Yu, B.-Y.; Lin, W.-C.; Lee, S.-H.; Kuo, C.-H.; Shyue, J.-J., Tailoring the Surface Potential of Gold Nanoparticles with Self-Assembled Monolayers with Mixed Functional Groups. *J. Colloid Interface Sci.* **2009**, *340*, 126-130.
70. O'Leary, L. E.; Johansson, E.; Brunschwig, B. S.; Lewis, N. S., Synthesis and Characterization of Mixed Methyl/Allyl Monolayers on Si(111). *J. Phys. Chem. B* **2010**, *114*, 14298-14302.
71. Wong, K. T.; Lewis, N. S., What a Difference a Bond Makes: The Structural, Chemical, and Physical Properties of Methyl-Terminated Si(111) Surfaces. *Acc. Chem. Res.* **2014**, *47*, 3037-3044.
72. O'Leary, L. E.; Rose, M. J.; Ding, T. X.; Johansson, E.; Brunschwig, B. S.; Lewis, N. S., Heck Coupling of Olefins to Mixed Methyl/Thienyl Monolayers on Si(111) Surfaces. *J. Am. Chem. Soc.* **2013**, *135*, 10081-10090.
73. Johansson, E.; Boettcher, S. W.; O'Leary, L. E.; Poletayev, A. D.; Maldonado, S.; Brunschwig, B. S.; Lewis, N. S., Control of the Ph-Dependence of the Band Edges of Si(111) Surfaces Using Mixed Methyl/Allyl Monolayers. *J. Phys. Chem. C* **2011**, *115*, 8594-8601.
74. Smith, M. B.; Efimenko, K.; Fischer, D. A.; Lappi, S. E.; Kilpatrick, P. K.; Genzer, J., Study of the Packing Density and Molecular Orientation of Bimolecular Self-Assembled Monolayers of Aromatic and Aliphatic Organosilanes on Silica. *Langmuir* **2007**, *23*, 673-83.
75. Patrone, L.; Gadenne, V.; Desbief, S., Single and Binary Self-Assembled Monolayers of Phenyl- and Pentafluorophenyl-Based Silane Species, and Their Phase Separation with Octadecyltrichlorosilane. *Langmuir* **2010**, *26*, 17111-8.
76. Rissner, F.; Egger, D. A.; Romaner, L.; Heimel, G.; Zojer, E., The Electronic Structure of Mixed Self-Assembled Monolayers. *ACS Nano* **2010**, *4*, 6735-46.
77. Heimel, G.; Romaner, L.; Zojer, E.; Bredas, J. L., Toward Control of the Metal-Organic Interfacial Electronic Structure in Molecular Electronics: A First-Principles

Study on Self-Assembled Monolayers of Pi-Conjugated Molecules on Noble Metals. *Nano Lett.* **2007**, *7*, 932-940.

78. Romaner, L.; Heimel, G.; Zojer, E., Electronic Structure of Thiol-Bonded Self-Assembled Monolayers: Impact of Coverage. *Phys. Rev. B* **2008**, *77*, 045113-9.

79. Romaner, L.; Heimel, G.; Ambrosch-Draxl, C.; Zojer, E., The Dielectric Constant of Self-Assembled Monolayers. *Adv. Funct. Mater.* **2008**, *18*, 3999-4006.

80. Heimel, G.; Romaner, L.; Brédas, J.-L.; Zojer, E., Interface Energetics and Level Alignment at Covalent Metal-Molecule Junctions: Pi-Conjugated Thiols on Gold. *Phys. Rev. Lett.* **2006**, *96*, 196806.

81. Wang, L.; Rangger, G. M.; Romaner, L.; Heimel, G.; Bučko, T.; Ma, Z.; Li, Q.; Shuai, Z.; Zojer, E., Electronic Structure of Self-Assembled Monolayers on Au(111) Surfaces: The Impact of Backbone Polarizability. *Adv. Funct. Mater.* **2009**, *19*, 3766-3775.

82. Heimel, G.; Romaner, L.; Zojer, E.; Bredas, J. L., The Interface Energetics of Self-Assembled Monolayers on Metals. *Acc. Chem. Res.* **2008**, *41*, 721-729.

83. Heimel, G.; Rissner, F.; Zojer, E., Modeling the Electronic Properties of Pi-Conjugated Self-Assembled Monolayers. *Adv. Mater.* **2010**, *22*, 2494-2513.

84. Natan, A.; Kronik, L.; Haick, H.; Tung, R. T., Electrostatic Properties of Ideal and Non-Ideal Polar Organic Monolayers: Implications for Electronic Devices. *Adv. Mater.* **2007**, *19*, 4103-4117.

85. Cornil, D.; Olivier, Y.; Geskin, V.; Cornil, J., Depolarization Effects in Self-Assembled Monolayers: A Quantum-Chemical Insight. *Adv. Funct. Mater.* **2007**, *17*, 1143-1148.

86. Sushko, M. L.; Shluger, A. L., Intramolecular Dipole Coupling and Depolarization in Self-Assembled Monolayers. *Adv. Funct. Mater.* **2008**, *18*, 2228-2236.

87. Natan, A.; Zidon, Y.; Shapira, Y.; Kronik, L., Cooperative Effects and Dipole Formation at Semiconductor and Self-Assembled-Monolayer Interfaces. *Phys. Rev. B* **2006**, *73*, 193310-4.

88. Rusu, P. C.; Giovannetti, G.; Brocks, G., Dipole Formation at Interfaces of Alkanethiolate Self-Assembled Monolayers and Ag(111). *J. Phys. Chem. C* **2007**, *111*, 14448-14456.

89. Wang, J.-g.; Prodan, E.; Car, R.; Selloni, A., Band Alignment in Molecular Devices: Influence of Anchoring Group and Metal Work Function. *Phys. Rev. B* **2008**, *77*, 245443.

90. Fukagawa, H.; Yamane, H.; Kera, S.; Okudaira, K. K.; Ueno, N., Experimental Estimation of the Electric Dipole Moment and Polarizability of Titanyl Phthalocyanine Using Ultraviolet Photoelectron Spectroscopy. *Phys. Rev. B* **2006**, *73*, 041302.

# Chapter 7

## Final Remarks and Perspectives

### 7.1 Summary of results and conclusion

With the ultimate aim of microscopic understanding of the functionalized H:Si(111) surface from both electronic and structural point of view, DFT-based calculations have been carried out. Building our knowledge step-by-step, a series of investigations were performed on a range of terminating species, different alkyl chain lengths, variety of head- and/or tail-group and binary mixture of the linker-chains. Results were shown to be consistent with available relevant measurements.

Applying several polar and non-polar experimentally accessible adsorbates such as halogens (F, Cl, Br, I), chalcogens (O, S, Se, Te) and second row elements (B, C, N, O, F) in the periodic table we studied the modified H:Si(111) surface as the starting step. We have shown that different chemical trends apply to each category of terminations. Our comprehensive and predictive study of the work function variation from first-principles provides reasonable interpretation to the results. Radical dipole, bond dipole, the electronegativity and range of interatomic interaction of the tether atoms primarily contribute to explaining the changes of the work function for different adsorbates at different coverage.

Also in agreement with electrostatic rules, our results indicate that a larger radical dipole component along the surface normal induces a bigger shift in the work function. The direction of the dipole in this case determines the sign of the

WF shift. Another form of dipole, namely the bond dipole, is also created by charge reorganization across the tether bond with the surface silicon. Therefore, a dipole field is formed at the surface whose strength and direction is governed by the amount and sign of the charge transferred across the surface. This generates the surface dipole layer which affects the electron acceleration towards the vacuum and the corresponding work function (WF).

Based on our charge analysis results, the number of valence electrons and electronegativity of the linker control the transferred charges. All of our selected tethers have higher electronegativity compared to silicon which results in electron withdrawal from the silicon surface and the inward (bond) dipole field is expected to increase the WF. This is however true for the case of surface termination with halogens in which a near-linear behaviour is predicted with respect to halogen's electronegativity. For other adsorbates with nonzero radical dipole moment along the surface normal, it can reduce or even reverse this effect. Excluding H:Si(111)-OH, modification of H:Si(111) by other chalcogen tethers tends to increase the work function, but to a lesser degree compared to halogen terminated surfaces. Also for the surfaces covered with -CH<sub>3</sub> and -NH<sub>2</sub> terminations, the WF reduced compared to the hydrogenated silicon surface. The electronic profile may also depend on the surface coverage. However, due to the covalent radius of the tether atoms, there are no large changes occurring in local charges on the surface Si atoms and therefore the work function shows an overall weak dependence on coverage percentage. Considering general changes in the WF, halogens seem to create bigger shifts compared to other species. This is with the exception of iodine, which can be rationalized once we realize that it has the largest size and the lowest electronegativity among the studied halogens. Surface passivation is an important part of the surface functionalization process, playing a key-role in controlling the reactivity and electronic properties of the surface. Our obtained results here on passivating H:Si(111) with different terminations can help experimentalists to choose proper terminating species with the knowledge of how each terminating atom modifies the surface properties. Also one can get more insight of how reactive a surface might be by using each

termination as reactivity can be related to the shifts in the WF or substantial charge transfer into/from the surface.

At the second step, in order to understand the role played by the nature of the linker and the chain length on the adsorption structures and stabilities of H:Si(111) modified with molecular chains with the general formula H:Si-(X)-(CH<sub>2</sub>)<sub>n</sub>-CH<sub>3</sub>, where X = NH, O, S and n = (0, 1, 3, 5, 7, 9, 11), we presented a systematic DFT study of these assemblies. Due to the importance of the long-range interaction in the low-charge density systems such as self-assembled monolayers, we applied the van der Waals correction to our DFT calculation which is implemented as vdW-DF(2) in the quantum espresso package. Through various adsorption calculations and structural analysis with and without including vdW correction for different lengths of alkyl chains attached to silicon, first we showed the absolute necessity of taking into account the van der Waals interaction between the alkyl chains. Our comprehensive investigation on this matter emphasizes how strongly vdW interactions can affect the structural properties and consequently the electronic profile.

Irrespective of chain length, oxygen delivers the strongest binding energy followed by sulfur and nitrogen. Direct binding of the alkyl chains to silicon is the least stable. This ordering was rationalized through analyzing the bridging bond distances, the electronegativity of the bridging atoms and silicon, and their oxidation state. For all bridging atoms apart from sulfur, structural properties, such as surface-(linker)-chain angles, are converged once  $n > 3$ . For sulfur, there are three regimes, namely  $n = 0 - 3$ ,  $n = 5 - 7$  and  $n = 9 - 11$ , which were attributed to substantial changes in adsorption structures. Attaching the alkyl chain to the Si surface via linkers other than carbon influences the optimum surface coverage. We have shown that NH, O and S linkers allow more packing density up to 75% coverage. However the sequence of the stability order seems to be independent of the coverage.

Functionalized surfaces have a broad range of application in bio/opto-electronic devices in which monolayers' stability and dense packing is one of the primary concerns. The predicted improvement in stability by using different linker

species rather than carbon in contact with silicon which was shown here, offers a new approach to achieve the goal of enhanced stability and dense packing. The role of the linker in inducing various structural effects predicted in this part is also important while dealing with opto-electronic devices, where we showed that for the same length of the alkyl there is a significant difference in thickness for monolayer with sulfur and carbon linkers compared to oxygen and nitrogen head-groups. This can significantly affect optical indices and adsorption spectra in those devices. More importantly, the potential for higher coverages as a result of grafting monolayers via linkers other than carbon, that we systematically investigated for the first time, may convince the experimentalist to consider it in the future for device design.

As a more expanded study compared to previous investigations and in the light of obtained insights, for the third step, we considered three classes of monolayers with the general formula of  $-X\text{-Alkyl}$ ,  $\text{-Alkyl-X}$  and  $-X\text{-Alkyl-X}$  ( $X = \text{C, O, N, S}$ ) grafted on the H:Si(111) surface at half coverage. Our comprehensive DFT-vdW analysis achieved interesting results.

Overall we have shown that the WF of the H:Si(111) surface can be modified by up to 1.73 eV by adsorption of alkyl chains with judicious choice of head groups for strong surface binding and tail-groups for WF modulation. Irrespective of which head- or tail-groups are combined, for short chains the WF depends on chain length with amplified effects arising from the choice of head and tail groups alongside showing weak odd-even effect. With different head-groups the WF converges quickly displaying no significant odd-even effects at long chain lengths. The WF shift compared to bare H:Si(111) in this case is dominated by the nature of the used head-group.

For functionalization with different tail-groups or with both head and tail-groups a strong oscillatory behavior of the work function is observed, with WF changes of up 1.73 eV compared to bare H:Si(111). For functionalization by alkyl chains with 12 or more carbons that is often applied by experimentalists, and terminated with  $-\text{SH}$  and  $-\text{NH}_2$ , the WF shift is dominated by the used tail-group. The odd-even effect due to the number of carbons in the alkyl chain plays a significant



role in controlling the WF. Hence highly stable SAMs with substantial tunability in the WF can be obtained by functionalizing with both head and tail-groups. While the head-group determines the stability of the SAM, the tail-group is able to induce large shifts in the surface WF. Furthermore, the WF can also be controlled by utilizing the odd-even effect in monolayers with long alkyl chains. This large tuning interval can be a valuable option in modifying various silicon-organic based devices. For example, to get higher sensitivity in FET-based nanowire sensors it is important to keep the threshold voltage around zero, as close as possible. It is shown that alkyl monolayers are capable of modifying the threshold voltage and including this large odd-even tuning interval predicted here can substantially improve our control of the threshold voltage or sensor sensitivity in the next generation of organic-inorganic devices. Considering the large predicted peak-to-peak amplitude of oscillations this can also be implemented in the future as an alternative molecular switch with application in nanosensors or as an option for reaction monitoring and control of the monolayer thickness.

Gathering all understandings from a single type of functionalization of different alkyl chain lengths and bearing in mind how utilizing head-group, tail-group or both as well as monolayer coverage affects the electronic and structural properties, at the final step of this Thesis we functionalized the H:Si(111) with binary mixtures of component SAMs. Aiming at increasing WF adjustment along with SAM stability and coverage, we chose a range of terminations and linker-chains  $-X-(\text{alkyl})$  with  $X = \text{CH}_3, \text{O(H)}, \text{S(H)}, \text{NH}_2$  and investigated the stability and WF of various binary components grafted onto the H:Si(111) surface.

At the first part we fixed the total coverage up to 50% and applied terminations and linker-chains with the same alkyl length each by 25% and calculated the WF and adsorption energy. We compared the results with the corresponding single type functionalization of each component at 50% coverage. The results clearly show a possibility to obtain further WF tuning with the values within the extremes of single type functionalization. For the binary mixture the WF is

roughly the average value of the single type functionalization. However this picture seems to be distorted by chain-chain interactions when longer alkyl chains are applied, especially for chains with more than six carbons.

At the second part, we applied different ratios of hexyl monolayers directly attached to H:Si(111) combined with either –NH–hexyl or –O–hexyl, where the hexyl portion dominates mostly. We have shown that irrespective of ratio, the binary layer is always more stable compared to pure alkyl functionalization. The results also indicates that even using a small percentage of linker-chain combined with alkyl SAM allows coverage more than 50% which was shown to be the optimum coverage for the case of alkyl monolayers.

Bearing in mind that direct Si-alkyl monolayers are suffering from poor stability and low coverage over Si-linker-alkyl SAMs (with linkers such as S, O and N) but are still the most studied monolayers among different types of organic SAMs with established preparation methods, the strategy of binary functionalization with different linkers that is proposed here for the first time, can be utilised by experimentalists to improve the stability and increase the coverage of alkyl functionalization.

Controlling the structure of silicon surfaces, their chemical and physical and structural properties, is scientifically interesting and particularly important for technology. Overall the results presented here provide important microscopic insights into work function tuning of H:Si(111) by modification with functionalized alkyl chains and structural behavior. This analysis forms a basis for efforts in creating surfaces by design.

## 7.2 Future perspectives

There are still quite a few approaches to the mechanism of adjusting (both electronically and structurally) the interface and further insights to be obtained from future investigations. Possibilities include:

- Study of dielectric properties of the silicon surface by applying SAMs with different head and/or tail groups. Regarding the insulating nature of

aliphatic SAMs, this is potentially important for addressing dielectric materials in hybrid devices.

- Pi-conjugated SAMs and their combination with aliphatic counterparts (as secondary functionalization for example) is another interesting research topic. In this case, commonly used SAMs in experiments might be a good option to start.
- Considering that real devices use p/n-doped silicon substrates, including that in the simulation may further improve the comparison with the experiment and provide more options in design. Also investigations of more complex substrates, such as Si/SiO<sub>2</sub> or reconstructed substrates or structures with defects, will improve the realism of the model.

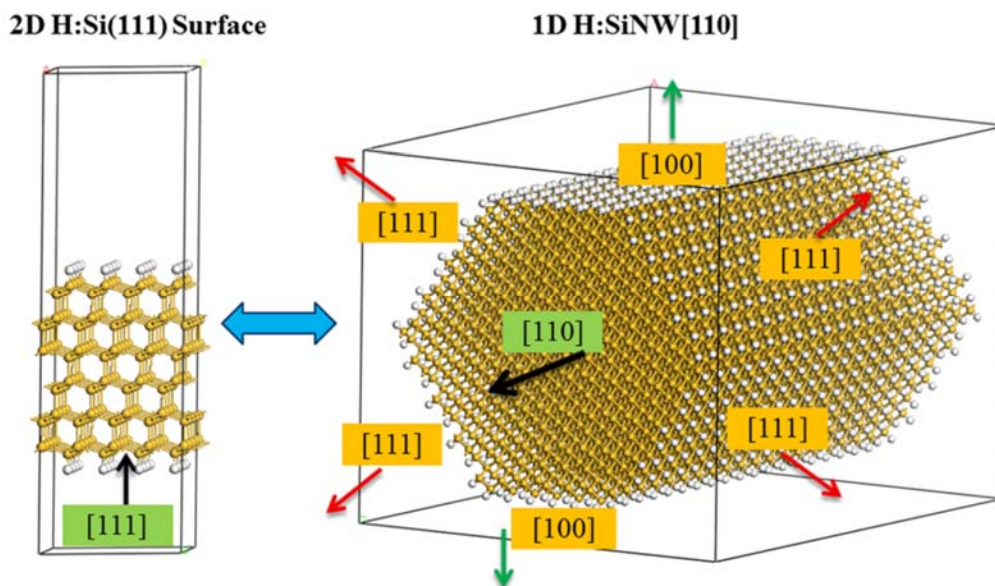


Figure 7.1. H:Si(111) 2D surface on the left and H:SiNWs along [110] crystallography direction on the right. For a thick NW and far from the edges, the (111) facets are comparable with their 2D counterpart.

Silicon nanowires (SiNWs) as a new class of quantum size materials have also proven to be very interesting for technology applications such as nanowire sensors and optical devices. In principle their general physical/chemical

properties can be extracted from their two dimensional analogue (2D surfaces). Therefore the overall results obtained from the functionalized H:Si(111) surface are transferable to SiNW surfaces. However, quantum confinement can make a substantial distinction between 2D and 1D structures and this is highly dependent on the NW diameter. Also in such NW-based devices, more than one surface is involved at a time and due to high surface-to-volume ratio, surface termination/functionalization can completely change the characteristics compared to 2D surfaces.

Therefore, these NW structures need to be studied independently and the comparison of the results with 2D surfaces will further improve our understanding and give us new insights.

Overall we propose that further work on this subject can be done as below:

- A detailed study of structural and electronic properties for a range of NW diameters (and cross-sections) functionalized with those linker-chains that show desired results in the surface studies and comparison with 2D. Determine the estimated diameter that both structures show the same properties. Investigate the symmetrical effect in multi facet functionalization. Establish a way to define the total WF for a multi-facet structure such as NW.
- Optical and dielectric properties of the functionalized NWs and finding how they can be controlled by SAMs. This can highly enhance the rational design of an efficient hybrid miniaturized optoelectronic device or sensor.
- Implementing all the obtained information and coupling ab-initio calculations to a larger scale simulation method, one could directly study the real device. Perhaps circuit-implantation (making circuits by grafting molecular layers on the surface) by molecular assembly will change our thinking in ways we have not imagined.